Effects of Surgical Repair or Reconstruction on Radiocarpal Mechanics from Wrists with Scapholunate Ligament Injury

by

Joshua E Johnson

MSc (ME), University of Kansas, Lawrence, Kansas, USA
BEng (ME), University of Botswana, Gaborone, Botswana

Submitted to the graduate degree program in Mechanical Engineering
and the Graduate Faculty of the University of Kansas School of Engineering
in partial fulfillment of the requirements for the degree of
Doctor of Philosophy

Committee: _____

Chairperson: Kenneth J Fischer, PhD

_____

Phil Lee, PhD

_____

Terence E McIff, PhD

_____

Carl W Luchies, PhD

_____

Michael Detamore, PhD

Date defended: _____

The Dissertation Committee for Joshua E Johnson certifies
that this is the approved version of the following dissertation:

Effects of Surgical Repair or Reconstruction on Radiocarpal Mechanics from Wrists with Scapholunate Ligament Injury

Committee: _____

Chairperson: Kenneth J Fischer, PhD

_____

Phil Lee, PhD

_____

Terence E McIff, PhD

_____

Carl W Luchies, PhD

_____

Michael Detamore, PhD

Date approved: _____

Table of Contents

This page left intentionally blank.

ACKNOWLEDGEMENTS

I would like to thank God for this opportunity and privilege, with whom all things are possible (Matthew 19:26). I would like to thank my adviser, Dr. Fischer, for accepting me as his graduate student and for all his invaluable help and mentoring, which made the successful completion of this work possible. I would like to thank my committee members, Dr. Lee, Dr. Luchies, Dr. McIff and Dr. Detamore for their valuable feedback. I would like to thank Allan Schmitt and Franklin Hunsinger at the Hoglund Brain Imaging Center, for their assistance with MR imaging. I am grateful for grant support. I would like to thank my colleagues in the Musculoskeletal Biomechanics Lab both past (Michael Humphrey, Eric Tobaben and Mahender Mandala) and present (Saman Modaresi, Qi Zheng and Isaac Chappell), for their help and support. Last but not the least, I would like to thank my mom (Vina), my dad (Johnson), my brother (Enoch) and Amy for being there for me through every step of the way. I am also grateful to my family and friends for all their prayers and support during my time of study.

This page left intentionally blank.

TABLE OF FIGURES

LIST OF ACRONYMS

3D:	three dimensional
3T:	three Tesla
ACL:	anterior cruciate ligament
ANOVA:	analysis of variance
AP:	anteroposterior
APL:	abductor pollicis longus
CH:	capitohamate
CIA:	carpal instability adaptive
CIC:	carpal instability complex
CID:	carpal instability dissociative
CIND:	carpal instability nondissociative
Cine-PC:	cine phase contrast
CISS:	constructive interference steady state
CT:	computed tomography
DASH:	disabilities of the arm, shoulder and hand
DEA:	discrete element analysis
DESS:	dual echo steady state
dGEMRIC:	delayed gadolinium enhanced MRI of cartilage
DIC:	dorsal intercarpal
DISI:	dorsal intercalated segment instability

DRC: dorsal radiocarpal

DTM: dart-throwers motion

ECRB: extensor carpi radialis brevis

ECRL: extensor carpi radialis longus

ECU: extensor carpi ulnaris

EMG: electromyogram

FCR: flexor carpi radialis

FCU: flexor carpi ulnaris

FE: finite element

FEM: flexion-extension motion

GAG: glycosaminoglycan

GRE: gradient recall echo

LRL: long radiolunate

LSD: least significant difference

LT/LTIO/LTIL: lunotriquetral/lunotriquetral interosseous/lunotriquetral interosseous ligament

MR/MRI: magnetic resonance imaging

NSAIDs: nonsteroidal anti-inflammatory drugs

OA: osteoarthritis

P/DRU: palmar/dorsal radioulnar

P/DST: palmar/dorsal scaphotriquetral

PA: posteroanterior

PG: proteoglycan

PRC: proximal row carpectomy

PSM: pronation-supination motion

PTOA: posttraumatic osteoarthritis

RBSM: rigid body spring modeling

RL: radiolunate

RMS/RMSE: root mean square error

RS: radioscaphoid

RSC: radioscaphocapitate

RSL: radioscapholunate

RUD: radial-ulnar deviation

RV: rotation vector

S/CNR: signal/contrast-to-noise ratio

SC: scaphocapitate

SCM: surface contact modeling

SL: scapholunate

SLAC: scapholunate advanced collapse

SLI/SLIL: scapholunate interosseous/scapholunate interosseous ligament

SLId/dSLIO: dorsal scapholunate interosseous

SLIp/vSLIO: palmar scapholunate interosseous

SLIpx/pSLIO: proximal scapholunate interosseous

SRL:	short radiolunate
STT:	scaphotrapezium-trapezoid
TC:	trapezocapitate
TC:	triquetrocapitate
TFCC:	triangular fibrocartilage complex
TH:	triquetrohamate
TT:	trapeziotrapezoid
TV:	translation vector
UC:	ulnocapitate
UL:	ulnolunate
UT:	ulnotriquetral
VISI:	volar intercalated segment instability

ABSTRACT

Osteoarthritis as a result of injury/trauma is a significant problem, and there is still a need to develop tools for evaluating joint injuries and the effectiveness of surgical treatments. For the wrist in particular, injury to the scapholunate ligament from impact loading, can lead to scapholunate joint instability. Without treatment, this can lead to progressive development of wrist osteoarthritis. Joint contact pressures are important mechanical factors in the etiology of osteoarthritis, and these can be determined non-invasively through computer modeling. Hence, the goal of this work was to investigate the effects of scapholunate ligament injury and surgical repair on radioscapholunate contact mechanics, through surface contact modeling (SCM) and finite element modeling (FEM). The modeling process required geometries, boundary conditions and a contact relationship. Magnetic resonance imaging (MRI) was used to acquire images of the normal, injured and post-operative wrists, while relaxed and during active grasp loading. Surface and volumetric models were generated from the relaxed images, while kinematic boundary conditions were determined from image registration between the relaxed and loaded images. To improve the automatic image registration process, the effects of initial manual registration on the outcome of final registration accuracy, were investigated. Results showed that kinematic accuracy and subsequent contact mechanics were improved by performing a manual registration to align the image volumes as close as possible, before auto-registration. Looking at the effects of scapholunate ligament injury, results showed that contact forces, contact areas, peak and mean contact pressures significantly increased in the radioscaphoid joint. The locations of contact also shifted with injury. This novel data showed that contact mechanics was altered for the worse after injury. Novel contact mechanics data on the effects of surgical repair were also obtained. Results showed that radiolunate peak and mean contact pressures decreased significantly compared to injured, which indicated the possibility of restoring normal mechanics post surgery. SCM results were compared to FEM results to demonstrate the feasibility of the surface contact modeling approach for clinical applications. Contact parameters compared well between the two techniques. This work demonstrated the potential of MRI-based SCM as a tool to evaluate joint injuries and subsequent treatments, for clinical applications.

This page left intentionally blank.

MOTIVATION

The goal of this study was to investigate *in vivo* changes in radiocarpal joint mechanics associated with scapholunate ligament injury and surgical repair, during active functional grasp. The long-term goal is to relate changes in joint contact mechanics to the risk of osteoarthritis (OA), to possibly prevent the onset of degeneration. Normal wrist function is the result of a complex interaction between articulating carpal bones and ligamentous constraints. These facilitate motion and load transfer between the hand and forearm. Instability of any joint can lead to abnormal motion and altered mechanics.

The scapholunate interosseous ligament (SLIL) is the primary stabilizer of the scapholunate (SL) joint. SL dissociation is a commonly occurring wrist injury caused by disruption of the SLIL due to hyperextension or intercarpal rotation. This ligament injury results in SL instability with associated changes in kinematics and load transfer through the radiocarpal joint. Without treatment, SL dissociation generally leads to a progressive osteoarthritic pattern known as scapholunate advanced collapse. The prevalence and incidence rates for symptomatic OA are second highest for the hand and wrist. While the mechanism is still not clearly understood, joint contact pressure is believed to be an important mechanical factor. Progressive instability/deformity of the SL joint as a result of SLIL injury, may cause an elevation in joint contact pressures in the normal contact regions or in shifted regions of contact. A tool to evaluate changes in contact pressure that occur *in vivo* may provide insight into the mechanism of post-traumatic OA. Surgical techniques such as direct ligament repair (with capsulodesis), tendon weaves, arthrodesis (various limited/total intercarpal fusions) etc., are performed to minimize pain, restore joint function and prevent the onset of OA. The postoperative effectiveness in restoring normal joint mechanics and function still remains a question. Several cadaveric experimental studies have investigated normal and pathologic wrist biomechanics (kinematics and kinetics). However, *in vivo* conditions are much more complex. Magnetic resonance imaging (MRI) is limited in its diagnostic value for wrist ligament injuries. However, MRI can be used to acquire *in vivo* data (such as model geometry and kinematics) and can be an effective tool when combined with computational modeling. Computer simulation can be a valuable tool to tailor patient-specific treatment procedures. MRI-based surface contact modeling is very useful to determine *in vivo* joint mechanics noninvasively, in a relatively simple and computationally

efficient manner, without the need for complex nonlinear analyses. Very few studies have investigated *in vivo* wrist joint mechanics and there does not appear to be any prior work on the *in vivo* effects of SLIL injury/repair on mechanics.

Specific aim 1

To investigate the effects of SLIL injury on normal joint mechanics through subject-specific functional data. The current goal was to investigate changes in peak contact pressure and contact pressure distribution on the cartilage surface as a result of injury, as well as other contact mechanics factors (contact area, contact force and average contact pressure).

Research question

How does scapholunate ligament disruption/injury affect normal joint mechanics? How are articular surface contact areas, contact forces, peak contact pressures and pressure distributions and average contact pressures altered as a result of injury?

Hypothesis

With SLIL disruption/tear and the stage of injury during the time of diagnosis, progressive scapholunate diastasis and instability may occur. This can cause changes in kinematics due to abnormal alignment that can lead to changes in load transfer and location in the joint. *Hence, peak contact pressures and average contact pressures were expected to increase with injury when compared to the normal wrist.*

It is possible there exists a range of contact pressures that are required to maintain physiological function, and that exceeding this limit maybe one of the factors that initiate the onset of OA. The ability to monitor the location of peak contact pressure and contact pressure distribution, may help predict tissue wear or the onset and progression of degradation.

Specific aim 2

To evaluate the efficacy of surgical repair to restore normal joint mechanics. The current goal was to investigate the immediate benefits of surgical treatment by looking at changes in peak contact pressure and contact pressure distribution on the cartilage surface after surgery (as well as other contact mechanics parameters).

Research question

How does surgical repair/reconstruction alter contact mechanics affected by injury? Do postoperative joint mechanics appear normal? Is the surgical technique effective at restoring near normal joint mechanics postoperatively?

Hypothesis

The goal of surgery is to minimize pain and deformity resulting from SLIL tears and attempt to restore normal carpal alignment. Depending on the surgery, patients present varying degrees of improvement in function, range of motion and radiographic evidence of reduction of the scapholunate interval. *Hence, peak contact pressures and average contact pressures were expected to decrease postoperatively to values near normal.*

Due to the different stages of injury and instability, there is still much controversy concerning the right choice of treatment. The ideal timing of SLIL repair is not yet known. It is also believed that the ideal treatment when the SLIL is irreparable, without the presence of OA, has not yet been determined. The severity of instability at the time of diagnosis is a confounding factor, which determines the type of surgery that is performed and thus has an impact on the outcome. The postoperative outcomes of various treatments have been inconsistent. Physicians try different surgical techniques and visually and/or functionally monitor the outcomes. It may be possible to more effectively differentiate between treatments based on pre and postoperative contact mechanics data. It may also be possible to use the contact mechanics data to devise strategies/surgical plans to address the different stages/patterns of injury and predict the future outcome of surgeries.

Specific aim 3

To compare contact mechanics data between surface contact modeling and finite element modeling. The goal was to demonstrate that MRI-based surface contact modeling results can be used to distinguish between normal and abnormal joint mechanics and surgical treatments, in a computationally efficient manner.

Research question

How do contact mechanics results from surface contact modeling compare with those from finite element (FE) modeling (which is considered the gold standard)? How complex does a model need to be to obtain clinically useful, accurate, and relevant data?

Hypothesis

FE modeling is the most commonly used technique but is also very involved. Surface contact mechanics can provide a reasonable idea of changes in mechanics associated with injury and surgical repair. This can be achieved through surface contact modeling without the need for complex 3D FE analyses. *To be considered reliable, contact parameters from surface contact modeling should compare well with contact parameters from a similar analysis performed using FE modeling.*

To evaluate changes in joint mechanics as a result of injury/surgical intervention, it may be sufficient to look at contact mechanics data from surface contact modeling. Also, the geometry and boundary conditions from surface contact modeling can be directly implemented in an FE model. FE modeling can also be used determine stress and strain distribution within cartilage. This may provide further insight into the mechanism of degradation by understanding how functional integrity is compromised by breakdown within the tissue. This data may also be useful for tissue engineering applications. The mechanics data was based on *in vivo* functional loading, which may be able to provide experimental parameters for chondrocyte biosynthesis for cartilage tissue culture and transplanting, or provide information on the functional stresses that regenerating tissue may experience *in situ*.

Since, there does not appear to be any prior work on the *in vivo* effects of SLIL injury/repair on radiocarpal joint mechanics, this study can potentially improve the understanding of the pathomechanics of injury, and the effectiveness of corrective measures.

Other studies in our lab are also investigating the effects of SLIL injury on physiological changes in cartilage based on T2 relaxation times. It may be possible to correlate microscopic degenerative changes (before any visual changes) with changes in contact mechanics to predict the risk of OA.

The short-term benefits of surgery based on a 1 to 2 year follow-up after postoperative assessment, and the effects of conservative treatment (for patients that do not opt for surgery), are also planned for future investigation. It is not uncommon to observe degenerative changes even after surgical intervention. Using surface contact modeling, it may be possible to monitor load transmission through the joint for different treatments (apart from visual/functional outcomes) to further refine the treatment process. Clinically observed patterns of cartilage degeneration can be compared to model contact pressure intensities or patterns on the surface (contact modeling) or within the tissue (FE modeling). Treatments for joint injuries can be designed to minimize high stresses on or within the cartilage (unload the cartilage) as a result of instability/deformity, to allow intervention for preventing OA.

Additional contact mechanics data from the short-term follow-ups and conservative treatments (together with further studies looking at the effectiveness of splints/braces, and joint mechanics at different wrist positions), may provide useful information for physical therapy and rehabilitation techniques on how to manage the progression and minimize the effects of instability.

Due to its subtlety, SLIL injuries are often dismissed as minor sprains and diagnosis is rarely performed in the early stages of instability, but rather in the advanced stages. MRI-based surface contact modeling has the potential for early diagnosis. With advances in MRI techniques in the future, it may be possible to incorporate the entire process into an MRI system to obtain contact pressure data in real time and regularly monitor the health of the joint, as part of a general physical exam. With data from sufficient subjects, it may be possible to generate a database of *in vivo* peak contact pressures and pressure distributions for comparison, in order to predict different levels of instability thereby providing a means to diagnose ligament injuries noninvasively and detect the future risk of OA. This technique can be further extended to evaluate other joints and joint pathologies.

This page left intentionally blank.

1. BACKGROUND

1.1. Introduction

The hand is integral in the physical expression of human behavior and has a vital function in daily living. A loss of this function can therefore prove very debilitating. The wrist, which connects the hand to the forearm, plays a key role in hand function. It allows for positioning and orientation of the hand in space and also for load transfer between the hand and the forearm. This is largely due to the intricate mechanisms and interactions between the bones and soft tissue (such as ligaments) that constitute the wrist joint complex.

1.1.1. Basic anatomy and function

The distal radius and ulna, the metacarpals and the carpus constitute the bones of the wrist complex (Fig. 1.1). The carpus is an organization of eight carpal bones. Until the 15th century, the carpus was considered physiologically insignificant and hardly any anatomical or functional information existed. The first descriptive illustrations of the wrist bones were published in 1543 wherein the carpal bones were numbered 1 to 8 [1]. Carpal bone nomenclature first appeared in 1653 and the present nomenclature was proposed at the start of the 20th century and adopted in 1955 [1]. From radial to ulnar, the scaphoid, the lunate, the triquetrum and the pisiform constitute the bones of the proximal row, while the trapezium, the trapezoid, the capitate and the hamate collectively comprise the distal row (Fig. 1.1). Due to its location within the flexor carpi ulnaris tendon, the pisiform is often considered more of a sesamoid bone [1-4] and as such does not contribute to proximal carpal row function [5]. The scaphoid, which is the second largest carpal bone, spans the proximal and distal rows and functions as an intermediary and supporting structure between the two rows [1-4]. The sigmoid notch region of the distal radius and the ulna head together with the triangular fibrocartilage complex [(TFCC) composed of the articular disc and radioulnar ligaments] articulate to form the distal radioulnar joint. Proximally, the scaphoid and the lunate articulate with the distal radius to form the radiocarpal joints. The sagittally oriented interfacet prominence (interfossal ridge) separates the triangular scaphoid fossa from the quadrangular lunate fossa proximally on the radius articular surface [6, 7]. There is no direct contact between the distal ulna and the proximal row, however, the articular disc functions as an interface between the distal ulna, the triquetrum, the hamate and the base of the fifth metacarpal [2]. This interface between the ulna and the distal wrist bones forms the ulnocarpal joint. The

proximal row articulates distally with the proximal surface of the distal row to form the midcarpal joints. The distal row articulates distally with the bases of the metacarpals. Within the proximal and distal rows, adjacent bones articulate to form various intercarpal joints. The entire carpus is bound together by a complex and finely tuned network of ligaments. Interaction between the carpal bones, highly specialized ligamentous connections and balanced muscle forces allow for proper joint function.

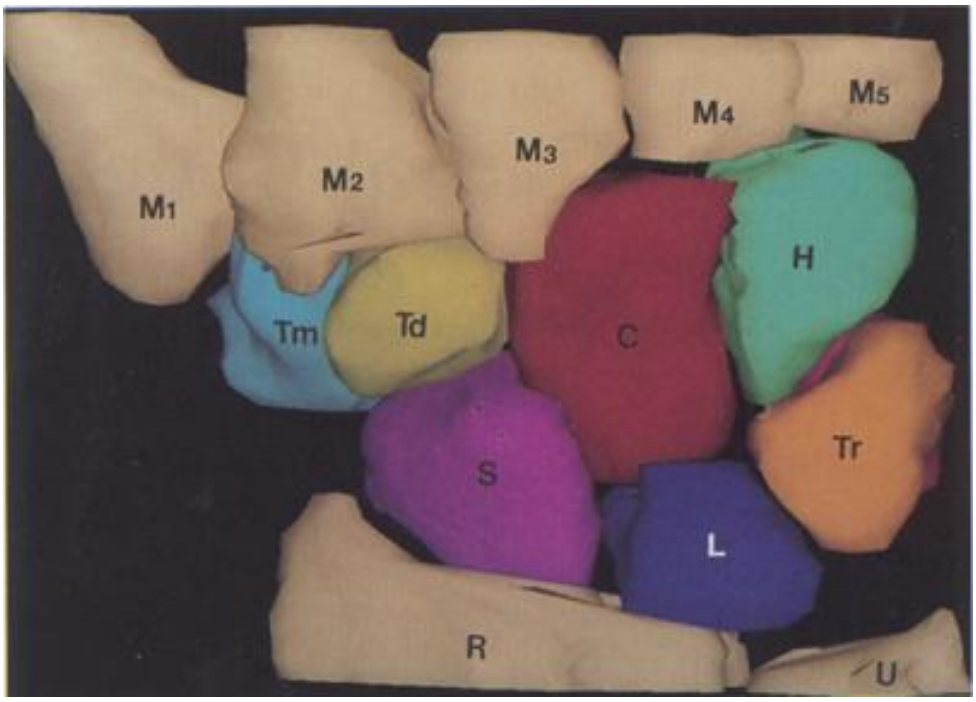

Figure 1.1. Osseous anatomy of the wrist from a dorsal perspective. Shown are the bones of the proximal (S: scaphoid, L: lunate, Tr: triquetrum, pisiform not shown) and distal (Tm: trapezium, Td: trapezoid, C: capitate, H: hamate) rows and the various articulating joints. Also shown are the radius (R), ulna (U) and metacarpals (M1-M5). Reprinted from The Journal of Hand Surgery, Volume 20, Patterson, R.M., Elder, K.W., Viegas, S.F., and Buford, W.L., Carpal bone anatomy measured by computer analysis of three-dimensional reconstructions of computed tomography images, Pages 923-929, Copyright (1995), with permission from Elsevier.

Except for the pisiform within the flexor carpi ulnaris tendon, there are no direct motor attachments to the carpal bones to provide dynamic stability. The flexors and extensors that contribute to carpal motion, insert into the metacarpals or phalanges from their origins at the

elbow/proximal forearm [5]. The flexor carpi radialis (FCR) and the flexor carpi ulnaris (FCU) are the primary wrist flexors, the extensor carpi radialis longus (ECRL) and brevis (ECRB) are the primary extensors, the abductor pollicis longus (APL) and the extensor carpi ulnaris (ECU) are the primary radial and ulnar deviators respectively [5]. The extensor carpi ulnaris, the abductor pollicis longus and the extensor pollicis brevis tendons contribute to and aid in dynamic stability [2, 4, 5]. Hence the arrangement of the carpal bones and the various ligamentous interconnections play a primary role in wrist stabilization [3, 4]. The ligaments of the wrist have been identified and named as early as the 18th century [8]. Since then, various individuals (Henke in 1863, Poirier in 1899, Destot in 1923, Testut in 1931, Lewis in 1970, Mayfield in 1976, Taleisnik in 1985, Sennwald in 1986, etc.) have progressively contributed to the further understanding of ligamentous functional anatomy [1, 9]. This understanding keeps evolving with improved knowledge of carpal function and mechanisms. Wrist injuries (ligamentous in particular) are difficult to treat, hence a better description of normal and pathologic physiology and mechanics can help identify the cause, and in turn improve treatment efficacies of wrist abnormalities.

Ligaments are made up of a dense bundle of collagen fibers called fascicles surrounded by connective tissue, which also transmits the neurovasculature [8]. Towards the surface, the connective tissue groups together to form a continuous protective cover called the epiligamentous sheath [8]. Ligaments of the wrist are generally classified as capsular (within joint capsule layers) or intra-articular (entirely within the joint). The epiligamentous sheath of capsular ligaments has a fibrous stratum on the superficial surface and a synovial stratum on the deep or joint surface, while the intra-articular ligaments are covered completely by a synovial stratum [8]. Depending on orientation, ligaments can be further classified as extrinsic or intrinsic (Fig. 1.2). Extrinsic ligaments originate from the distal radius and ulna and attach to the carpal bones while the origins and insertions of the intrinsic ligaments are within the carpal bones [1, 4, 7]. The intrinsic ligaments are stronger and thicker palmarly than dorsally and assist with intercarpal stability [4]. The majority of the extrinsic ligaments are capsular while the intrinsic ligaments are intra-articular or interosseous [6, 8, 9]. Depending on location, the extrinsic ligaments can be subdivided into palmar (volar) or dorsal. The stronger palmar ligaments are the major wrist stabilizers and provide a greater resistance to instability (especially against

hyperextension) while the lesser developed dorsal ligaments are the secondary stabilizers of the scapholunate (SL) joint and help prevent volar instability [4, 7]. Intercarpal motion and carpal stability is reliant on and facilitated by the complex arrangements of these ligaments [3, 4, 6-9].

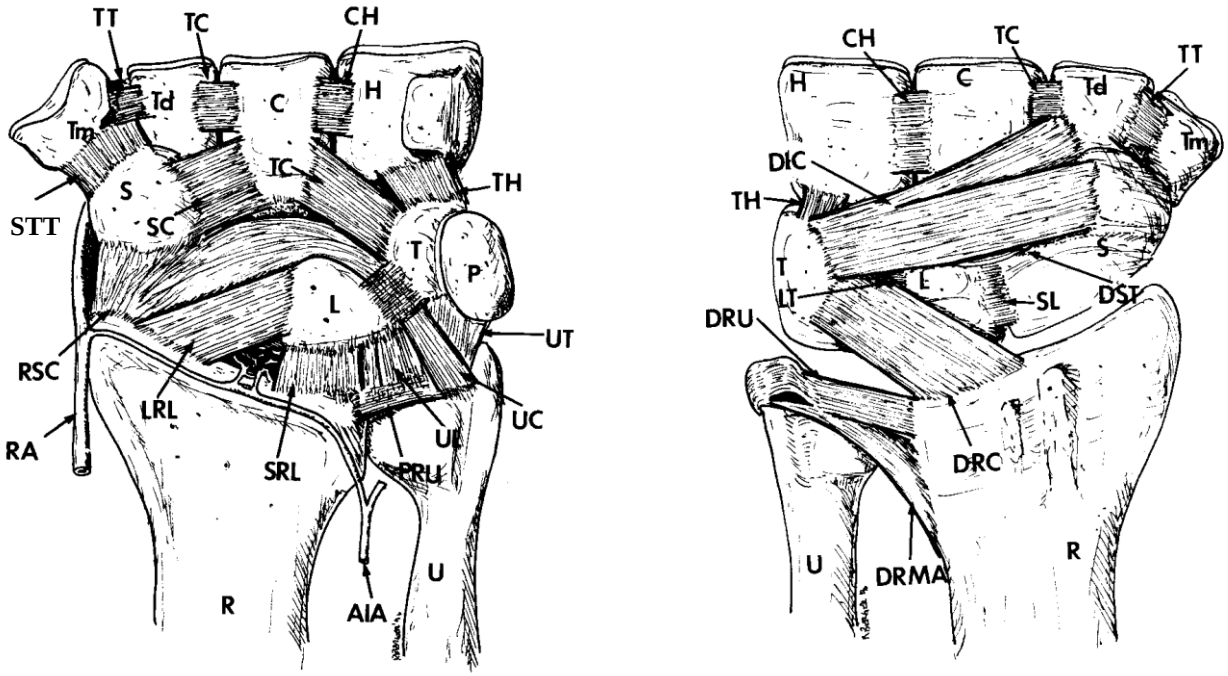

Figure 1.2. Ligamentous anatomy of the wrist from the palmar (left) and dorsal (right) perspective. The palmar view shows the extrinsic ulnocarpal and palmar radiocarpal ligaments, the intrinsic palmar midcarpal ligaments and the distal row interosseous ligaments. The dorsal view shows the extrinsic dorsal radiocarpal ligament, the intrinsic dorsal midcarpal ligaments and the proximal and distal row interosseous ligaments. The palmar and dorsal radioulnar ligaments are also shown. The palmar view also shows vascular insertion into the radiocarpal joint capsule through the radioscapholunate ligament. Reprinted from Hand Clinics, Volume 13, Berger, R.A., The ligaments of the wrist. A current overview of anatomy with considerations of their potential functions, Pages 63-82, Copyright (1997), with permission from Elsevier.

The distal radioulnar ligaments are important for the stability of the distal radioulnar joint [palmar and dorsal radioulnar (P/DRU) ligaments]. The ulnocarpal ligaments help stabilize the ulnocarpal joint and are thought to guide lunate and triquetrum motion [ulnolunate (UL) and ulnotriquetral (UT) ligaments], while also assisting with distal radioulnar joint stability [ulnocapitate (UC) ligament]. The palmar radiocarpal ligaments help with scaphoid distal pole

stability [radioscaphocapitate (RSC) ligament], constrain lunate rotation [short radiolunate (SRL) ligament] and translocation [long radiolunate (LRL) ligament] and maintain the functional integrity of the wrist [radioscapholunate (RSL) ligament]. From their proximal radial and ulnar origins, the palmar extrinsic ligaments tend to merge toward the middle of the carpus (Fig. 1.2, left). There also exists a weak spot in the palmar capsule between the radioscaphocapitate and the long radiolunate ligaments at the level of the midcarpal joint called the space of Poirier [1, 8]. The dorsal radiocarpal (DRC) ligament helps with carpal alignment and stability and constrains the carpus against ulnar translocation. The palmar midcarpal ligaments are thought to stabilize the distal pole of the scaphoid, trapezium and trapezoid [scaphotrapezium-trapezoid (STT) and scaphocapitate (SC) ligaments], help prevent midcarpal dissociative [triquetrohamate (TH) ligament] and non-dissociative [triquetrocapitate (TC) ligament] instability and are important to the mechanical integrity of the proximal carpal row [palmar scaphotriquetral (PST) ligament]. The dorsal midcarpal ligaments help to constrain midcarpal rotation and provide indirect scapholunate dorsal stability [dorsal intercarpal (DIC) ligament] and also facilitate proximal row interosseous ligament stability [dorsal scaphotriquetral (DST) ligament]. From their origins, the dorsal extrinsic and intrinsic ligaments tend to converge on the triquetrum (Fig. 1.2, right). The distal row interosseous ligaments assist in stabilizing the distal row and the carpal arch system and provide structural integrity to the joints [trapeziotrapezoid (TT), trapezocapitate (TC) and capitohamate (CH) interosseous ligaments]. The proximal row interosseous ligaments help stabilize the proximal row, allowing for normal scapholunate and lunotriquetral joint function [scapholunate (SL) and lunotriquetral (LT) interosseous ligaments]. These are but a few of the many known (and still unknown) functions and from this it is clear that the ligaments of the wrist form an intricate arrangement with a complex function beyond just a simple passive constraining of the carpal bones. The scapholunate interosseous ligament is considered one of the most important intrinsic interosseous ligaments [7].

1.1.2. Anatomy and function of the scapholunate interosseous ligament

A ligament connecting the scaphoid and the lunate was first mentioned in Destot's posthumous publication in 1923 [9, 10]. This ligament, now known as the scapholunate interosseous (SLI) ligament, is compared to a "lateral ligamentous bolt" that holds the proximal row together [10] and is thought to be the primary stabilizer of the scapholunate joint [7]. Except

for the distal region, the SLI ligament joins all edges (dorsal, proximal and palmar) of the scapholunate articulation [10, 11]. Hence the possible need for secondary stabilizers RSC, STT, SC and DST to provide distal stability to the scaphoid and the scapholunate articulation [7, 8]. The SLI ligament is a "C" shaped ligament which is structurally divided into the dorsal (SLId), proximal (SLIpx) and palmar (SLIp) sections (Fig. 1.3) [7, 8, 10, 11].

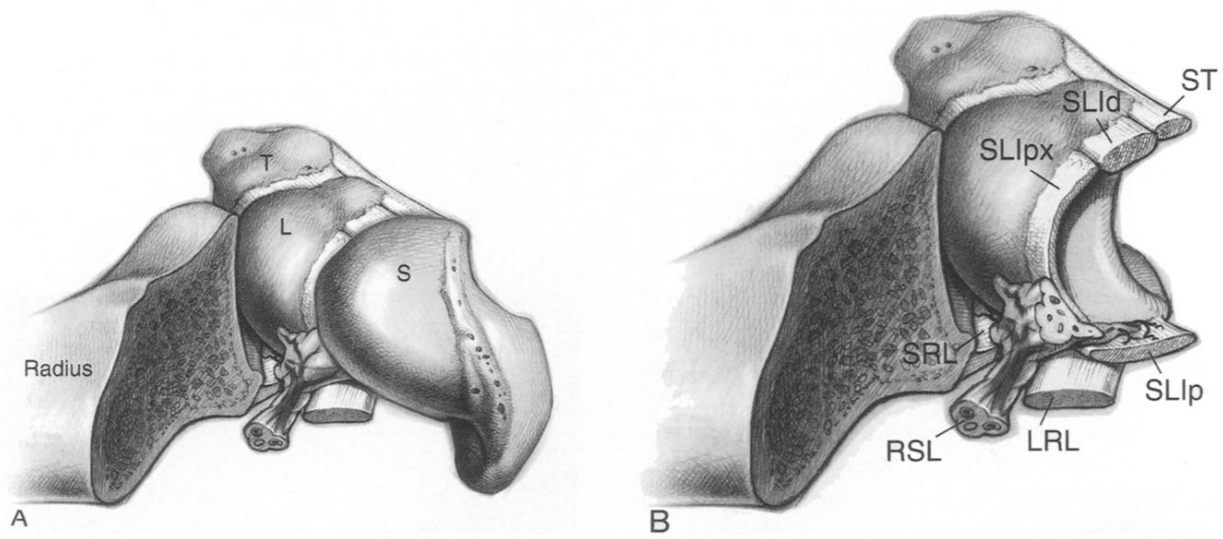

Figure 1.3. Anatomy of the scapholunate interosseous (SLI) ligament shown with the scapholunate joint intact (A) and with the scaphoid removed (B) from a radial and proximal perspective. Shown are the dorsal (SLId), proximal (SLIpx) and palmar (SLIp) sections, with the RSL interrupting the continuity of the SLIpx and the SLIp sections. Also shown are the palmar capsular ligaments that attach to the lunate and the distal attachment of the dorsal section. The radial styloid process has been sectioned for clarity. Reprinted from The Journal of Hand Surgery, Volume 21, Berger, R.A., The gross and histologic anatomy of the scapholunate interosseous ligament, Pages 170-178, Copyright (1996), with permission from Elsevier.

The SLId is a true ligament histologically, with transversely oriented collagen fibers between the radial aspect of the tip of the lunate dorsal horn and the corresponding ulnar-dorsal aspect of the proximal pole of the scaphoid (Fig. 1.4, right). This is the strongest and thickest of the three sections, usually 3 – 5 mm long (proximal-distal) and 2 – 4 mm thick [8, 10, 11]. The transverse fibers shorten in length from dorsal to palmar, giving the SLId a trapezoidal cross-section in the saggital and transverse planes. The superficial fibers of the SLId are oriented perpendicular and

tangential to the bulk fibers. The perpendicular fibers in the dorsal region attach to the dorsal radiocarpal joint capsule, thereby isolating contact between the distal half to three-quarters portion of the SLId and the radiocarpal joint. The tangential fibers in the dorsal region merge distally with the dorsal ST ligament. The most dorsal region of the SLId also merges with the DIC ligament. The SLId merges proximally with the SLIpx. This is characterized by a continuous transition from highly oriented fibers to a loose rubbery texture, which is otherwise not visible. This transition is gradual to sudden with increasing SLIpx thickness.

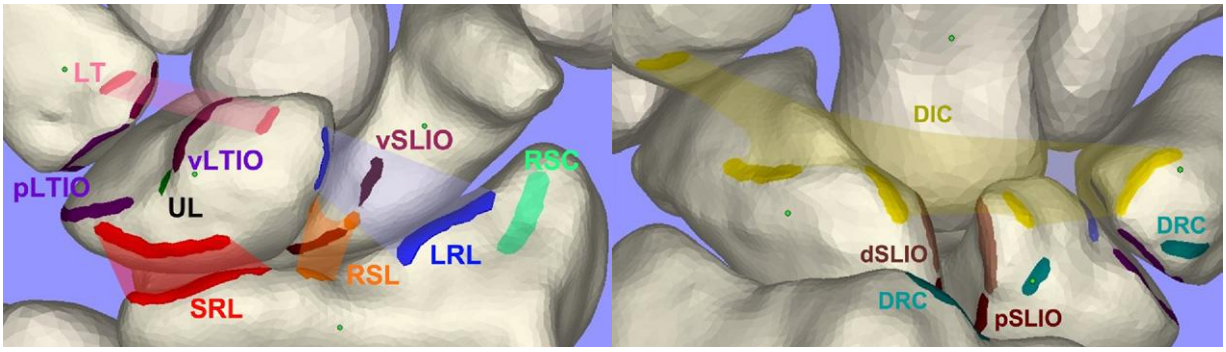

Figure 1.4. Showing attachment sites of the palmar (vSLIO), proximal (pSLIO) and dorsal (dSLIO) sections of the scapholunate interosseous ligament on the scaphoid and lunate from a palmar (left) and dorsal (right) perspective. Also shown are the pathways and attachment sites of the extrinsic palmar (UL) ulnocarpal and palmar (RSC, LRL, SRL, RSL) and dorsal (DRC) radiocarpal ligaments, the intrinsic dorsal (DIC) midcarpal ligament and the lunotriquetral (LTIO) interosseous ligament. Reprinted from The Journal of Hand Surgery, Volume 34, Kijima, Y. and S.F. Viegas, Wrist anatomy and biomechanics, Pages 1555-1563, Copyright (2009), with permission from Elsevier.

The SLIpx is distinctly anisotropic and appears as a minor disruption in the proximal scapholunate joint surface, which is otherwise continuous and smooth. This section does not display true ligamentous histology and is composed mostly of fibrocartilage throughout its length, and is avascular and aneural with little connective tissue. There is some longitudinal fiber organization in the central and most superficial surfaces. The thickness of the SLIpx varies but is generally the thinnest of the three sections [7, 8, 10, 11]. The fibrocartilage is particularly dense at the scaphoid and lunate attachment sites and blends with the articular cartilage. It is not easy to

identify the boundary between the articular cartilage and the ligamentous fibrocartilage. In instances where the SLIpx is relatively thicker, it pushes into the scapholunate joint space. The tip of this protrusion is wedge-shaped and forms two articulating surfaces with the scaphoid and lunate, similar to a knee meniscus. The pliable consistency of the SLIpx (compared to the taut SLId) and structure continues till gradually merging with the RSL ligament palmarly. Histologically, the RSL is also not a true ligament, but rather a neurovascular pedicle with loose connective tissue and neurovascular network forming its core, often referred to as the "intra-articular fat pad" [6, 8]. The RSL penetrates the palmar joint capsule to merge with the SLIpx, separating the SLIpx and SLIp sections (Fig. 1.4, left). At the merging zone, the core of the RSL replaces the fibrocartilage of the SLIpx and blends into the longitudinally oriented fibers within the fibrocartilage. This unique anatomical arrangement is not found elsewhere in the body. The distal extension of this region covers the dorsal joint surface of the SLIp.

The SLIp is histologically similar to the SLId, with proximal-ulnar to distal-radial obliquely oriented fibers (Fig. 1.4, left). This section is usually 4 – 5 mm long and not more than 1 mm thick [8, 10, 11]. The SLIp merges proximally with the joined RSL and SLIpx region. It is easy to visualize this sudden transition because of the oblique fiber orientation. There can be some interconnections of varying density between the SLIp and the RSC distally. Connective tissue usually separates the SLIp from the LRL ligament. Extensions of the RSL attach to the proximal-palmar aspects of the scaphoid and lunate covering the surface of the SLIp thereby isolating it from the radiocarpal joint. It is therefore impossible to visualize the SLIp with the RSL intact.

The SLI ligament is a complex structure that allows relative motion between the scaphoid and lunate [10, 11]. Isolation and sectioning of the SLI ligament has been observed to cause scapholunate joint instability and an abnormal transmission of forces through the wrist [10]. This leads to pressure modification on the intercarpal and radiocarpal joints resulting in secondary arthrosis [10]. The transversely orientated SLId is critical for resisting palmar-dorsal translation, distraction and torsional moments [7, 8] and facilitating control of flexion and extension motion [10]. The obliquely oriented SLIp is critical for constraining flexion-extension rotation [8] and facilitates rotational control [10]. The SLId and SLIp sections are therefore important for the scapholunate pair to function normally [8, 10]. The fibrocartilagenous SLIpx is not a substantial

mechanical structure [8]. It appears to play a very minor role in constraining motion [8] and in isolation, does not restrain abnormal scapholunate joint motion [7]. However, the SLIpx helps with scapholunate joint rotational stability and is suited to bear compressive and shear loads [7, 8]. Age-related degenerative tears occur in the SLIpx region probably due to its unique histology [10, 11]. Due to less vascularity on the scaphoid proximal pole, the SLIpx commonly tears on the scaphoid side following trauma or degeneration, leaving most of the ligament still attached and intact on the lunate side [10]. The SLId is the strongest of the three sections requiring more than 300 N to fail in tension, the SLIp fails within 150 N while the SLIpx being the weakest can only withstand 25 – 50 N [8, 10]. The inhomogeneity of the SLI ligament should be taken into account when considering ligamentous reconstruction. Treating the SLId, the SLIpx and the SLIp sections as a homogeneous unit can lead to failure of ligamentous reconstruction [10]. When performing ligamentous reconstruction, especially direct repair, it is important to note which sections are likely to heal and to recognize which tissues are strong enough to hold sutures securely in place while healing takes place [11].

1.1.3. Kinematics and carpal stability

The highly complex motion of the wrist joint is achieved through a combination of morphology (shapes of the carpal bones and their articulations), soft-tissue constraints (extrinsic and intrinsic ligaments) and motor attachments (to the bases of the metacarpals) that act indirectly through the distal carpal row. Complex interactions between these allow for normal and stable carpal joint function. Stability is defined as "the ability of a joint to maintain a normal relationship between the articulating bones and soft-tissue constraints under physiologic loads for its entire range of motion" [12]. Instability can lead to abnormal load transfer between articulations causing increased articular cartilage stresses and can also affect carpal alignment leading to abnormal motion. It is therefore important to understand normal joint function in order to understand the effects of injuries and pathologies that cause instability and abnormal motion.

Attempts have been made to describe cadaveric carpal motion since Henke in 1859 [1] but true descriptions of carpal kinematics began after the discovery of x-rays in the late 19th century, when Bryce first studied motions of his own wrists on radiographs in 1896 [1, 13]. Since then several techniques have been used to investigate carpal motion, such as cineradiography,

stereophotogrammetry, goniometry, magnetic and video tracking, magnetic, spatial and sonic digitization, biplanar radiography and non-invasive markerless registration [13, 14]. Initially, the wrist was thought to behave as a universal joint with a single transverse axis of motion having a single pivot point [6]. Despite some controversy, the center of rotation is commonly believed to be located in the capitate head (proximal pole) [6, 9, 13]. While the capitate is still considered to have a "keystone" position, it is now believed that *in vivo* carpal motion is much more complex with multiple axes of rotation [13, 14]. There exist three primary axes of carpal motion (Fig. 1.5); flexion-extension motion (FEM) in the saggital plane, radial-ulnar deviation (RUD) in the coronal plane and pronation-supination motion (PSM) in the transverse plane [6, 13, 15]. These axes of motion are still located at the capitate head but are shifted by 4 mm; the FEM axes being the most proximal and the ulnar deviation axis being the most distal [13, 14].

The range of motion varies from 140 – 150° in FEM (80° in flexion, 70° in extension), 50 – 60° in RUD (15 – 20° in radial, 30 – 35° in ulnar) and 150° in PSM [4, 5, 15]. The distal radius has a slight palmar tilt (11°) in the saggital plane that allows for more flexion than extension [4, 12]. The radiocarpal and midcarpal joints contribute differently to carpal motion. In flexion the midcarpal joint contributes 60% while the radiocarpal joint contributes 40% [5, 15]. In extension the midcarpal joint contributes 33 – 33.5% while the radiocarpal joint contributes 66 – 66.5% [5, 15]. In RUD the midcarpal joint contributes 60% of the motion while the radiocarpal joint contributes 40% [5]. The entire carpus moves primarily with the forearm in PSM (less than 10° of relative rotation) [6]. However, there exists slight intercarpal pronation and supination during FEM and RUD.

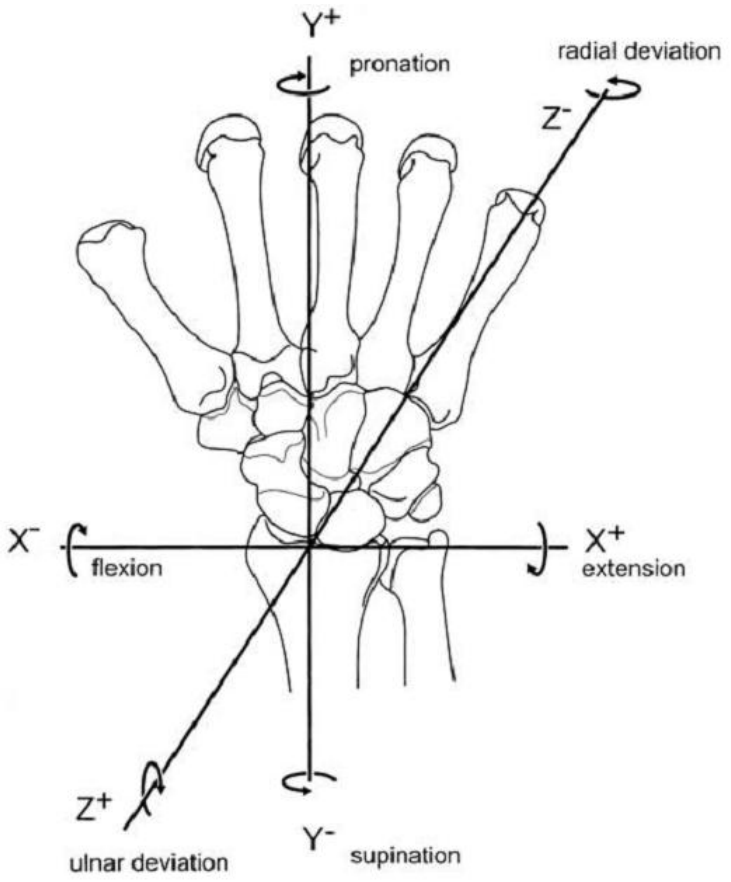

Figure 1.5. Showing the three primary axes about which carpal motion occurs. These are the flexion-extension axis (X) in the saggital plane, the pronation-supination axis (Y) in the transverse plane and the radial-ulnar deviation axis (Z) in the coronal plane. Reprinted from The Journal of Hand Surgery, Volume 28, Moojen, T. M., Snel, J. G., Ritt, M. J. P. F., Venema, H. W., Kauer, J. M. G., and Bos, K. E., In vivo analysis of carpal kinematics and comparative review of the literature, Pages 81-87, Copyright (2003), with permission from Elsevier.

The motions of the proximal and distal carpal rows also vary with direction of wrist motion. The bones of the distal carpal row interlock articularly and are tightly bound to each other and to the bases of the metacarpals (second and third) by intrinsic ligaments, such that there is hardly any intercarpal or distal carpal-metacarpal motion. In essence, the distal carpal row bones behave as a functional unit with the metacarpals (motor attachments) to transfer motion (direction and magnitude) and load [6, 9, 13]. In contrast there is more relative motion between the bones of the proximal carpal row to facilitate range of motion and stability [6, 13]. In flexion, both the

proximal and distal carpal rows undergo flexion [6, 15]. Within the proximal carpal row, scaphoid and lunate contributions to flexion are 69% and 51%, respectively [5, 16, 17]. Similarly in extension, both the proximal and distal carpal rows undergo extension [6, 15]. Within the proximal carpal row, scaphoid and lunate contributions to extension are 83 – 86% and 45 – 48%, respectively [5, 16, 17]. There is also intercarpal rotation between the scaphoid and lunate during FEM (13° and 21° in-plane motion in flexion and extension, respectively) [5, 16, 17]. In extension the scaphoid tends to supinate while the lunate tends to pronate causing a palmar separation [6]. In flexion the scaphoid tends to pronate while the lunate tends to supinate [6]. Proximal and distal carpal row motion is more complex in RUD and a reciprocal pattern is observed. In radial deviation, the distal row moves radially [4, 6] combined with extension and supination [7], while the proximal row moves ulnarly and also flexes (20°) [4-6, 9, 15]. Within the proximal carpal row, scaphoid and lunate contributions to radial deviation are 29% and 25% respectively [5, 6, 16]. In ulnar deviation, the distal row moves ulnarly [4, 6] combined with flexion and pronation [7], while the proximal row moves radially and also extends (20°) [4-6, 9, 15]. Within the proximal carpal row, scaphoid and lunate contributions to ulnar deviation are 49% and 54% respectively [5, 6, 16]. Though small, there is also intercarpal rotation between the scaphoid and lunate during RUD (1° in-plane motion for both radial and ulnar deviation) [5, 6, 16]. Scaphoid and lunate motion occurs predominantly in the saggital plane (of FEM) and there is minimal motion outside this plane for all wrist positions [13]. It is now believed that *in vivo* carpal bone motion is much more complex than what can be defined by the traditional axes of motion in the anatomic planes, and cannot be explained by any one theory. Rather than limiting motion to the three orthogonal planes, majority of functional activities such as combing, throwing, swinging an object etc., involve coupled motion in an oblique plane [7, 13, 18]. This is the plane of the dart-throwers motion (DTM), which occurs from extension-radial deviation to flexion-ulnar deviation. The midcarpal joint contributes most of the motion in this plane with no proximal carpal row rotation [13]. This plane of motion is thought to provide more stability and agility, allowing one to maintain power during grip throughout the motion [13]. The scapholunate joint is believed to have a dorsal rotation axis, which becomes a factor as most carpal injuries are caused by hyperextension and intercarpal supination [14]. The position of neutral scaphoid and lunate rotation (zero flexion-extension rotation) lies along the DTM path

[13]. Thus the most natural and physiologically intended path of motion, least affects scapholunate stability.

Several theories have been used in literature to describe carpal motion and stability during normal joint function [1-3, 5, 6, 12-15, 19]. Traditionally different patterns have been used to categorize carpal bones having similar motion. The *row theory* divided the carpal bones into two independent rows; distal and proximal, where motion within rows was fixed (Destot, de Lange, Berger) [1, 3, 13, 14]. The rows were considered rigid and rotating about fixed axes with the scaphoid acting as a link between the two rows. Since there are no direct tendon attachments to the proximal carpal row, it was considered to behave as an intercalated segment between the distal row and radius, with its motion facilitated by the distal row articulations and ligamentous constraints (Landsmeer) [1, 13]. It was later thought that the bones of the distal row were tightly bound together and that the bones of the proximal row were more mobile but still moved together within the row (Ruby) [14]. The *ring theory* was a modification of the row theory where the radial and ulnar ends of the proximal and distal rows were connected by ligaments and articulations, thereby facilitating function (Lichtman) [1, 6, 14]. In radial deviation, the motion (dorsal sliding) of the trapezium and the trapezoid on the distal end of the scaphoid was thought to push the scaphoid into flexion. The lunate in turn would be pulled into flexion with the scaphoid through the SLIL. In ulnar deviation, the STT ligament would pull the scaphoid into extension and the opposite would happen. The *column theory* divided the carpal bones into three longitudinal columns; the radial stability column (trapezium, trapezoid, scaphoid and radius), the central flexion-extension column (capitate, lunate and radius) and the ulnar rotation column (hamate, triquetrum and ulnar articular disc) [Navarro] [1, 13-15]. This was later modified to include the trapezium, trapezoid and hamate in the central column (Taleisnik) [1, 13-15]. It was also proposed that the three longitudinal columns performed as a three-bar link system, with centers of rotation located at the radiocarpal and midcarpal levels and the proximal row bones functioning as intercalated segments in the three chains (Gilford, Fisk, Taleisnik) [2, 3, 12, 14, 19]. This arrangement is inherently unstable in compression, therefore, it was proposed that the oblique placement of the scaphoid provided stability to the capitate, lunate and radius links (central column) similar to a slider-crank mechanism (Linscheid) [3, 12]. Also, the shape and geometry of the proximal row was thought to play a role in stability, since it has no direct motor

control and behaves as an intercalated segment (Kauer) [1, 12]. The proximal joint surfaces of the scaphoid and lunate are unequally curved and this results in palmar separation of the two bones during extension, which is constrained by the SLIp. Also, the proximal poles of the scaphoid and lunate are wedge-shaped in the saggital plane but in opposite directions. Under load, the oblique orientation of the scaphoid causes it to flex. On the other hand the palmar wedge shape of the lunate causes it to extend thereby resisting scaphoid flexion. Normal interaction between these opposing motions was believed to provide proximal row stability. Another theory proposed that the helicoid articulation of the triquetrohamate joint, and not the wedge shape of the lunate, provided stability to the proximal row (Weber) [1, 5, 12]. Under axial compressive load, this unique articulating configuration would cause the triquetrum to extend thereby resisting scaphoid flexion (the lunate balanced between the two). It is now believed that no single theory is sufficient to explain carpal stability. Since the wrist is a complex joint with many articulations, a combination of four stabilizing mechanisms at the distal row, the midcarpal joint, the proximal row and the radiocarpal joint provide stability under load [12]. For instance, under axial compressive loading, the proximal row bones undergo different rotations (5.1° scaphoid, 4.2° lunate and 3.8° triquetrum) likely due to the different biomechanical properties of the constraining intrinsic ligaments (STT, SC, TC and TH) [12]. The intact SLIL and LTIL constrain these rotations and provide stability to the proximal row. The distal radius has a 14 – 23° ulnar tilt in the coronal plane [12, 15]. The radiocarpal joint is therefore easily stabilized in ulnar deviation. However in maximal grip (35° extension and slight ulnar deviation), the carpus tends to move ulnarly [12]. The palmar and dorsal radiocarpal ligaments contribute significantly to resist this ulnar-sliding to provide radiocarpal joint stability.

Carpal bone motion is dependent on wrist position during loading, direction of transferred forces and the geometry and orientation of the articulating surfaces. The ligaments constrain these motions and facilitate stability. The SLIL constrains scaphoid flexion and dorsal translation of the scaphoid proximal pole (SLId) to maintain normal radioscaphoid contact [12]. Disease or injury to any of these stabilizing mechanisms leads to carpal instability.

1.1.4. Overview of carpal injuries

Carpal injuries occur as a result of damage to osseous and ligamentous anatomy. The resultant damage observed on clinical scans can be categorized generally into pure dislocations, fractures or fracture-dislocations. These injuries are determined by the type of loading, the duration and magnitude of loading, hand position at initiation and the biomechanical properties of the anatomy involved. Hyperextension, ulnar deviation and intercarpal supination are believed to be the main pathomechanics leading to injury [20].

Pure dislocations occur as a result of damage to the extrinsic and intrinsic ligaments. This damage can occur due to progressive wear or more commonly, due to trauma [20, 21]. These include lunate dislocation and perilunate dislocation (scaphoid, capitate, triquetrum and lunate dislocations) [20]. Hyperextension and ulnar deviation causes disruption of the RSC, the STT and the RSL ligaments and intercarpal supination causes progressive palmar to dorsal disruption of the SLIL, resulting in scaphoid dislocation and rotation [20]. Progressive capitate, triquetrum and lunate dislocations occur with increased severity of ligamentous damage. Fractures occur as a result of trauma to the bones. These include scaphoid fractures, radial styloid fractures, palmar/dorsal intra-articular distal radius fractures (Barton's fracture), triquetral fractures and the less frequently occurring capitate fractures [20, 22]. The most common carpal injury is the scaphoid fracture (71.2%) followed by the triquetrum (20.4%) [20, 22]. Depending on the type of loading, scaphoid fractures occur at the waist (70 – 80%, in hyperextension propagating from palmar to dorsal), the proximal pole (in hyperextension) or the distal tuberosity (in compression) [20, 22]. Malunion can cause osteonecrosis of the fracture fragment (Preiser's disease) which may lead to progressive loosening of the ligaments [22]. Scaphoid fractures normally occur with the wrist loaded in 95 – 100° of extension [5]. Lesser extension usually results in distal radius fractures [Colles' fracture (fracture fragment extended) or Smith's fracture (fracture fragment flexed) in flexion] [5]. Fractures can also be associated with ligamentous damage, known as fracture dislocations. These include transscaphoid or transtriquetral perilunar fracture-dislocations [20]. Fracture to the lateral side of the distal radius is usually associated with scaphoid dislocation [22]. Scaphoid fractures are almost always accompanied by SLIL failure (partial tear to complete disruption) [20]. Damage to the carpal ligaments (traumatic disruption

or progressive laxity) as a result of fractures and dislocations can lead to carpal instability [12, 20, 22].

1.1.5. Classification of carpal instability

Changes in carpal alignment have been observed since the invention of the radiograph; however, carpal instabilities and post-traumatic deformities and their clinical significance have only recently (1972) been recognized [1, 13, 23, 24]. Carpal instabilities as a result of disease or injury cause changes in normal carpal alignment, that can lead to abnormal motion and load transfer through the carpus [12, 23, 24]. When functioning normally, the central column of the wrist (the radius, the lunate, the capitate and the third metacarpal) displays an almost collinear alignment. Changes in alignment to any of the individual links of more than 5 to 10°, indicate the possibility of instability [25]. Carpal instabilities have been classified into six categories. These categories explain the chronicity, constancy, etiology, location, directions and pattern leading to and following the instability [5, 7, 20, 23-27]. Descriptions of instabilities should present information in all these categories [25].

Based on the time between injury and diagnosis (chronicity), instabilities can be divided into *acute*, *subacute* or *chronic*. Acute is when less than one week passes and therefore has the maximum chance of healing. Subacute is between one and six weeks with some chance of healing, while chronic is greater than 6 weeks with little chance of healing without surgical repair or reconstruction.

Based on the severity of the injury (constancy), instabilities can be divided into *static*, *dynamic* or *predynamic*. Static is used to describe instabilities that are constant (reducible or irreducible) and can be observed on static radiographs (standard lateral and posteroanterior). Dynamic is used to describe instabilities that can only be observed on standard radiographs when a stress/load or motion is applied, which otherwise appear normal. Predynamic is when there is clinical evidence and symptoms of instability but the radiographs appear normal.

Carpal instabilities can also be categorized based on the cause (etiology). The most common cause is injury (*traumatic*) and instability can occur at the time of injury or later. The cause of instabilities can also be diseases such as rheumatoid, neurologic, Kienbock's [osteonecrosis of

the lunate], calcium pyrophosphate crystal deposition, infection or osteonecrosis of the capitate (*inflammatory*, *arthritis*); birth related (*congenital*); due to cancerous tissue growth (*neoplastic*); less commonly induced inadvertently by surgery (*iatrogenic*); or any other cause (*miscellaneous*) or *combinations* of causes.

Depending on the location, instabilities can be divided into *radiocarpal*, *midcarpal*, *intercarpal*, *carpometacarpal* or affecting *specific bones/ligaments*. These provide general information on where the abnormality can be found. Radiocarpal instabilities arise from individual or combinations of palmar, dorsal and ulnar dislocations or from fracture-dislocations such as Barton's and radial styloid fractures. Midcarpal instabilities arise from corresponding ligament attenuation or disruption. In rare instances, carpometacarpal instabilities arise from axial injury to the carpus such as axial-ulnar dislocation, axial-radial dislocation or both.

Instabilities can also be classified based on similar pathologies leading to deformity (direction). Instabilities can be caused by a translational shift of the carpal bones which are divided into *radial, ulnar, palmar, dorsal, proximal, distal* or *combinations* of these. Instabilities can also be *rotary* as a result of angular deformity observed by the flexion or extension of part or whole of the proximal carpal row. Disruption to its distal stabilizers will cause the scaphoid to flex. Further scapholunate diastasis due to SLIL tear (or secondary from disease such as Kienbock's), causes the scaphoid to collapse into a horizontal position perpendicular to the forearm long axis, known as rotary subluxation. Progressive disruption of the DIC and DRC ligaments and also the SLIL can lead to a deformity where the scaphoid collapses into flexion, along with extension of the lunate together with the triquetrum. This is known as *dorsal intercalated segment instability* (DISI). DISI also often occurs with nonunion or malunion of scaphoid fractures. Progressive disruption of the LTIL causes the triquetrum to extend, while the scaphoid and lunate collapse into flexion. This is known as *volar intercalated segment instability* (VISI). A more severe deformity occurs with significant global disruption of the palmar and dorsal extrinsic ligaments resulting in the carpus sliding down the ulnar slope of the distal radius. This is known as ulnar translocation.

Depending on the pattern, instabilities can be divided into *carpal instability dissociative* (CID), *carpal instability nondissociative* (CIND), *carpal instability complex* (CIC) or *carpal*

instability adaptive (CIA). CIA occurs as a result of the normal carpus adapting to malalignments extrinsic to the wrist, as in the case of distal radius fracture malunion. CID occurs within the proximal or distal rows as a result of disruption to the intercarpal or interosseous ligaments (disruption of the SLIL or LTIL leading to scapholunate or lunotriquetral instabilities respectively), or distal row dissociation as a result of axial injury. Scaphoid fractures with SLIL tear without capsular injury are still classified as CID. CIND occurs between the proximal or distal rows as a result of disruption to the capsular ligaments as in the case of radiocarpal or midcarpal instabilities. CIC is a more severe pattern of injury occurring from a combination of CID and CIND such as perilunate instability. Perilunate instability begins with scapholunate instability due to SLIL disruption, followed by capitate dislocation, triquetral dislocation due to disruption of LTIL, and eventually lunate dislocation due to disruption of the palmar and dorsal radiocarpal ligaments. SLIL disruption with capsular injury, as in the case of distal radius fractures or transscaphoid perilunate dislocation, also fall under CIC.

1.2. Scapholunate ligament injury/scapholunate instability

Scapholunate instability is the most frequently occurring carpal instability [28-31]. Widening of the scapholunate interval as a result of injury, was first documented by Destot in 1926 [29, 32]. Scapholunate instability can clinically range from partial tear of the SLIL and minor loss of function, to complete tear and incapacitating pain. The term scapholunate dissociation has only recently (1972) been created to refer to the mechanical disruption of the scapholunate link [29]. Pain can be a result of the injured wrist not being able to withstand normal/physiologic loads [28, 29].

1.2.1. Pathophysiology and mechanism of injury

As mentioned earlier, the SLIL is the primary stabilizer of the scapholunate joint. The intact SLIp and SLId are critical for normal joint motion. However, the palmar extrinsic and intrinsic ligaments (RSC, RSL, STT, SC) and dorsal capsular ligaments (DRC, DIC) also contribute to secondary stability. It is also believed that SLIL disruption alone may not show considerable changes on plain radiographs [29, 31]. SLIp tear alone shows minimal widening of the scapholunate gap. Further tear of the SLId shows some widening of the scapholunate interval, but significant widening is observed after disruption to the RSC ligament [29]. Also SLIL

disruption alone does not produce static lunate malrotation, but further disruption of the DIC and DRC produces DISI deformity [7, 29]. Thus, the secondary stabilizers are important to facilitate SLIL function. These ligaments may suffer progressive damage after SLIL injury as a result of continued usage without treatment, finally causing failure and further instability [29, 30]. When scapholunate diastasis and scapholunate malalignment are visible on plain radiographs, this may indicate injury not only to the SLIL but also to the secondary stabilizers.

SLIL injury and scapholunate dissociation is the first stage of perilunate dislocation [20, 32]. The mechanism of injury is still unclear but is believed to occur as a result of an impact load to the base of the thenar/hypothenar region (fall on outstretched hand) in extension, ulnar deviation and supination, or during repetitive twisting motion (swinging a bat) [29, 30, 33]. This causes the capitate to drive proximally and palmarly, causing a palmar separation of the scaphoid and lunate (the scaphoid and lunate are forced radial-dorsal and ulnar-palmar respectively, in opposite directions). SLIL tears therefore initiate at the palmar section (SLIp) and progress dorsally [29]. Clinical examinations usually reveal early tears in the SLIp region [29, 34].

1.2.2. Diagnosis

The earlier the diagnosis, the better the chance will be for a successful surgical intervention. However in most cases, SLIL injury is not diagnosed until the latter stages when radiographs clearly show the presence of abnormality. Sometimes a patient will consult a physician for treatment following a sudden impact load or fall on the wrist. More often than not, patients forgo treatment because they feel the injury is not significant enough (dismissed as a sprain), or that the symptoms they experience initially are manageable and not worth the time, effort and money involving a physical examination. They may not remember when the injury happened, or the injury may happen over time due to minor repetitive trauma. Also, SLIL injury may happen secondary to a more severe extracarpal trauma such as a distal radius fracture and may go unnoticed on radiographs due to the more obvious abnormality [29, 30, 33, 35].

Though symptoms vary between patients, common complaints are pain or weakness during normal usage and sometimes swelling. Upon careful examination, other causes of radial sided wrist pain such as dorsal ganglion, dorsal wrist impaction syndrome, tendinitis, de Quervain's disease, scaphotrapezial arthritis, radioscaphoid arthritis, carpal tunnel syndrome, scaphoid

fracture and perilunate instability, can be eliminated. Another common complaint is a clicking or snapping feeling that causes pain and, rarely is loss of motion an issue initially, but can be later with progression [29, 30, 32, 33].

Upon physical examination, some tenderness or swelling may be noticed in the scapholunate area and pain localized to that area is cause to suspect the possibility of scapholunate dissociation. Watson's scaphoid shift test can be performed for further verification. This involves placing the injured hand first in ulnar deviation. Pressure is then applied to the scaphoid tuberosity and the hand is moved from ulnar to radial deviation. This prevents normal flexion of the scaphoid and with the presence of instability, causes the scaphoid proximal pole to dorsally sublux over the dorsal rim of the distal radius causing pain. When the pressure is released, the scaphoid jumps back into its radial fossa with a snap or clunk. A positive result may also occur due to other pathologies such as joint laxity, synovitis etc., hence the contralateral normal hand is used for additional verification by comparing pain levels (injured more painful) [29, 30, 33]. This test is not very specific and additional evaluation is required for more accurate diagnosis.

Radiographic evaluation involves at least the anteroposterior (AP) view (in full supination) and the lateral view (in neutral flexion/extension) [21, 29, 30, 32, 33, 36]. The AP view may show widening of the scapholunate gap known as scapholunate diastasis or the "Terry Thomas sign". The widening is more pronounced in the AP supinated view compared to the posteroanterior (PA) view in pronation. A gap of more than 2 mm indicates the presence of abnormality, and scapholunate dissociation is suspect if the gap is more than 3 mm. The "scaphoid ring sign" may also be visible in the AP view. This happens when the scaphoid collapses in flexion and the distal pole projection looks similar to a ring. In addition, a less than 7 mm decrease in distance between the distal and proximal poles (foreshortened scaphoid) indicates rotary subluxation. As a result, the lunate may appear trapezoid-shaped in extension. Other signs include disruption of Gilula's lines (c-shaped lines defined at the radiocarpal and midcarpal levels) and reduction in carpal height ratio (< 0.54). The lateral view may indicate rotary subluxation of the scaphoid, with abnormal flexion and extension of the scaphoid and lunate (radiolunate angle greater than 15°), respectively. In the lateral view, the angle between the long axes of the scaphoid and lunate varies from 30° to 60° (average 46°) in normal

alignment. Scapholunate dissociation is suspect with scapholunate angle more than 70°. Capitolunate angle more than 30° and scapholunate angle more than 80° suggests DISI deformity. Also, in the lateral view, the long axis of the scaphoid and a line tangent to the distal radius volar flare form a “V sign” in the presence of abnormality, which are otherwise almost parallel normally. If the static AP or lateral radiographs appear normal, additional stress radiographs may be required to identify a dynamic instability. This can either be an ulnar deviated PA view or a clenched fist AP view. A preexisting gap will be further widened indicating abnormality, but always must be compared to the contralateral normal wrist. Fluoroscopy and cineradiography may also be used to detect abnormal motion [21, 29, 30, 32, 33, 36].

Arthrographic evaluation can also be used to identify partial or complete SLIL tears, but is less commonly used due to low sensitivity and the problem of differentiating between degenerative and traumatic tears. While magnetic resonance imaging (MRI) can provide anatomical information, the quality (resolution, signal to noise ratio) of the images are usually not high enough to interpret the information accurately due to complex anatomy and small size of the ligament, compared to a larger joint such as the knee. MR arthrograms do not provide much further improvement. It is generally agreed that MRI is not very reliable for diagnosis [21, 29, 30, 33].

Arthroscopy is considered the gold standard for diagnosing SLIL injuries [21, 29, 30, 33]. This technique allows the examiner to visually inspect and accurately assess the extent of tearing, damage to the internal ligament structures and changes in scapholunate articular surfaces, which may not be as clear using the other methods. A grading system (Giessler) is used to categorize SLIL tears into four grades as follows. *Grade 1*: attenuation of SLIL from the radiocarpal side with no midcarpal step-off (incongruency); *Grade 2*: attenuation of SLIL from the radiocarpal side with a step-off between the scaphoid and the lunate from the midcarpal side, 1 mm probe can be placed in between; *Grade 3*: step-off can be seen from both the radiocarpal and midcarpal sides, 1 mm probe can be place into and freely rotated between the bones; *Grade 4*: complete SLIL disruption with gross instability, 2.7 mm probe can be passed between the gap [21, 29, 30, 33].

1.2.3. Clinical classification

Scapholunate instability can be classified into four stages, based on how severely the scapholunate joint is injured [29, 30]. The first stage is known as *predynamic instability,* which is the earliest stage of injury. This involves partial tear to the scapholunate membrane resulting in abnormal scapholunate motion with synovitis and subsequent pain. All radiographs will appear normal and Grade 1 Giessler pattern may be observed. Lack of treatment can lead to attenuation of the secondary stabilizers causing further SLIL disruption, which may progress to dynamic or static instability. The second stage is *dynamic instability*, which involves tear of the SLIp or SLId. Plain radiographs may still appear normal, but the scapholunate gap may increase when viewed on stress radiographs. Damage to the ligament may also be observed on an arthrogram. SLIL disruption follows Grade 2 or 3 Giessler pattern. The third stage is *static instability,* which involves additional damage to the secondary stabilizers. In this stage the deformity is fixed and appears on plain radiographs (scapholunate gap $\geq$ 3 mm, scapholunate angle > 70°). Grade 4 Giessler pattern is observed. This stage can also be subdivided as occurring with or without DISI deformity. Depending on the duration of the malalignment, static instability can either be reducible or irreducible. The final stage is *scapholunate advanced collapse* (SLAC), where continued use with altered mechanics as a result of scapholunate dissociation can cause progressive degenerative changes [29, 30].

1.2.4. Treatment

Since scapholunate dissociation is not often diagnosed in its early stages, treatment of the instability is an ongoing challenge, with not very consistent results [29, 32, 33]. The ideal procedure for treatment still remains elusive. Depending on the time from injury, scapholunate injuries are described as acute (2 to 4 weeks from injury), subacute (4 weeks to 6 months from injury) or chronic (more than 6 months from injury) [21, 29, 30, 33]. Due to the variation in injuries between patients, many factors other than time can influence the choice for the most appropriate patient-specific treatment.

A series of five questions have been proposed (Garcia-Elias) to address the treatment procedures for scapholunate dissociation [21, 29, 31, 37]. These questions are: “1) is the SLId partially or completely torn, 2) if complete, can the ligament be repaired and what is the healing

potential, 3) what is the status of the secondary scaphoid stabilizers (is radioscaphoid angle < 45°), 4) is the carpal malalignment reducible, and 5) are the cartilaginous surfaces normal". Depending on the answers, the following six stages of scapholunate dissociation have been proposed: "1) partial scapholunate injury, 2) complete SLIL tear with repairable SLId, 3) complete SLIL tear with nonrepairable SLId but a normally aligned scaphoid, 4) complete SLIL tear with nonrepairable tissue and a reducible rotary subluxation of the scaphoid, 5) complete SLIL tear with irreducible malalignment but no evidence of cartilage degeneration, and 6) complete SLIL tear with irreducible malalignment and cartilage degeneration [21, 29, 31, 37]". Therefore, the treatment approach can be more specific to the stage of injury. In general, if the deformity is not fixed, the treatment should try to restore mechanical relationship between the scaphoid and lunate, with necessary soft tissue augmentation. However, if the deformity is fixed there is less chance of soft tissue methods succeeding, hence procedures to salvage the joint may be required to minimize pain.

Patients with *stage 1* injury may have pain on the dorsal side of the scapholunate joint. Radiographs may appear normal and arthroscopy is normally used for diagnosis. In *stage 2*, the SLIL shows good potential for healing as a result of early diagnosis of SLIL tear or with avulsion of the SLIL from the bone, where the ligament is still intact and attached to the osteochondral fragment. Radiographs may still appear normal due to intact secondary stabilizers and arthroscopy is normally used for diagnosis. With *stage 3*, the SLIL tears in the middle and the ends usually shrink and degenerate within a week of injury, thus displaying poor potential for healing. Normal alignment is still observed due to intact secondary stabilizers. In *stage 4*, malalignment and DISI deformity are observed on radiographs due to additional disruption of the secondary stabilizers but because of the early stages of the deformity, reduction of the scapholunate gap is possible [29]. The following treatment methods have been applied to the first four stages.

With acute scapholunate dissociation, casting and immobilization (in full supination, ulnar deviation, and mid-extension) have been performed, but this technique is now considered unreliable because it is difficult to achieve sufficient immobility in the different positions of cast

fixation to facilitate healing. The positions either widen the gap (in extension) or further flex the scaphoid (in flexion) [21, 29, 33].

In the acute stages of injury, closed reduction with Kirschner wire (K-wire) fixation is also performed and has demonstrated good results [21, 29]. The scapholunate gap is reduced and held in place by K-wires till healing takes place without the need to surgically open the joint [21, 29].

Arthroscopic debridement (with pin reduction) is also performed in the acute stage for partial SLIL tears [21, 29, 31]. Torn fragments of the SLIL are thought to cause synovitis and irritation in the joint. The fragments are arthroscopically cleaned or removed to facilitate healing. This technique is found to be more effective in lowering symptoms for partial versus complete tears, and offers a minimally invasive treatment option for patients [21, 29, 31].

Electrothermal collagen shrinkage has also been performed in addition to arthroscopic debridement [29]. This technique uses heat (75°C) to reduce SLIL laxity by changing the mechanical properties of type I collagen and increasing stiffness. There is potential for risk as collagen damage occurs beyond 80°C, including damage to articular surfaces and neurovascular tissue due to their proximity to the ligament [29].

Open reduction, internal fixation and SLIL repair (direct repair) is also performed in the acute stage, if the secondary stabilizers appear intact and no degenerative changes are observed [21, 29, 31, 34, 38, 39]. With this technique, the effectiveness of scapholunate joint reduction can be directly visualized and the SLId can also be repaired. The joint is accessed from the dorsal side near the Lister's tubercle. K-wire joystick reduction of the joint is performed. Drill holes are made through the scaphoid proximal end. The SLIL and scaphoid are held together by sutures secured to the scaphoid waist. Additional pinning of the scaphoid and lunate is performed (6 to 8 weeks) to keep the joint immobile (including wrist splinting), while healing takes place. Only repair of the SLId can be performed and results show improvement in pain and grip strength with some loss of motion [21, 29, 31, 34, 38, 39].

Capsulodesis is used to augment SLIL repair and provide further stability [21, 29, 30, 40, 41]. This treatment is also used when there is insufficient ligament for direct repair or in the subacute stage where disruption to the secondary stabilizers is also present. A portion of the

dorsal capsule (Blatt/dorsal capsulodesis) or DIC ligament (DIC capsulodesis) is used to stabilize the scaphoid and prevent it from collapsing into flexion. Results show improvement in pain and function but with some loss of flexion motion [21, 29, 30, 40, 41].

Bone-tissue-bone grafts have also been performed with varying degrees of success in the subacute and chronic stages when the SLIL is insufficient for successful healing to take place [29-31, 42]. Various autografts are used to reestablish the scapholunate relationship. These include bone-retinaculum-bone grafts (extensor retinaculum) and bone-ligament-bone grafts (tarsometatarsal ligament, dorsal CH ligament, dorsal trapeziometacarpal ligament) [29-31, 42].

Tenodesis is another approach used in the subacute and chronic stages, where injury to the scapholunate joint is reducible [21, 37, 43-47]. This is used to augment fixation of the scapholunate interval. Several techniques have been used including four-bone ligament construction (a strip of the extensor carpi radialis brevis tendon passed through the capitate, scaphoid, lunate and radius), a strip of extensor carpi radialis longus tendon passed through the scaphoid, across the lunate and triquetrum (Linscheid), a strip of the flexor carpi radialis tendon passed through the distal scaphoid pole and attached to the distal radius (Brunelli reconstruction) or dorsal lunate (Van Den Abbeele) or the three-ligament tenodesis (Garcia-Elias) which is a further modification of the Brunelli, Linscheid and Van Den Abbeele techniques. The three-ligament tenodesis procedure involves accessing the joint from the dorsal side near the Lister's tubercle. A groove is made in the cortical dorsal distal lunate. A strip of the FCR tendon is passed through the scaphoid tuberosity along the region of the SLId and suture anchored into the lunate groove. It is then passed through the DRC ligament and sutured onto itself. Additional K-wire pinning (6 weeks) of the scapholunate and scaphocapitate joints is performed and the wrist is placed in a splint for another 4 weeks. This provides stability to both the proximal and distal scaphoid and results indicate lessened pain, improved grip strength and motion and decreased scapholunate gaps [21, 37, 43-47].

Less commonly, scaphoid and lunate reduction is performed using screws in the subacute stage. However this causes problems with scapholunate motion in RUD and the long-term effectiveness of this method remains a question [29].

Newer soft tissue reconstruction techniques have also been recently introduced to address the first four stages of injury. These involve minimally invasive arthroscopic repair of the volar section [48], minimally invasive arthroscopic repair of the dorsal section with dorsal capsuloplasty [49], minimally invasive arthroscopic bone-tendon-tenodesis ligamentoplasty (which aims to improve on the three-ligament tenodesis by reducing soft tissue trauma and providing more mobility postoperatively) [50], or combination of an extensor carpi radialis longus tenodesis and DIC capsulodesis [51].

Stage 5 of scapholunate dissociation occurs when the static deformity has been present for a while causing fibrosis, resulting in a fixed irreducible malalignment. In such instances, soft tissue techniques are highly likely to fail. Hence, limited carpal fusions are performed to reduce pain and deformity and preserve motion [21, 29, 52-54]. These techniques include scaphoid-trapezium-trapezoid (STT, triscaphe) arthrodesis, scaphocapitate arthrodesis, scapholunate arthrodesis and scapholunocapitate arthrodesis. Since the scaphoid and lunate have a tendency to separate, scapholunate arthrodesis has a higher rate of nonunion and is considered unreliable. Additional procedures such as radial styloidectomy, may be required to improve effectiveness (STT fusion). Overall, there is improvement in pain levels and function, while resulting in greater loss of motion [21, 29, 52-54].

With degenerative changes associated with *stage 6* of scapholunate dissociation, more extreme salvage procedures are required to minimize wrist pain but with considerable loss of motion [21, 29, 30, 55, 56]. These include four-corner (capitate, lunate, triquetrum and hamate) fusion with scaphoid excision (also known as the SLAC procedure or midcarpal arthrodesis) and proximal row carpectomy (PRC). Dorsal distal radius limited resection (SLAC procedure) and radial styloidectomy (PRC) may be required as well. Additional salvage procedures such as total wrist arthrodesis and total wrist arthroplasty are also performed as last resort options, but only after considering all associated factors (age, degree of pathology, occupation, physical demands etc.) [21, 29, 30, 55, 56].

Patients may also opt for conservative treatment as an alternative to surgery. Different options are available to aid the healing process. These include periodic immobilization, using braces that support the wrist during functional activity, nonsteroidal anti-inflammatory drugs

(NSAIDs), physical therapy (stretching and strength exercises) and gradual loading of the injured hand [33]. It is also believed that repetitive usage following injury will lead to progressive damage to the secondary stabilizers, causing further instability [29, 30, 33]. Scapholunate dissociation is usually diagnosed several weeks or months after injury, when pain becomes intolerable and patients start experiencing limited mobility. Therefore, conservative treatment is not often recommended [33]. The goal of surgery is to reduce the ensuing pain and deformity and to restore normal alignment and functional relationship. Though the mechanism is still unclear, scapholunate dissociation is known to progress to SLAC in its final stages and associated radiocarpal osteoarthritis [57-61].

1.3. Osteoarthritis and associated factors

Osteoarthritis (OA) is a degenerative joint disease that affects the middle aged and elderly population more than any other joint disease [62, 63]. Primary OA commonly occurs due to unknown causes and predominantly affects the elderly. On the other hand, secondary OA can be initiated by trauma/injury to a joint and this can affect anyone, especially from the younger active populace [62, 63]. OA is believed to affect approximately 10% of the world's population over 60 [62, 63]. Over 20 million Americans are estimated to suffer from OA, which accounts for 13.9% of the population over 25, and 33.6% over 65 [64]. The prevalence of radiographic OA is highest for the hand (7.3/100), and the prevalence of symptomatic OA of the hand (8/100) is second only to the knee (12.1/100) [65, 66]. Hand OA has the second highest age and sex-standardized incidence rate (100/100,000 person years) compared to the knee (240/100,000 person years) and hip (88/100,000 person years) for symptomatic OA [67]. Functional debilitating effects are commonly seen in the weight bearing joints (knee or hip), but with hand OA, people also often complain about considerable difficulty in grasping and even the inability to grasp in more severe cases. While figures are speculative, it is estimated that overall OA job-related economic losses range from $3 to $14 billion annually [62]. This is mainly due to the debilitating effects of the disease that impact quality of life and function, especially in the working class. There is no effective way to prevent or cure OA, and with the onset of OA, there is no generally accepted medical treatment to prevent the loss of cartilage [63].

Age is believed to be the primary risk factor for OA. The capacity of cartilage cells (chondrocytes) to repair and maintain a healthy joint is thought to diminish with age, thereby causing progressive deterioration of the articular surfaces [62, 63]. While normal regular use and physical activity aid normal joint health and function, excessive loading or repetitive loading that exceeds physiological limits can lead to joint degeneration [62, 63]. Disruption of normal joint function as a result of injury (intra-articular fractures, dislocations, ligament/capsule tears) can cause post-traumatic OA [62, 63]. The risk of post-traumatic OA maybe further increased with age [62]. It is important to understand how the risk of developing OA varies with injuries to different joints (the wrist, for instance); how the risk of developing OA varies with the type of injury to a particular joint (SLIL injury, for instance); how long it takes to develop OA once a joint is injured and the rate and mechanism of progression after onset of OA. Insight into these areas may supplement our understanding of the relationship between joint injuries and OA.

The mechanism of post-traumatic OA is not well understood. It is hypothesized that injury to a joint may cause changes in positions and orientations of the various bones and articulations, which correspondingly alter normal load transfer through the joint. While there is still much controversy concerning the effects of SLIL tears on scapholunate motion, it is commonly accepted that disruption to the ligament can cause changes in the normal scapholunate relationship, leading to loss of alignment [14, 28, 57, 58, 68]. This is the beginning of scapholunate instability. With continued usage, there is further damage to the secondary stabilizers that leads to progressive instability, thereby causing further malalignment/deformity. As mentioned previously, apart from global motion of the proximal carpal row, the individual bones also move relative to each other within the row, the scaphoid being the most mobile. With its oblique orientation, scaphoid motion is constrained at both its proximal and distal ends by the primary (SLIL) and secondary stabilizers (RSC, STT, SC), respectively. Disruption of the SLIL causes the scaphoid to collapse into flexion (while the lunate extends more), and its mobility is further increased. Further disruption to its secondary stabilizers causes rotary subluxation of the scaphoid. These changes in alignment (positions and orientations) can lead to abnormal kinematics [68-71]. Loss of normal alignment and abnormal kinematics can lead to changes in load transfer through the joint. Cadaveric experiments have shown that under simulated normal conditions, 80 – 83% of the load is transferred from the wrist to the forearm through the

radiocarpal joint, and 17 – 20% through the ulnocarpal joint [5, 6]. Of the load transferred through the radiocarpal joint, 60% is transferred through the radioscaphoid joint and 40% percent through the radiolunate joint [5, 27, 72]. On average, only 20.6% of the radius articular surface is in contact with the scaphoid and lunate (scaphoid contact area being 1.47 times greater than lunate), and does not exceed 40% despite the magnitude of loading [5, 6, 27, 72]. The magnitude and location of contact vary with wrist position and direction of motion. Abnormal load transfer characteristics can lead to changes in articular surface contact locations and distributions. The scaphoid articular facet on the radius fossa is elliptical (triangular region of contact), while the lunate articular facet is spherical (quadrangular region of contact) [35, 73, 74]. Under normal conditions, the oblique scaphoid is congruent in its radius facet. With rotary subluxation of the scaphoid, the proximal articular surface looses it congruency with its radius facet and contact is shifted to the volar and dorsal rims of the distal radius [35, 73, 74]. This leads to a progressive pattern of degeneration known as SLAC. Degenerative changes do not appear to occur as a consequence of original insult to the joint (injury event), but rather due to abnormal changes in kinematics and contact locations that progressively occur following SLIL injury. As such, restoring kinematics and normal alignment may prevent the onset of degeneration.

About 95% of wrist degeneration occurs around the periscaphoid region [73, 74]. Of these, SLAC pattern of degeneration is the most common (55%), followed by triscaphe OA (26%) or a combination of the two (14%) [73, 74]. In other words, SLAC pattern of degeneration is the most common form of wrist OA [55, 56, 60, 61, 73, 74]. While the mechanism is not clearly understood, scapholunate advanced collapse follows a consistent, predictable pattern [61, 73-75]. Degenerative changes are first observed between the radius and scaphoid in the radial styloid region, which is the most radial portion of the distal radius articular surface (stage I). In stage II, the entire radioscaphoid joint is affected by OA. With further degeneration and scapholunate diastasis, the proximal capitate is driven between the scaphoid and lunate. Hence, with stage III along with radioscaphoid OA, degeneration of the midcarpal joint at the capitate-lunate interval is also observed. Due to its spherical fossa, the radiolunate articulation is thought to maintain its congruency even with instability [55, 61, 73, 74]. Therefore, degenerative changes are not often seen at the radiolunate interval. However, the entire radiocarpal joint can be affected eventually (pancarpal OA) with progressive perilunar instability [76].

Since scapholunate dissociation is not often diagnosed in its acute stages, but rather well into the injury stage, it is possible that degenerative changes, though not yet visible, may have already begun to take place (microscopic changes). Due to the different stages of injury and instability, there is still much controversy concerning the right choice of treatment, which is not easy to choose [37, 43]. The ideal timing of SLIL repair is not yet known [39]. It is also believed that the ideal treatment when the SLIL is irreparable, without the presence of OA, has not yet been determined [46]. For this stage of injury, Blatt dorsal capsulodesis is the most common treatment used in the US and Canada [46]. With evidence of degeneration, the choice of salvage procedures for treatment is more obvious. No matter what the surgical treatment used, the goal is to minimize/eliminate pain, correct the malalignment/deformity, restore normal function and halt the progression of OA [46, 75]. However, the outcome of surgery is less positive for static deformity compared to dynamic, and surgical effectiveness decreases with increasing severity of the stage of injury at the time of diagnosis [34]. Also, the results of SLIL repair vary with the type of occupational activities (strenuous vs. non-strenuous) performed postoperatively [39]. Hence, it is not uncommon to observe degenerative changes even after surgical intervention [34, 39, 43, 46, 53]. Even the more successful three-ligament tenodesis procedure has up to 20% failure rates [50]. Therefore, it is important to identify the mechanisms that cause these degenerative changes. Rates of degenerative changes are not uniform – they can remain unchanged, manifest intermittently over a long period or rapidly progress in a short amount of time [62]. During the time of degeneration, partial repair of the degenerated articular surface has been observed, indicating the possibility for treatment by identifying the biological and mechanical factors that facilitate restoration of the joint [62, 77]. Joint contact pressures and pressure distributions are considered to be important mechanical factors.

The relationship between joint contact pressures and OA is complex. It is accepted that the risk of OA is increased with increase in articular surface contact pressures [78-84]. However, the mechanism is unclear and the role played by joint contact pressures is still under debate. Excessive loading of the joint (as a result of obesity, strenuous physical activity, post-traumatic incongruity/deformity and dysplasia) is thought to increase the risk of OA [62, 63, 79, 85-88], but cartilage thickness and properties have also been shown to increase in areas exposed to higher contact pressures [78, 85, 89, 90]. Once the tissue begins to degrade, further loading is

thought to increase the rate at which OA progresses [85]. On the other hand, unloading the joint surface (joint distraction) has been shown to both cause degenerative changes (progressive thinning/atrophy) [77, 78, 80, 89-92], and also improve the health of degenerating cartilage [93]. There appears to be a connection between cartilage loading and tissue response to the mechanical stimulus [77, 78, 85, 87, 89, 90]. The impact of loading on degeneration may vary from the subchondral level to the articular surface (3D stresses), and also be influenced by the properties of the cells and the extra cellular matrix (anisotropy and biphasic nature) [62, 80, 84, 89]. With SLIL tears, changes in pressure distribution are observed following abnormal kinematics and load transfer through the radiocarpal joint [69]. Under simulated normal conditions, cadaveric experiments have shown peak contact pressures to be relatively low, averaging 3.17 MPa, and varying with wrist position [27]. With fixed position and static loading, an increase in contact pressure in the radioscaphoid joint has been observed after SLIL sectioning [69]. With SLIL sectioning under dynamic motion, a decrease in scaphoid contact and an increase in lunate contact was observed, with contact pressure shifting from the scaphoid to the lunate fossa [69]. With instability/deformity, a shift in the location of contact to regions of the articular surface that are not normally loaded (80% of the available surface) maybe a more critical factor, apart from an increase in peak contact pressures in the normal contact regions. It is possible there exists a range of contact pressures that are required to maintain physiological function, and that exceeding this limit maybe one of the factors that initiate the onset of OA. A tool to evaluate changes in contact pressure that occur *in vivo* may provide insight into the mechanism of post-traumatic OA. The ability to monitor the location of peak contact pressure and contact pressure distribution, may help predict tissue wear or the onset and progression of degradation.

1.4. The role of magnetic resonance imaging

Magnetic resonance imaging is an excellent 3D imaging modality that can be used to obtain qualitative and quantitative information, to evaluate the structure (anatomy/morphology) and function (physiology) of tissue. MRI allows for direct visualization of soft tissue, such as articular cartilage, non-invasively. However, in order to correctly differentiate between the various soft tissue morphologies, the MR images must have sufficient *signal/contrast-to-noise ratio* ([S/CNR] to delineate different interfaces and to minimize chemical shift artifacts), *spatial*

resolution (to precisely capture the geometry) and reasonable *image acquisition times* (to minimize motion artifacts and patient fatigue) [94].

MRI has been primarily used for diagnostic purposes in the wrist, especially with regards to identifying pathologies in their early stages of progression [95-100]. MRI has been used to evaluate ulnar-sided wrist pain (such as TFCC disorders/tears, ulnar impaction syndrome, distal radioulnar joint instability), nerve impaction syndromes (such as carpal tunnel syndrome, Guyon's canal syndrome), benign soft tissue masses (such as giant cell tumor, dorsal ganglion), osteonecrosis/avascular necrosis (such as Kienbock's disease, Preiser's disease), occult fractures (scaphoid, distal radius), carpal instabilities, tendinopathies (such as tendinitis, tenosynovitis, ruptures), synovial abnormalities (inflammation, edema, effusions), ligament abnormalities/tears and arthritis (rheumatoid, OA). Depending on the imaging sequence, the signal intensity varies between low and intermediate for the intact SLIL. With disruption, one can observe discontinuities/fragments within the ligament with higher signal intensity, morphological distortion of the ligament, or complete absence with synovial fluid in the ligament space [95, 96]. MRI is very useful for the early diagnosis of OA, as it is possible to characterize the progressive degrading of articular cartilage (increase in signal intensity from effusion, focal thinning, narrowing of joint space, to complete loss) [94, 95].

MRI has been used to evaluate morphological and biochemical changes in articular cartilage *in vivo*. Degenerative changes may already begin to occur at the microscopic level before any visible changes are present (partial/full-thickness focal defects). It may be possible to indentify the onset of degenerative changes by evaluating associated changes in proteoglycan (PG) and glycosaminoglycan (GAG) content, which alter normal physiology. This has been achieved through measurements such as T1 relaxation time in the presence of Gd-DTPA (T1[Gd]) also known as delayed gadolinium enhanced MRI of cartilage ([dGEMRIC] sensitive to PG content and GAG distribution) [101, 102], T2 relaxation times (sensitive to collagen integrity and orientation) [103], and T1rho (sensitive to bound water) [104]. However, these measures are not completely effective and do not provide any information about the biomechanical properties. With injury, cartilage may still have good structural and biochemical properties initially, which may suddenly change as a result of abnormal mechanics. Correlating structural and biochemical

changes with *in vivo* biomechanical properties, may provide useful insight into the pathology of OA.

MRI has been used to obtain *in vivo* 3D geometry for model construction. Computed tomography (CT) provides images with better contrast and higher resolution, however, there is the risk of radiation exposure and also the inability to directly acquire soft tissue information [94]. Bone and cartilage anatomy have been segmented from MRI images primarily to construct 3D models, especially for finite element analyses [105-110]. Studies involving these models have focused more on the lower extremity, where loading (force) or boundary (kinematics) conditions were acquired separately through experiments (subject-specific EMG or motion capture), or from pre-existing resources (standards or literature) [105, 107, 108]. Due to the relatively low contrast between the soft tissue interfaces, no fully automatic segmentation method is available and substantial manual work is required [106]. However, with techniques such as fat suppression (by fat saturation or water excitation), it is possible to improve contrast (especially at the subchondral level) and minimize chemical shift artifacts, which allows for semi-automated segmentation [94]. The technique to obtain model geometry has been further extended to also obtain direct *in vivo* contact area measurements from MRI scans. MRI scans of different joints have been acquired in various static or quasi-static positions or loading conditions. The effective contact areas (patellofemoral, tibiofemoral, for example) were obtained by segmenting regions of articular surface contact or by constructing models of the joint [111-115]. More advanced MRI techniques have also been used to acquire muscle geometry (diffusion tensor MRI) and moment arm data (dynamic MRI) [106]. Future advances in body or parallel imaging methods and pulse sequences may improve the process of acquiring model geometry [106].

MRI has been used to evaluate *in vivo* joint kinematics, mainly in the load bearing joints. As mentioned earlier, *in vivo* carpal kinematics is very complex (position and direction dependent). The majority of the wrist kinematic studies have been experimental studies involving invasive marker techniques [13, 14]. However, *in vitro* conditions may not accurately represent *in vivo* conditions and these studies do not consider the impact of disrupting the surrounding tissue by marker placement, or account for the effects of dynamic motor stabilization *in vivo* [13, 14]. *In*

vivo kinematics can also be acquired using surface markers and motion capture systems but this may not accurately represent internal motion, especially in the complex joints such as the wrist [106]. Recently, a CT-based markerless surface registration technique has been used to precisely measure 3D *in vivo* carpal kinematics, but radiation usage is still a limitation, even with quasi-static positioning and low-dosage protocols [13]. Markerless volume-based registration using MRI may not be as sensitive to errors from segmentation, and has been shown to have a similar/better accuracy compared to the surface registration techniques (mean translation error of 0.21 mm and rotation error of 1.29° compared to mean translation error of 0.8 mm and rotation error of 1.5° for CT-based surface registration), without the risk of exposure to radiation [13, 16, 116]. MRI, from images acquired at static or quasi-static positions (kinematic MRI) or loading conditions, has been frequently used to determine 3D wrist motion (scaphoid, lunate, capitate contributions to radiocarpal and midcarpal joint motion in FEM, RUD and DTM; triquetrum-hamate joint motion etc.) and also flexor tendon motion in the carpal tunnel [116-120]. Cine phase-contrast (cine-PC) MRI has also been used to determine motion in dynamic conditions [106]. Future advances, which include real-time MRI and rapid MRI techniques (ultrafast gradient recall echo [GRE], echo planar), have the potential to provide more accurate *in vivo* kinematics [99, 106]. MRI together with volume-based registration, may provide accurate 3D *in vivo* kinematics non-invasively, representative of actual normal bone motion and changes in motion from injury, in order to evaluate surgical treatments at different time points.

MRI has also been used to evaluate *in vivo* deformation of soft tissues. While, there is no non-invasive way to directly evaluate *in vivo* deformation of cartilage under dynamic motion/load, it is possible to quantify *in vivo* deformation based on images acquired at different static positions/loading conditions [121, 122]. Cartilage surfaces are segmented from images acquired before and after different positions and loading conditions, from which volumetric (surface area, thickness) measurements are made (quantitative MRI). These measures have been used to quantify, for example, patellar, tibiofemoral cartilage thinning/deformation with static and dynamic loading, or with age [94, 121-125]. However, the measures determined from dynamic conditions, do not represent deformation during the loading activity, but rather residual deformation after. This method is also very sensitive to segmentation errors (from multiple sets of images) and it is not easy extrapolate surface strains, contact stresses and contact force data

from the deformation maps. Cine-PC MRI, along with other advanced techniques such as MR tagging and MRI with displacement encoding with stimulated echoes (DENSE), have also been used to image muscle deformation and directly visualize and quantify myocardial tissue deformation/strains [106]. Future advances, such as ultra short echo-time (UTE) pulse sequences and MR elastography, may improve signal from structures with short transverse (T2) relaxation times (such as cartilage), and provide information on mechanical response [106].

While MRI is limited in its diagnostic value for wrist ligament injuries, it can be very useful to obtain *in vivo* data such as geometry and kinematics. The data can be incorporated in computational models to provide insight into changes in joint contact mechanics that may trigger the onset of OA. This combination may also be very useful to provide clinically relevant information that can help evaluate different surgical treatments.

1.5. Modeling approach

Computational modeling is a very helpful tool to evaluate joint abnormalities and simulate the outcomes of surgical treatments. Models can be used to estimate parameters, which are otherwise difficult to obtain experimentally (dynamic muscle forces for instance). Currently, computational modeling is the only technique by which prediction of joint contact mechanics may be possible, noninvasively [126]. However, many models are generic, with input parameters derived from a wide range of resources (experiments, standards, literature) [106]. These models are limited in their applicability for patient-specific treatments and therefore highlight the importance of subject-specific results.

Several cadaveric experiments have been performed to evaluate normal carpal joint mechanics. Contact areas, contact forces, contact pressures and pressure distributions have been measured using sensors inserted into the joint space under different positions and/or loading conditions [5, 6, 27, 72]. Several cadaveric experiments have also been used to investigate how diseases (such as Kienbock's) and injuries such as carpal instabilities (SLIL injury/scapholunate instability and progressive perilunate instability, DISI, VISI, ulnar translocation), fractures (scaphoid proximal pole, ulnar styloid) and fracture malunions (distal radius), alter normal joint mechanics and the biomechanical results of corresponding surgical treatments (limited intercarpal fusions [SC, STT, CH, scaphoid nonunion limited fusion], implant arthroplasties

[silastic scaphoid implant], joint leveling procedures [radial shortening, ulnar lengthening], etc) [69, 72, 127]. However, as mentioned previously, loading conditions and mechanisms are different *in vivo*. *In vivo* conditions are much more complex and cadaveric experiments may not accurately represent these conditions (for instance soft tissue interactions and dynamic motor stability). The magnitude and direction of loading vary with condition (static/dynamic), and also with the position and direction of wrist motion. It has been determined that actual forces transferred from the metacarpals to the distal carpal row, may exceed ten times the applied finger force [12]. While useful, cadaveric studies that evaluate surgical repair only provide immediate mechanics results, and cannot be used to assess prolonged effects at future time points. They also do not account for the effects of tissue healing response.

The majority of *in vivo* wrist studies have focused on carpal bone kinematics. These studies have investigated normal carpal bone positions and orientations during different functional activities, and how normal kinematics are adversely affected by SLIL injury [13, 14, 16-18]. Some *in vivo* wrist biomechanics studies have looked at contact forces and stress on the median nerve resulting from carpal tunnel syndrome [118, 128]. Most of the *in vivo* studies involving SLIL repair, have focused only on the visual or functional outcome of surgeries used to treat the different stages of injury (predynamic, dynamic, static or SLAC). These studies have compared visual/functional data between pre and post surgical repair and also to the normal hand, to assess the effectiveness of the surgery. Improvements in pain level (visual analogue scale), function scores (disabilities of the arm, shoulder and hand [DASH] questionnaire), grip strength (pinch, grasp), range of motion (FEM, RUD), bone angles/height, scapholunate gap and patient satisfaction (have the same surgery again or not) have been used to determine a positive or a negative outcome of treatment [34, 37-41, 52, 53, 55, 56]. As mentioned previously, contact pressures are an important mechanical factor associated with OA risk. Hence, it may be more clinically relevant to compare *in vivo* contact pressures and other contact parameters before and after surgery, to evaluate the different surgical procedures. Most of the modeling studies investigating normal, injured and postoperative *in vivo* joint mechanics have focused on the lower extremity. These studies have used patient-specific model geometries to simulate ACL injury, patellofemoral joint mechanics and the Maquet procedure, tibial tuberosity transfers, total knee arthroplasty, tibio-menisco-femoral contact behavior with variations in kinematics, hip

implant design, femoral osteotomies and various other orthopedic procedures [79, 106, 108, 110, 129, 130]. Most of the computer simulation joint mechanics studies of the wrist have been cadaveric studies (normal radiocarpal mechanics during simulated grasp, effects of injuries [intra-articular distal radius fracture and Colles' fracture], and surgical treatments [CH, SC, STT fusions for Kienbock's disease and four-corner arthrodesis], etc) [131-136], with only a few *in vivo* studies [137-142]. The *in vivo* wrist joint mechanics studies have investigated normal mechanics (radiocarpal mechanics during active grasp [142], radiocarpal and midcarpal mechanics in maximal extension [141], load transmission through the neutral wrist during static loading [139]) and simulations of some injuries and treatments (scaphoid fracture [140] and scaphoid nonunion surgery; such as screw reduction [138] and distal fragment resection [137]), but there does not appear to be any prior modeling work on the *in vivo* effects of SLIL injury/repair.

The common general approach to musculoskeletal modeling involves acquiring model geometry using CT or MR images, from which surface or volume meshes are generated [106, 108]. If models are constructed from CT images for joint contact analyses, then alternate methods may be required to obtain/define cartilage geometry/surfaces. These include using additional contrast agents or separate MRI scans to visualize cartilage anatomy, projecting cartilage surfaces from the bone surfaces (to a specified thickness or to half the joint space), or replacing cartilage with a mechanical equivalent (compression springs). Kinematics are acquired separately using motion capture systems or by matching/registering bone models to dynamic images acquired from biplanar fluoroscopy, and muscle forces are acquired using EMG. These are input into the model to obtain joint kinematics and joint reaction forces. The kinematics and force outputs from the model are implemented in a finite element model to determine contact stresses on the articular surface, or even volumetric stresses and strains.

Finite element (FE) modeling and rigid body spring modeling (RBSM) are commonly used for joint contact analyses. Computer models need to be validated with experimental studies to ensure sufficient accuracy of the model results [126, 129]. RBSM has been used to evaluate joint contact forces and ligament tension [107, 135, 137, 141, 143]. In this method, bones are modeled as rigid, while ligaments and cartilage are modeled as tensile and compressive springs,

respectively. Joint reaction forces are determined from the stiffness and deformation of the springs when equilibrium is reached, upon application of a known external load. While this technique is computationally efficient compared to FE modeling, the major drawback is replacing the actual articular surface with discrete springs [135, 143].

Combining MRI with modeling may prove to be a useful tool to determine *in vivo* joint mechanics during functional loading, and this method has not been extensively used. MRI is believed to be the best technique to obtain subject-specific geometries [108]. MRI can be used to obtain bone and cartilage geometry simultaneously within the same coordinate system, thus eliminating the need for coordinate system registration and transformation when acquiring geometries from different imaging modalities. Also, MRI can be used to obtain kinematics non-invasively from scans acquired during functional loading. Surface contact modeling is very useful to determine contact parameters from interpenetration of rigid bodies based on a contact rule [130, 136, 138, 144, 145]. However, there are limited studies that combined MRI with surface contact modeling for joint contact analyses. MRI-based surface contact modeling has been shown to be very useful to determine contact parameters in the wrist [133, 134, 142, 146]. This technique has been sufficiently validated with experimental studies for models constructed from research (9.4T) [133, 134] and clinical (3T) [146] MRI scanners. Displacement driven contact mechanics data (contact areas, contact forces, peak contact pressures and pressures), were determined using a contact algorithm that defined contact force as linearly proportional to strain. These studies showed that contact area and contact force outputs from model simulations were reliable, but there was more variability in mean and peak contact pressure data. To evaluate changes in joint mechanics as a result of injury/surgical intervention, it may be sufficient to look at surface contact mechanics data. Hence, MRI-based surface contact modeling has the potential to provide clinically relevant data in a relatively simple and computationally efficient manner, without the need for complex nonlinear analyses. Since the models are displacement controlled, there are no a priori force assumptions, thereby making the technique more accurate and reliable. Also with this technique, model geometries and boundary conditions are already available, and therefore can be directly implemented in an FE model, without the need for additional modeling steps.

FE modeling is the most common and accurate technique to obtain joint contact stresses [108]. This involves discretization of a complex system into finite elements and analyzing the behavior of the individual elements to approximate the response of the entire system. The process involves generating FE meshes of the model, defining geometric and material properties, specifying loading and boundary conditions, and solving a system of matrix equations for prescribed interactions to obtain displacements, stresses and strains throughout the model. Studies have used linear (4 node)/quadratic (10 node) tetrahedral or linear (8 node)/quadratic (20 node) hexahedral (brick) elements to generate bone and cartilage meshes [79, 110, 126]. Cartilage is usually modeled as a deformable, homogeneous, linear elastic, isotropic solid [79, 107-110]. If time (creep, stress relaxation) and loading (hysteresis, strain-rate) are factors that need to be considered (as in the case of dynamic motion), then cartilage is usually modeled as viscoelastic or hyperelastic [126], which are accurate representations of its material properties. Initially, the compressive loads on the articular surfaces are supported by the fluid pressure from the PG bound water within the cartilage. With fluid efflux and matrix compaction, the cartilage begins to deform. Fluid redistribution occurs and when equilibrium is reached (hydrostatic fluid pressure approaches zero, no fluid flow), the loads are borne entirely by the extra cellular matrix (PG-collagen) [121, 122]. Hence, the poroelastic or biphasic nature of cartilage has also been taken into account for more detailed analyses of cartilage behavior [89, 108]. Cartilage is considered incompressible (interstitial fluid) and functions to transfer loads evenly through the joint and allows joint motion with minimal friction [121, 122]. Therefore, frictionless interaction is commonly assumed between articular surfaces. Static or quasi-static analyses are often performed to determine joint contact stresses [108]. These are obtained by solving a set of nonlinear equations iteratively under static equilibrium for each time step, till criteria for convergence are met. To obtain reliable output from the models, it has to be ensured that the governing equations are performing as intended (code verification), and that the numerical solution from these equations is consistent (calculation verification) [107, 129]. When using commercial software, code verification is achieved by discarding results of iterations where discontinuities arise, not relaxing the convergence criteria (force residuals, displacement corrections), and only accepting equilibrium iteration results that have converged for all the analyses steps [129]. Calculation verification is performed by mesh convergence studies to

minimize discretization errors [129]. Converged results are typically accepted after a change of less than 5% percent is observed (solution asymptotes) in output parameters, after progressive mesh refinement [126, 129]. Validation studies are performed to ensure that the governing equations accurately represent the physical problem [126, 129, 147]. Sensitivity studies are also performed to evaluate the influence of geometry, material properties and boundary conditions to match results obtained from experiments under similar conditions, and thus improve model fidelity [126, 129]. FE modeling can be used to determine stress and strain distribution within cartilage, which is useful to understand effects of *in vivo* loading during functional activity. This may provide further insight into the mechanism of degradation, by understanding how functional integrity is compromised by breakdown within the tissue. This data may also be useful for tissue engineering applications, by providing information on the functional stresses that cultured/transplanted tissue may experience *in situ*. However, generating a quality FE model and solving the complex nonlinear contact problem is difficult and time consuming. Even performing a more computationally efficient rigid body FE analysis, requires considerable time to generate geometry with good mesh quality metrics [148].

1.6. References

1. Dobyns, J.H. and R.L. Linscheid, *A short history of the wrist joint.* Hand clinics, 1997. **13**(1): p. 1-12.
2. Kauer, J.M., *Functional anatomy of the wrist.* Clinical orthopaedics and related research, 1980(149): p. 9-20.
3. Kauer, J.M. and A. de Lange, *The carpal joint. Anatomy and function.* Hand clinics, 1987. **3**(1): p. 23-9.
4. Stuchin, S.A., *Wrist anatomy.* Hand clinics, 1992. **8**(4): p. 603-9.
5. Ruby, L.K., *Wrist biomechanics.* Instructional course lectures, 1992. **41**: p. 25-32.
6. Berger, R.A., *The anatomy and basic biomechanics of the wrist joint.* Journal of hand therapy, 1996. **9**(2): p. 84-93.
7. Kijima, Y. and S.F. Viegas, *Wrist anatomy and biomechanics.* Journal of Hand Surgery. American Volume, 2009. **34**(8): p. 1555-63.
8. Berger, R.A., *The ligaments of the wrist. A current overview of anatomy with considerations of their potential functions.* Hand clinics, 1997. **13**(1): p. 63-82.
9. Mayfield, J.K., R.P. Johnson, and R.F. Kilcoyne, *The ligaments of the human wrist and their functional significance.* The Anatomical record, 1976. **186**(3): p. 417-28.
10. Sokolow, C., *Anatomy and histology of the scapholunate ligament.* Hand clinics, 2001. **17**(1): p. 77.
11. Berger, R.A., *The gross and histologic anatomy of the scapholunate interosseous ligament.* The Journal of Hand Surgery, 1996. **21**(2): p. 170-178.
12. Garcia-Elias, M., *Kinetic analysis of carpal stability during grip.* Hand clinics, 1997. **13**(1): p. 151-8.
13. Gardner, M.J., J.J. Crisco, and S.W. Wolfe, *Carpal kinematics.* Hand clinics, 2006. **22**(4): p. 413-20.
14. Crisco, J.J., et al., *Advances in the in vivo measurement of normal and abnormal carpal kinematics.* The Orthopedic clinics of North America, 2001. **32**(2): p. 219-31.
15. Linscheid, R.L., *Kinematic considerations of the wrist.* Clinical orthopaedics and related research, 1986(202): p. 27-39.

16. Moojen, T.M., et al., *In vivo analysis of carpal kinematics and comparative review of the literature.* The Journal of Hand Surgery, 2003. **28**(1): p. 81-87.
17. Wolfe, S.W., C. Neu, and J.J. Crisco, *In vivo scaphoid, lunate, and capitate kinematics in flexion and in extension.* The Journal of Hand Surgery, 2000. **25**(5): p. 860-869.
18. Crisco, J.J., et al., *In vivo radiocarpal kinematics and the dart thrower's motion.* Journal of Bone & Joint Surgery, American Volume, 2005. **87**(12): p. 2729-2740.
19. Kauer, J.M., *The mechanism of the carpal joint.* Clinical orthopaedics and related research, 1986(202): p. 16-26.
20. Mayfield, J.K., *Mechanism of carpal injuries.* Clinical orthopaedics and related research, 1980(149): p. 45-54.
21. Tanaka, T., *Ligamentous injuries of the wrist.* Seminars in musculoskeletal radiology, 2008. **12**(4): p. 359.
22. Fisk, G.R., *An overview of injuries of the wrist.* Clinical orthopaedics and related research, 1980(149): p. 137-44.
23. Taleisnik, J., *Classification of carpal instability.* Bulletin of the Hospital for Joint Diseases Orthopaedic Institute, 1984. **44**(2): p. 511.
24. Taleisnik, J., *Post-traumatic carpal instability.* Clinical orthopaedics and related research, 1980(149): p. 73-82.
25. Larsen, C.F., et al., *Analysis of carpal instability: I. Description of the scheme.* Journal of Hand Surgery. American Volume, 1995. **20**(5): p. 757-764.
26. Watson, H.K. and D.M. Black, *Instabilities of the wrist.* Hand clinics, 1987. **3**(1): p. 103-11.
27. Patterson, R. and S.F. Viegas, *Biomechanics of the wrist.* Journal of hand therapy, 1995. **8**(2): p. 97-105.
28. Cohen, M.S., *Ligamentous injuries of the wrist in the athlete.* Clinics in sports medicine, 1998. **17**(3): p. 533-52.
29. Manuel, J. and S.L. Moran, *The diagnosis and treatment of scapholunate instability.* Hand clinics, 2010. **26**(1): p. 129-44.
30. Walsh, J.J., *Current status of scapholunate interosseous ligament injuries.* Journal of the American Academy of Orthopaedic Surgeons, 2002. **10**(1): p. 32.

31. Kuo, C.E. and S.W. Wolfe, *Scapholunate Instability: Current Concepts in Diagnosis and Management.* Journal of Hand Surgery. American Volume, 2008. **33**(6): p. 998-1013.
32. Linscheid, R.L., *Scapholunate ligamentous instabilities (dissociations, subdislocations, dislocations).* Annales de chirurgie de la main, 1984. **3**(4): p. 323.
33. Atkinson, L.S., *Scapholunate dissociation.* American family physician, 1994. **49**(8): p. 1845-50.
34. Saffar, P., C. Sokolow, and L. Duclos, *Soft tissue stabilization in the management of chronic scapholunate instability without osteoarthritis. A 15-year series.* Acta orthopaedica belgica, 1999. **65**(4): p. 424-33.
35. Watson, H.K., J. Weinzweig, and J. Zeppieri, *The natural progression of scaphoid instability.* Hand clinics, 1997. **13**(1): p. 39-49.
36. Pliefke, J., et al., *Diagnostic accuracy of plain radiographs and cineradiography in diagnosing traumatic scapholunate dissociation.* Skeletal Radiology, 2008. **37**(2): p. 139-145.
37. Garcia-Elias, M., A.L. Lluch, and J.K. Stanley, *Three-Ligament Tenodesis for the Treatment of Scapholunate Dissociation: Indications and Surgical Technique.* Journal of Hand Surgery. American Volume, 2006. **31**(1): p. 125-134.
38. Lavernia, C.J., M.S. Cohen, and J. Taleisnik, *Treatment of scapholunate dissociation by ligamentous repair and capsulodesis.* The Journal of hand surgery (American ed.), 1992. **17**(2): p. 354-9.
39. Pomerance, J., *Outcome After Repair of the Scapholunate Interosseous Ligament and Dorsal Capsulodesis for Dynamic Scapholunate Instability Due to Trauma.* Journal of Hand Surgery. American Volume, 2006. **31**(8): p. 1380-1386.
40. Luchetti, R., et al., *Dorsal intercarpal ligament capsulodesis for predynamic and dynamic scapholunate instability.* The Journal of hand surgery, European volume, 2010. **35**(1): p. 32-7.
41. Muermans, S., L. De Smet, and H. Van Ransbeeck, *Blatt dorsal capsulodesis for scapholunate instability.* Acta orthopaedica belgica, 1999. **65**(4): p. 434-9.
42. Harvey, E.J., et al., *Bone-Tissue-Bone Repairs for Scapholunate Dissociation.* The Journal of Hand Surgery, 2007. **32**(2): p. 256-264.

43. Chabas, J.-F., et al., *Results of the Modified Brunelli Tenodesis for Treatment of Scapholunate Instability: A Retrospective Study of 19 Patients.* Journal of Hand Surgery. American Volume, 2008. **33**(9): p. 1469-1477.
44. Brunelli, G.A. and G.R. Brunelli, *A new surgical technique for carpal instability with scapholunate dissociation.* Surgical technology international, 1996. **5**: p. 370-4.
45. Links, A.C., et al., *Scapholunate Interosseous Ligament Reconstruction: Results With a Modified Brunelli Technique Versus Four-Bone Weave.* The Journal of Hand Surgery, 2008. **33**(6): p. 850-856.
46. Pollock, P.J., et al., *Radiographic Evaluation of the Modified Brunelli Technique Versus the Blatt Capsulodesis for Scapholunate Dissociation in a Cadaver Model.* Journal of Hand Surgery. American Volume, 2010. **35**(10): p. 1589-1598.
47. Talwalkar, S.C., et al., *Results of tri-ligament tenodesis: a modified Brunelli procedure in the management of scapholunate instability.* Journal of hand surgery, British volume, 2006. **31**(1): p. 110-7.
48. del Piñal, F., et al., *An All-Inside Technique for Arthroscopic Suturing of the Volar Scapholunate Ligament.* Journal of Hand Surgery. American Volume, 2011(0): p. (in press).
49. Mathoulin, C., N. Dauphin, and V. Sallen, *Arthroscopic dorsal capsuloplasty in chronic scapholunate ligament tears: a new procedure; preliminary report.* Chirurgie de la Main, 2011. **30**(3): p. 188-97.
50. Corella, F., et al., *Arthroscopic ligamentoplasty (bone-tendon-tenodesis). A new surgical technique for scapholunate instability: preliminary cadaver study.* Journal of Hand Surgery, European Volume, 2011. **36**(8): p. 682-9.
51. De Carli, P., et al., *Chronic scapholunate dissociation: ligament reconstruction combining a new extensor carpi radialis longus tenodesis and a dorsal intercarpal ligament capsulodesis.* Techniques in Hand and Upper Extremity Surgery, 2011. **15**(1): p. 6-11.
52. Chantelot, C., et al., *Étude rétrospective de 13 arthrodèses scaphocapitatum pour instabilité scapholunaire chronique.* Chirurgie de la Main, 2005. **24**(2): p. 79-83.

53. Fortin, P.T. and D.S. Louis, *Long-term follow-up of scaphoid-trapezium-trapezoid arthrodesis.* Journal of Hand Surgery. American Volume, 1993. **18**(4): p. 675-81.
54. Pettersson, K. and P. Wagnsjö, *Arthrodesis for chronic static scapholunate dissociation: a prospective study in 12 patients.* Scandinavian Journal of Plastic and Reconstructive Surgery and Hand Surgery, 2004. **38**(3): p. 166-171.
55. Vanhove, W., et al., *Proximal row carpectomy versus four-corner arthrodesis as a treatment for SLAC (scapholunate advanced collapse) wrist.* The Journal of hand surgery, European volume, 2008. **33**(2): p. 118-25.
56. Dacho, A., et al., *Long-term results of midcarpal arthrodesis in the treatment of scaphoid nonunion advanced collapse (SNAC-Wrist) and scapholunate advanced collapse (SLAC-Wrist).* Annals of plastic surgery, 2006. **56**(2): p. 139-44.
57. Hergenröeder, P.T., *Bilateral scapholunate dissociation with degenerative arthritis.* The Journal of hand surgery (American ed.), 1981. **6**(6): p. 620.
58. Ira, D., *Injury of the scapholunate interosseal ligament--scapholunate dissociation.* Časopis lékařů českých, 2006. **145**(6): p. 460.
59. Krimmer, H., *Post-traumatic carpal collapse (SLAC- and SNAC-wrist)--stage classification and therapeutic possibilities.* Handchirurgie, Mikrochirurgie, plastische Chirurgie, 1997. **29**(5): p. 228.
60. Roberts, C., et al., *The association of scapho-trapezio-trapezoid osteoarthrosis and scapholunate dissociation.* Hand Surgery, 2006. **11**(3): p. 135-141.
61. Watson, H.K., *The SLAC wrist: scapholunate advanced collapse pattern of degenerative arthritis.* The Journal of hand surgery (American ed.), 1984. **9**(3): p. 358.
62. Buckwalter, J.A., C. Saltzman, and T. Brown, *The impact of osteoarthritis: implications for research.* Clinical orthopaedics and related research, 2004(427 Suppl): p. S6-15.
63. Buckwalter, J.A. and J.A. Martin, *Osteoarthritis.* Advanced Drug Delivery Reviews, 2006. **58**(2): p. 150-167.
64. Lawrence, R.C., et al., *Estimates of the prevalence of arthritis and other rheumatic conditions in the United States: Part II.* Arthritis & Rheumatism, 2008. **58**(1): p. 26-35.
65. Dillon, C.F., et al., *Symptomatic Hand Osteoarthritis in the United States: Prevalence and Functional Impairment Estimates from the Third U.S. National Health and Nutrition*

Examination Survey, 1991-1994. American Journal of Physical Medicine & Rehabilitation, 2007. **86**(1): p. 12-21.

66. Dillon, C.F., et al., *Prevalence of knee osteoarthritis in the United States: arthritis data from the Third National Health and Nutrition Examination Survey 1991-94.* Journal of rheumatology, 2006. **33**(11): p. 2271-9.
67. Oliveria, S.A., et al., *Incidence of symptomatic hand, hip, and knee osteoarthritis among patients in a health maintenance organization.* Arthritis and rheumatism, 1995. **38**(8): p. 1134-41.
68. Ruby, L.K., et al., *The effect of scapholunate ligament section on scapholunate motion.* Journal of Hand Surgery. American Volume, 1987. **12**(5 Pt 1): p. 767-71.
69. Short, W.H., et al., *A dynamic biomechanical study of scapholunate ligament sectioning.* Journal of Hand Surgery. American Volume, 1995. **20**(6): p. 986-999.
70. Short, W.H., et al., *Biomechanical evaluation of ligamentous stabilizers of the scaphoid and lunate.* The Journal of Hand Surgery, 2002. **27**(6): p. 991-1002.
71. Werner, F.W., W.H. Short, and J.K. Green, *Changes in Patterns of Scaphoid and Lunate Motion During Functional Arcs of Wrist Motion Induced by Ligament Division.* The Journal of Hand Surgery, 2005. **30**(6): p. 1156-1160.
72. Viegas, S.F. and R.M. Patterson, *Load mechanics of the wrist.* Hand clinics, 1997. **13**(1): p. 109-28.
73. Watson, H.K. and L.H. Brenner, *Degenerative disorders of the wrist.* Journal of Hand Surgery. American Volume, 1985. **10**(6 Pt 2): p. 1002-6.
74. Watson, H.K. and J. Ryu, *Evolution of arthritis of the wrist.* Clinical orthopaedics and related research, 1986(202): p. 57-67.
75. Weiss, A.P., *Osteoarthritis of the wrist.* Instructional course lectures, 2004. **53**: p. 31-40.
76. Weiss, K.E. and C.M. Rodner, *Osteoarthritis of the Wrist.* Journal of Hand Surgery. American Volume, 2007. **32**(5): p. 725-746.
77. Engh, G.A. and O.D. Chrisman, *Experimental arthritis in rabbit knees: a study of relief of pressure on one tibial plateau in immature and mature rabbits.* Clinical orthopaedics and related research, 1977(125): p. 221-6.

78. Andriacchi, T.P., et al., *A Framework for the in Vivo Pathomechanics of Osteoarthritis at the Knee.* Annals of Biomedical Engineering, 2004. **32**(3): p. 447-457.
79. Andriacchi, T.P., et al., *Rotational changes at the knee after ACL injury cause cartilage thinning.* Clinical orthopaedics and related research, 2006. **442**: p. 39-44.
80. Hall, M.C., *Cartilage changes after experimental relief of contact in the knee joint of the mature rat.* Clinical orthopaedics and related research, 1969. **64**: p. 64-76.
81. MacDonald, P., et al., *A biomechanical analysis of joint contact forces in the posterior cruciate deficient knee.* Knee surgery, sports traumatology, arthroscopy, 1996. **3**(4): p. 252-5.
82. Seedhom, B.B., *Conditioning of cartilage during normal activities is an important factor in the development of osteoarthritis.* Rheumatology (Oxford), 2006. **45**(2): p. 146-9.
83. Shi, Q., et al., *Finite element analysis of pathogenesis of osteoarthritis in the first carpometacarpal joint.* Acta medica Okayama, 1995. **49**(1): p. 43-51.
84. Swann, A.C. and B.B. Seedhom, *The stiffness of normal articular cartilage and the predominant acting stress levels: implications for the aetiology of osteoarthrosis.* British journal of rheumatology, 1993. **32**(1): p. 16-25.
85. Andriacchi, T.P., S. Koo, and S.F. Scanlan, *Gait mechanics influence healthy cartilage morphology and osteoarthritis of the knee.* Journal of bone and joint surgery. American volume, 2009. **91 Suppl 1**: p. 95-101.
86. Maly, M.R., *Abnormal and cumulative loading in knee osteoarthritis.* Current opinion in rheumatology, 2008. **20**(5): p. 547-52.
87. Martin, J.A. and J.A. Buckwalter, *Post-traumatic osteoarthritis: the role of stress induced chondrocyte damage.* Biorheology (Oxford), 2006. **43**(3-4): p. 517-21.
88. Wu, J.Z., W. Herzog, and M. Epstein, *Joint contact mechanics in the early stages of osteoarthritis.* Medical Engineering & Physics, 2000. **22**(1): p. 1-12.
89. Carter, D.R., et al., *The mechanobiology of articular cartilage development and degeneration.* Clinical orthopaedics and related research, 2004(427 Suppl): p. S69-77.
90. Chaudhari, A.M., et al., *Knee kinematics, cartilage morphology, and osteoarthritis after ACL injury.* Medicine and science in sports and exercise, 2008. **40**(2): p. 215-22.

91. Herzog, W., A. Clark, and D. Longino, *Joint mechanics in osteoarthritis.* Novartis Foundation symposium, 2004. **260**: p. 79-95; discussion 95-9, 100-4, 277-9.
92. Vanwanseele, B., et al., *Knee cartilage of spinal cord–injured patients displays progressive thinning in the absence of normal joint loading and movement.* Arthritis & Rheumatism, 2002. **46**(8): p. 2073-2078.
93. Van Valburg, A.A., et al., *Joint distraction in treatment of osteoarthritis (II): effects on cartilage in a canine model.* Osteoarthritis and Cartilage, 2000. **8**(1): p. 1-8.
94. Eckstein, F., et al., *Magnetic resonance imaging (MRI) of articular cartilage in knee osteoarthritis (OA): morphological assessment.* Osteoarthritis and Cartilage, 2006. **14**(Supplement 1): p. 46-75.
95. DiMarcangelo, M.T. and P.A. Smith, *Use of magnetic resonance imaging to diagnose common wrist disorders.* The Journal of the American Osteopathic Association, 2000. **100**(4): p. 228-31.
96. Brahme, S.K. and D. Resnick, *Magnetic resonance imaging of the wrist.* Rheumatic diseases clinics of North America, 1991. **17**(3): p. 721-39.
97. Pretorius, E.S., R.E. Epstein, and M.K. Dalinka, *MR imaging of the wrist.* The Radiologic clinics of North America, 1997. **35**(1): p. 145-61.
98. Steinbach, L.S. and D.K. Smith, *MRI of the wrist.* Clinical Imaging, 2000. **24**(5): p. 298-322.
99. Zlatkin, M.B. and T. Greenan, *Magnetic resonance imaging of the wrist.* Magnetic resonance quarterly, 1992. **8**(2): p. 65-96.
100. Siegel, S., L.M. White, and S. Brahme, *Magnetic resonance imaging of the musculoskeletal system. Part 5. The wrist.* Clinical orthopaedics and related research, 1996(332): p. 281-300.
101. Roos, E.M. and L. Dahlberg, *Positive effects of moderate exercise on glycosaminoglycan content in knee cartilage: A four-month, randomized, controlled trial in patients at risk of osteoarthritis.* Arthritis & Rheumatism, 2005. **52**(11): p. 3507-3514.
102. McAlindon, T.E., et al., *Change in knee osteoarthritis cartilage detected by delayed gadolinium enhanced magnetic resonance imaging following treatment with collagen*

hydrolysate: a pilot randomized controlled trial. Osteoarthritis and Cartilage, 2011. **19**(4): p. 399-405.

103. Stehling, C., et al., *Patellar Cartilage: T2 Values and Morphologic Abnormalities at 3.0-T MR Imaging in Relation to Physical Activity in Asymptomatic Subjects from the Osteoarthritis Initiative1.* Radiology, 2010. **254**(2): p. 509-520.
104. Souza, R.B., et al., *The effects of acute loading on T1rho and T2 relaxation times of tibiofemoral articular cartilage.* Osteoarthritis and Cartilage, 2010. **18**(12): p. 1557-1563.
105. Akbarshahi, M., et al., *Non-invasive assessment of soft-tissue artifact and its effect on knee joint kinematics during functional activity.* Journal of biomechanics, 2010. **43**(7): p. 1292-301.
106. Blemker, S.S., et al., *Image-based musculoskeletal modeling: Applications, advances, and future opportunities.* Journal of Magnetic Resonance Imaging, 2007. **25**(2): p. 441-451.
107. Elias, J.J. and A.J. Cosgarea, *Computational modeling: an alternative approach for investigating patellofemoral mechanics.* Sports medicine and arthroscopy review, 2007. **15**(2): p. 89-94.
108. Fernandez, J.W. and M.G. Pandy, *Integrating modelling and experiments to assess dynamic musculoskeletal function in humans.* Experimental Physiology, 2006. **91**(2): p. 371-382.
109. Wawro, M. and M. Fathi-Torbaghan, *A parallel framework for the FE-based simulation of knee joint motion.* IEEE transactions on biomedical engineering, 2004. **51**(8): p. 1490-4.
110. Yao, J., et al., *Sensitivity of tibio-menisco-femoral joint contact behavior to variations in knee kinematics.* Journal of Biomechanics, 2008. **41**(2): p. 390-398.
111. Besier, T.F., et al., *Patellofemoral joint contact area increases with knee flexion and weight-bearing.* Journal of Orthopaedic Research, 2005. **23**(2): p. 345-350.
112. Hinterwimmer, S., et al., *In vivo contact areas of the knee in patients with patellar subluxation.* Journal of biomechanics, 2005. **38**(10): p. 2095-101.

113. Patel, V.V., et al., *Magnetic resonance imaging of patellofemoral kinematics with weight-bearing.* Journal of bone and joint surgery. American volume, 2003. **85-A**(12): p. 2419-24.
114. von Eisenhart-Rothe, R., et al., *A new in vivo technique for determination of 3D kinematics and contact areas of the patello-femoral and tibio-femoral joint.* Journal of biomechanics, 2004. **37**(6): p. 927-34.
115. Ward, S.R., M.R. Terk, and C.M. Powers, *Patella alta: association with patellofemoral alignment and changes in contact area during weight-bearing.* Journal of bone and joint surgery. American volume, 2007. **89**(8): p. 1749-55.
116. Goto, A., et al., *In vivo three-dimensional wrist motion analysis using magnetic resonance imaging and volume-based registration.* Journal of Orthopaedic Research, 2005. **23**(4): p. 750-756.
117. Moritomo, H., et al., *In vivo three-dimensional kinematics of the midcarpal joint of the wrist.* Journal of Bone and Joint Surgery. American Volume, 2006. **88**(3): p. 611-621.
118. Keir, P.J. and R.P. Wells, *Changes in geometry of the finger flexor tendons in the carpal tunnel with wrist posture and tendon load: an MRI study on normal wrists.* Clinical Biomechanics, 1999. **14**(9): p. 635-645.
119. Moritomo, H., et al., *Capitate-based kinematics of the midcarpal joint during wrist radioulnar deviation: an in vivo three-dimensional motion analysis.* The Journal of Hand Surgery, 2004. **29**(4): p. 668-675.
120. Moritomo, H., et al., *The Triquetrum-Hamate joint: an anatomic and in vivo three-dimensional kinematic study.* The Journal of Hand Surgery, 2003. **28**(5): p. 797-805.
121. Eckstein, F., et al., *Functional analysis of articular cartilage deformation, recovery, and fluid flow following dynamic exercise in vivo.* Anatomy and Embryology, 1999. **200**(4): p. 419-424.
122. Eckstein, F., M. Hudelmaier, and R. Putz, *The effects of exercise on human articular cartilage.* Journal of Anatomy, 2006. **208**(4): p. 491-512.
123. Eckstein, F., et al., *In vivo cartilage deformation after different types of activity and its dependence on physical training status.* Annals of the rheumatic diseases, 2005. **64**(2): p. 291-5.

124. Eckstein, F., et al., *Patellar cartilage deformation in vivo after static versus dynamic loading.* Journal of Biomechanics, 2000. **33**(7): p. 819-825.
125. Hudelmaier, M., et al., *Age-related changes in the morphology and deformational behavior of knee joint cartilage.* Arthritis & Rheumatism, 2001. **44**(11): p. 2556-2561.
126. Anderson, A.E., et al., *Validation of finite element predictions of cartilage contact pressure in the human hip joint.* J Biomech Eng, 2008. **130**(5): p. 051008.
127. Werner, F.W. and A.K. Palmer, *Biomechanical evaluation of operative procedures to treat Kienbock's disease.* Hand Clin, 1993. **9**(3): p. 431-43.
128. Keir, P.J., *Magnetic resonance imaging as a research tool for biomechanical studies of the wrist.* Seminars in musculoskeletal radiology, 2001. **5**(3): p. 241-50.
129. Henninger, H.B., et al., *Validation of computational models in biomechanics.* Proc Inst Mech Eng H, 2010. **224**(7): p. 801-12.
130. Cohen, Z.A., et al., *Computer Simulations of Patellofemoral Joint Surgery.* The American Journal of Sports Medicine, 2003. **31**(1): p. 87-98.
131. Anderson, D.D., et al., *A three-dimensional finite element model of the radiocarpal joint: distal radius fracture step-off and stress transfer.* Iowa Orthop J, 2005. **25**: p. 108-17.
132. Varga, P., et al., *Validation of an anatomy specific finite element model of Colles' fracture.* J Biomech, 2009. **42**(11): p. 1726-31.
133. Thoomukuntla, B., et al., *Preliminary validation of MRI-based modeling for evaluation of joint mechanics.* J Musculoskelet Res, 2008. **11**(4): p. 161-171.
134. Fischer, K.J., et al., *MRI-Based Modeling for Radiocarpal Joint Mechanics: Validation Criteria and Results for Four Specimen-Specific Models.* J Biomech Eng, 2011. **133**(10): p. 101004.
135. Iwasaki, N., et al., *Biomechanical analysis of limited intercarpal fusion for the treatment of Kienbock's disease: a three-dimensional theoretical study.* J Orthop Res, 1998. **16**(2): p. 256-63.
136. Dvinskikh, N.A., et al., *The effect of lunate position on range of motion after a four-corner arthrodesis: A biomechanical simulation study.* Journal of Biomechanics, 2011. **44**(7): p. 1387-1392.

137. Matsuki, H., et al., *Scaphoid nonunion and distal fragment resection: analysis with three-dimensional rigid body spring model.* J Orthop Sci, 2009. **14**(2): p. 144-9.
138. Murase, T., et al., *Does three-dimensional computer simulation improve results of scaphoid nonunion surgery?* Clin Orthop Relat Res, 2005(434): p. 143-50.
139. Carrigan, S.D., et al., *Development of a three-dimensional finite element model for carpal load transmission in a static neutral posture.* Ann Biomed Eng, 2003. **31**(6): p. 718-25.
140. Ledoux, P., D. Lamblin, and R. Targowski, *Modifications to the mechanical behavior of the wrist after fracture of the scaphoid. Modeling by finite element analysis.* Acta Orthop Belg, 2001. **67**(3): p. 236-41.
141. Majima, M., et al., *Load transmission through the wrist in the extended position.* J Hand Surg Am, 2008. **33**(2): p. 182-8.
142. Pillai, R.R., et al., *MRI-based modeling for evaluation of in vivo contact mechanics in the human wrist during active light grasp.* J Biomech, 2007. **40**(12): p. 2781-7.
143. Schuind, F., et al., *Force and pressure transmission through the normal wrist. A theoretical two-dimensional study in the posteroanterior plane.* Journal of Biomechanics, 1995. **28**(5): p. 587-601.
144. Kwak, S.D., L. Blankevoort, and G.A. Ateshian, *A Mathematical Formulation for 3D Quasi-Static Multibody Models of Diarthrodial Joints.* Comput Methods Biomech Biomed Engin, 2000. **3**(1): p. 41-64.
145. Cohen, Z.A., et al., *Patellofemoral Stresses during Open and Closed Kinetic Chain Exercises.* The American Journal of Sports Medicine, 2001. **29**(4): p. 480-487.
146. Johnson, J.E., et al., *Validation of radiocarpal joint contact models based on images from a clinical MRI scanner.* Comput Methods Biomech Biomed Engin, 2012. Epub.
147. Anderson, A.E., et al., *Subject-specific finite element model of the pelvis: development, validation and sensitivity studies.* Journal of Biomechanical Engineering, 2005. **127**(3): p. 364-73.
148. Fitzpatrick, C.K., M.A. Baldwin, and P.J. Rullkoetter, *Computationally efficient finite element evaluation of natural patellofemoral mechanics.* Journal of Biomechanical Engineering, 2010. **132**(12): p. 121013.

2. RESULTS OF AUTOMATIC IMAGE REGISTRATION ARE DEPENDENT ON INITIAL MANUAL REGISTRATION

This page left intentionally blank.

Submitted to Computer Methods in Biomechanics and Biomedical Engineering

TECHNICAL NOTE

Results of Automatic Image Registration are Dependent on Initial Manual Registration

J.E. Johnson[a] and K.J. Fischer[a,b,*]

[a]*Department of Mechanical Engineering, University of Kansas, Lawrence, USA*

[b]*Department of Orthopedic Surgery, University of Kansas Medical Center, Kansas City, USA*

(Received 2012; final version received 2012)

Joshua E. Johnson[a]

1530 W. 15th St.

3138 Learned Hall, Lawrence, KS 66045, USA

Tel: +1 785 864 3191; Fax: +1 785 864 5254

a2joe@ku.edu

Kenneth J. Fischer[a,b,*]

1530 W. 15th St.

3138 Learned Hall, Lawrence, KS 66045, USA

Tel: +1 785 864 2994; Fax: +1 785 864 5254

fischer@ku.edu

2.1. Abstract

Accurate kinematics are important to investigate normal/pathologic joint function, and we propose a method to further improve accuracy of image-based registration using initial manual registration. MRI of two wrist specimens were acquired in relaxed position, and during simulated grasp. Kinematics were determined from image registration between the two volumes. The volumes were manually aligned as close as possible prior to auto-registration, from which standard kinematics were obtained. Then, translation/rotation perturbations were applied to the manual registration to obtain altered initial positions, from which altered auto-registration kinematics were obtained. Also, surface models of the radiolunate joint were constructed from relaxed images. Kinematics and contact mechanics were compared between the standard and altered initial conditions. Kinematic errors increased while contact data decreased, with increasing perturbations. Overall, initial registration conditions clearly influence final registration accuracy. Manual alignment of image volumes as close as possible prior to auto-registration, appears to minimize kinematics and contact errors.

Keywords: kinematics; image registration accuracy; voxel-based image registration; manual image registration; magnetic resonance imaging

2.2. Introduction

Kinematics are important to investigate normal joint function and pathologic effects of injuries or disease. This is particularly true for complex joints such as the wrist, where normal bone motion facilitates stability and abnormal motion can lead to instability (Gardner et al. 2006). Kinematics also have a broad application in computational simulations as input parameters for displacement driven models. Small errors initially can lead to incremental errors in final simulation results, hence kinematic accuracy is of utmost importance.

Several techniques, such as motion tracking, biplanar fluoroscopy or cine phase-contrast magnetic resonance imaging (MRI), have been used to measure in vivo kinematics (Crisco et al. 2001; Rogers et al. 2002; Gardner, et al. 2006; Moro-oka et al. 2007; Tay et al. 2008; Zheng and Zhang 2010; Borotikar et al. 2012; Svedmark et al. 2012; Zhu et al. 2012). Motion tracking requires surface markers, which may not accurately reflect actual bone motions. Markerless image-based registration has also been used and shown to have good accuracy (Crisco, et al. 2001; Goto et al. 2005). This method has an advantage over surface based marker techniques, due to its ability to directly quantify bone motion, especially for complex joints such as the wrist. However, when using registration to acquire kinematics from image sets such as MRI, initial registration conditions may potentially influence accuracy.

The goal of this study was to investigate effects of different initial conditions on lunate kinematics obtained from image registration and related contact mechanics (contact force, contact area and peak contact pressure). We propose a method to further improve the accuracy of image-based registration using initial manual registration. Registration accuracy and contact data were expected to differ with varying initial conditions.

2.3. Methods

MR images of two cadaveric wrist specimens were acquired in a 3T clinical scanner (Allegra, Siemens, USA) using a constructive interference steady state sequence. Images were acquired with the wrists relaxed (unloaded), and during simulated grasp (loaded). To simulate grasp, a total of 110 N was distributed across select extensor and flexor tendons (Johnson et al. 2012). The unloaded images were acquired at high resolution for model construction (0.15×0.15×0.5

mm voxel), while loaded images were acquired at lower resolution for image registration (0.3×0.3×1.0 mm voxel).

Radius and lunate bones with their cartilage surfaces, were segmented from the unloaded images to generate three dimensional (3D) surface models of the radiolunate articulation. The bones were assumed as rigid; hence, radius and lunate bones only (without cartilage) were segmented for image registration.

Volume-based 3D image registration was performed using Analyze 5.0 (Analyze Direct, Overland Park, KS), which compared normalized mutual pixel intensities, to obtain kinematics from unloaded to loaded configuration. First, the radius was used as a fixed reference to find a transformation that aligned the loaded and unloaded image sets. A manual registration was performed to align the two image sets as close as possible in 3D (defined as the standard initial condition). This was followed by 25 subsequent auto-registration iterations, from which a best match was visually selected. This best match was defined as the standard best match. Next, the best match from the reference transformation was used to move the loaded lunate into the unloaded image coordinate system. Finally, the unloaded lunate was registered to the loaded lunate (now in the unloaded coordinate system) to obtain the kinematic transformation to the loaded configuration. A standard initial condition and standard best match were also defined for this step.

To investigate the effects of different initial conditions on final radius and lunate kinematics, the results after a series of perturbations from the standard initial condition, were compared to the standard best match. Perturbations in the x, y and z directions of 1, 2 and 3 pixels (translation) and 1, 2 and 3° (rotation) were applied to the standard initial conditions, to obtain altered initial conditions. Each perturbation was again followed by 25 auto-registration iterations, from which best matches were selected (defined as perturbation best matches). The transformations were converted into translation and rotation vectors (Woltring 1994) for analyses. Root mean square error (RMSE) values were calculated for both translation (TV) and rotation (RV) vectors between the standard best match and each perturbation best match, using the equation;

$$RMSE_{TV/RV} = \sqrt{\frac{1}{n}\left((x_{sb} - x_{pb})^2 + (y_{sb} - y_{pb})^2 + (z_{sb} - z_{pb})^2\right)} \; mm/°$$

Where x_{sb}, y_{sb} and z_{sb} are the components of the standard best match translation/rotation vector and x_{pb}, y_{pb} and z_{pb} are the components of the perturbation best match vector.

To compare effects of different initial conditions on contact mechanics, standard best match kinematics and perturbation best match kinematics, were implemented for surface models in the Joint_Model software (Kwak et al. 2000). Contact area, local contact pressure and contact force were determined in Joint_Model, assuming an effective cartilage relaxation modulus of 4 MPa (Kwak, et al. 2000) and a uniform cartilage thickness of 1 mm for each articulation. Two-way repeated measures analysis of variance, with Tukey LSD post hoc analysis ($p < 0.05$), was used to identify differences between standard and perturbation best matches.

2.4. Results

Data is presented as means of the two specimens. Looking at the effects of initial conditions on kinematics, TV (Table 2.1) and RV (Table 2.2) RMS errors were significantly higher for lunate compared to radius, for both magnitude (1, 2 or 3) and direction (x, y or z) of perturbation ($p = 0.000$ for all cases). TV and RV RMS errors trended higher in the z direction, compared to x and y (Tables 2.1, 2.2). Averaging for direction of perturbation, we compared lunate TV and RV RMS errors with increasing magnitude of perturbation. TV RMS errors significantly increased from 2 to 3 pixel/° perturbations ($p = 0.002$), and RV RMS errors tended to increase with increasing perturbations (Table 2.3). For TV, errors tended to be higher from rotation than translation perturbation, and the opposite was true for RV errors (Table 2.3). A difference could be visually observed between the standard best match and best matches from altered initial conditions, especially at higher perturbation magnitudes (Figure 2.1).

We also investigated the effects of initial conditions on radiolunate contact mechanics, by comparing differences in contact parameters grouped for magnitude (Figure 2.2) and direction (Figure 2.3) of perturbation, and overall translation and rotation perturbations (Figure 2.4). For contact area, differences were significantly greater ($p = 0.047$) after 3 pixel/° perturbations compared to standard, and there was only a trend for higher differences for contact force and

peak pressure (Figure 2.2). A strong trend was also observed for higher differences in contact parameters from standard, after perturbations in the z direction (Figure 2.3). For contact force and contact area, there was a strong trend for higher differences between standard and translation perturbation best matches (Figure 2.4). Contact pressure distribution also changed with altered registration initial conditions (Figure 2.5).

2.5. Discussion

We investigated the effects of different initial registration positions on final radiolunate kinematics and contact mechanics. Results from a series of translation and rotation perturbations were compared to a standard, which indicated that initial manual alignment of registration volumes influences registration accuracy.

Markerless image registration is particularly useful to determine in vivo kinematics. Surface registration is often used, but volume-based image registration has been shown to have a similar/better accuracy (Goto, et al. 2005). There is still a need to improve image registration accuracy, especially for articulations that have small motions.

Lower registration errors for radius indicated that size and/or shape of the bone may be a factor affecting voxel-based registration accuracy. The larger the bone, the more the pixel information, which could minimize the effects of initial position. Similarly, more distinct features may improve registration.

The out of plane direction (z, in this case) generally appeared to have higher errors. Since in-plane resolution of MR images are usually higher than out of plane, mismatch in that direction may further compound errors. Rotation perturbations seem to cause larger translation errors, likely due to translations associated with rotations.

With increasing perturbations, contact mechanics appeared to be underestimated regardless of perturbation direction. Larger perturbations appear to result in kinematic errors that increase separation in the radiocarpal joint, resulting in lack of contact and lower values for contact data. This is evident from the reduction in contact area and contact pressure after perturbation (Figure 2.5). Larger differences in contact data from translation perturbations may be a bone-specific

result. Due to the relatively spherical shape of the radiolunate articulation, rotation may have a smaller effect on contact.

Lack of significant differences is likely due to the low specimen number. Only effects of pure translation and rotation perturbations were investigated. Combined perturbations should have a similar or worse effect. Results from perturbations may be software specific, but any automated voxel registration software should benefit from good initial manual registration.

We have shown kinematic errors to increase with larger perturbations in initial position and orientation. Overall, initial condition for registration clearly influences accuracy. We recommend a careful manual alignment of the image volumes, as closely as possible, prior to auto-registration to minimize kinematic and subsequent modeling errors.

Acknowledgements

We would like to acknowledge NIH R01EB008709 grant funding, Columbia University for use of Joint_Model software, and Allan Schmitt for technical assistance with MR imaging.

2.6. References

Borotikar BS, Sipprell WH, 3rd, Wible EE, Sheehan FT. 2012. A methodology to accurately quantify patellofemoral cartilage contact kinematics by combining 3D image shape registration and cine-PC MRI velocity data. J Biomech. 45(6):1117-1122.

Crisco JJ, Wolfe SW, Neu CP, Pike S. 2001. Advances in the in vivo measurement of normal and abnormal carpal kinematics. The Orthopedic clinics of North America. 32(2):219-231.

Gardner MJ, Crisco JJ, Wolfe SW. 2006. Carpal kinematics. Hand Clin. 22(4):413-420.

Goto A, Moritomo H, Murase T, Oka K, Sugamoto K, Arimura T, Masumoto J, Tamura S, Yoshikawa H, Ochi T. 2005. In vivo three-dimensional wrist motion analysis using magnetic resonance imaging and volume-based registration. J Orthop Res. 23(4):750-756.

Johnson JE, McIff TE, Lee P, Toby EB, Fischer KJ. 2012. Validation of radiocarpal joint contact models based on images from a clinical MRI scanner. Comput Methods Biomech Biomed Engin. Epub ahead of print

Kwak SD, Blankevoort L, Ateshian GA. 2000. A Mathematical Formulation for 3D Quasi-Static Multibody Models of Diarthrodial Joints. Comput Methods Biomech Biomed Engin. 3(1):41-64.

Moro-oka TA, Hamai S, Miura H, Shimoto T, Higaki H, Fregly BJ, Iwamoto Y, Banks SA. 2007. Can magnetic resonance imaging-derived bone models be used for accurate motion measurement with single-plane three-dimensional shape registration? J Orthop Res. 25(7):867-872.

Rogers BP, Haughton VM, Arfanakis K, Meyerand ME. 2002. Application of image registration to measurement of intervertebral rotation in the lumbar spine. Magn Reson Med. 48(6):1072-1075.

Svedmark P, Tullberg T, Noz ME, Maguire GQ, Jr., Zeleznik MP, Weidenhielm L, Nemeth G, Olivecrona H. 2012. Three-dimensional movements of the lumbar spine facet joints and

segmental movements: in vivo examinations of normal subjects with a new non-invasive method. Eur Spine J. 21(4):599-605.

Tay SC, van Riet R, Kazunari T, Koff MF, Amrami KK, An KN, Berger RA. 2008. A method for in-vivo kinematic analysis of the forearm. J Biomech. 41(1):56-62.

Woltring HJ. 1994. 3-D attitude representation of human joints: a standardization proposal. J Biomech. 27(12):1399-1414.

Zheng G, Zhang X. 2010. Computer assisted determination of acetabular cup orientation using 2D-3D image registration. Int J Comput Assist Radiol Surg. 5(5):437-447.

Zhu Z, Massimini DF, Wang G, Warner JJ, Li G. 2012. The accuracy and repeatability of an automatic 2D-3D fluoroscopic image-model registration technique for determining shoulder joint kinematics. Med Eng Phys. 34(9):1303-1309.

2.7. Tables

Table 2.1. RMS errors of translation vectors for the radius and lunate from initial conditions after translation and rotation perturbations, averaged for specimens.

RMSE of Translation Vector (pixels)							
Perturbation		*Radius*			*Lunate*		
		X	**Y**	**Z**	**X**	**Y**	**Z**
Translation (pixels)	**1**	0.0140	0.0243	0.0284	0.3604	0.2943	0.1857
	2	0.0000	0.0452	0.0427	0.2918	0.2440	0.3946
	3	0.0243	0.0555	0.0492	0.2918	0.2617	0.3915
Rotation (degrees)	**1**	0.1208	0.0396	0.0431	0.2605	0.3153	0.2895
	2	0.0387	0.0521	0.0593	0.2992	0.2915	0.2919
	3	0.0692	0.0410	0.0845	0.4283	0.3472	0.3755

Table 2.2. RMS errors of rotation vectors for the radius and lunate from initial conditions after translation and rotation perturbations, averaged for specimens.

RMSE of Rotation Vector (degrees)							
Perturbation		*Radius*			*Lunate*		
		X	**Y**	**Z**	**X**	**Y**	**Z**
Translation (pixels)	**1**	0.0071	0.0115	0.0502	0.7669	0.6889	0.4315
	2	0.0000	0.0219	0.0584	0.7067	0.5461	0.9789
	3	0.0115	0.0467	0.0435	0.7067	0.6026	0.6229
Rotation (degrees)	**1**	0.0653	0.0716	0.0398	0.3413	0.6500	0.5415
	2	0.0555	0.0485	0.0549	0.5055	0.5173	0.5667
	3	0.0357	0.0634	0.0756	0.9012	0.7325	0.6453

Table 2.3. RMS errors of lunate translation and rotation vectors with increasing magnitude of perturbation, averaged for direction of perturbation. * indicates significance.

	RMSE of Translation Vector (pixels)			**RMSE of Rotation Vector (degrees)**		
Perturbation (pixel/°)	**1**	**2**	**3***	**1**	**2**	**3**
Translation	0.2802	0.3102	0.3150	0.6291	0.7439	0.6441
Rotation	0.2884	0.2942	0.3837	0.5109	0.5298	0.7597

2.8. Figures

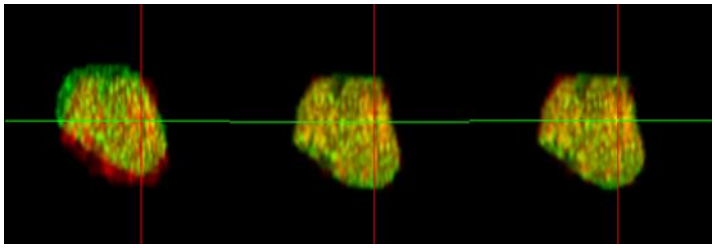

Figure 2.1. Transverse slice from unloaded (green) and transformed loaded lunate (red) volumes in the unregistered position (left), after standard best match kinematics was applied (center) and best match after a 3° rotation perturbation was applied (right).

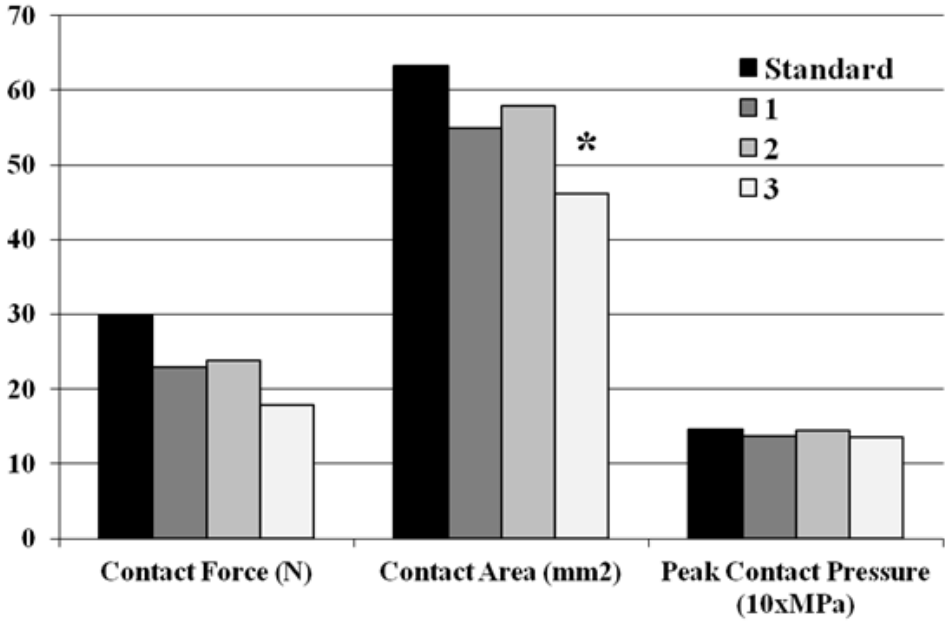

Figure 2.2. Contact data from standard best match kinematics, and from kinematics after 1, 2 and 3 pixels/° perturbations were applied (averaged for x, y and z directions). * indicates significant difference

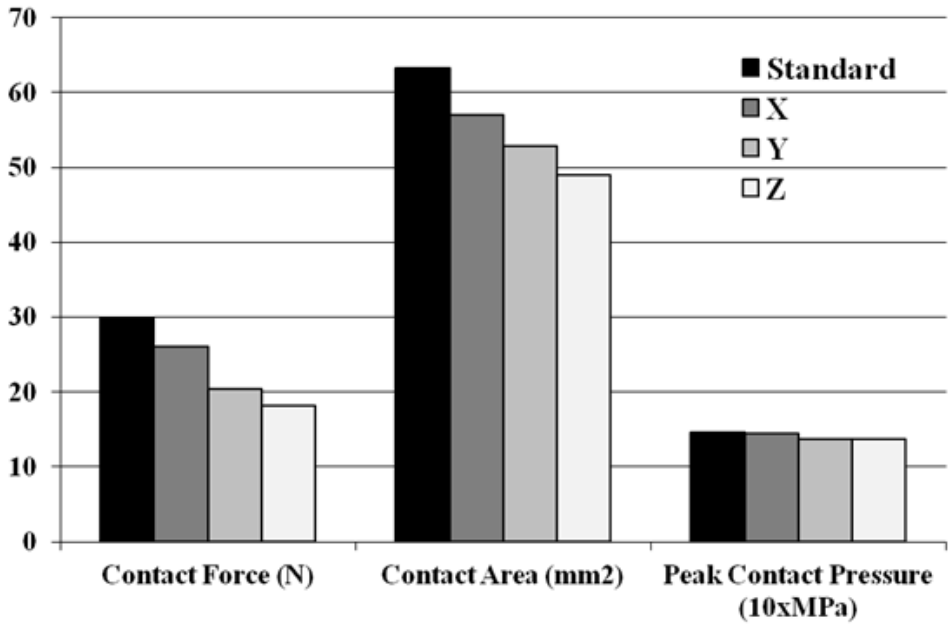

Figure 2.3. Contact data from standard best match kinematics, and from perturbations varying in x, y and z directions (averaged for 1, 2 and 3 pixels/°).

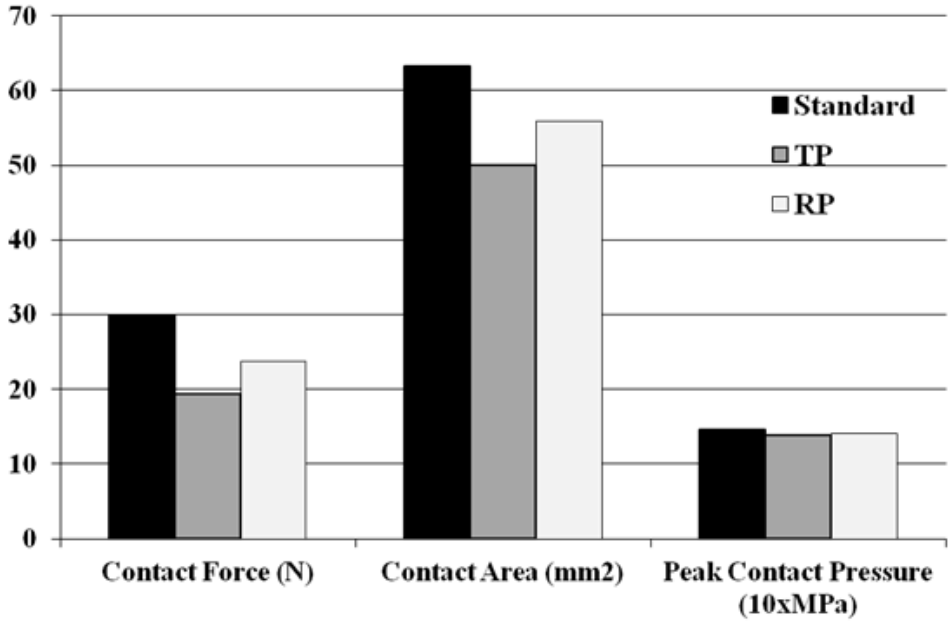

Figure 2.4. Overall means of contact data from translation (TP) and rotation (RP) perturbations compared to standard.

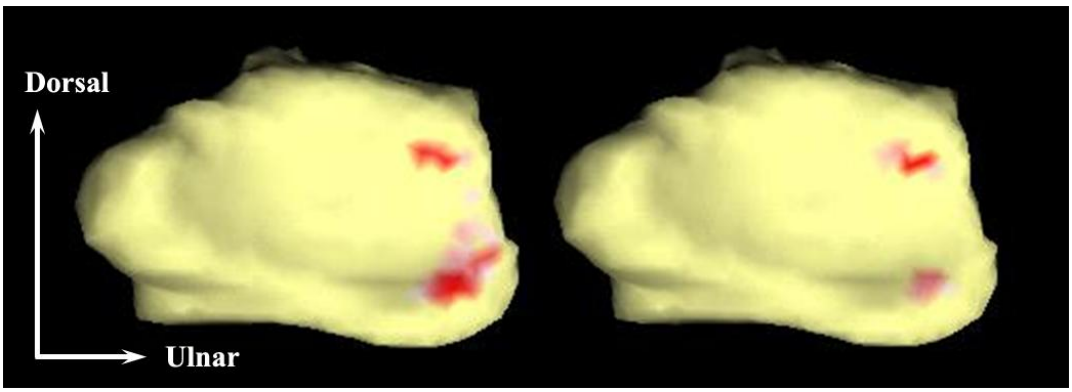

Figure 2.5. Sample radiolunate contact pressure distribution shown on the radius articular surface after a standard best match kinematics (left) and a 3° rotation perturbation best match kinematics (right) were applied.

3. SCAPHOLUNATE LIGAMENT INJURY ADVERSELY ALTERS IN VIVO WRIST JOINT MECHANICS. AN MRI-BASED MODELING STUDY

This page left intentionally blank.

Submitted to Journal of Orthopedic Research

Scapholunate Ligament Injury Adversely Alters In Vivo Wrist Joint Mechanics. An MRI-based Modeling Study.

Joshua E. Johnson,[1] Phil Lee,[2] Terence E. McIff,[3] E. Bruce Toby,[3] Kenneth J. Fischer[1,3]

[1]Department of Mechanical Engineering, University of Kansas, 3138 Learned Hall, Lawrence, Kansas, 66045

[2]Hoglund Brain Imaging Center, University of Kansas Medical Center, 3901 Rainbow Boulevard, Kansas City, Kansas, 66160

[3]Department of Orthopedic Surgery, University of Kansas Medical Center, 3901 Rainbow Boulevard, Kansas City, Kansas, 66160

Kenneth J. Fischer

1530 W. 15th St, 3138 Learned Hall, Lawrence, Kansas, 66045

Phone: 785 864 2994

Fax: 785 864 5254

fischer@ku.edu

3.1. Abstract

We investigated the effects of scapholunate ligament injury on *in vivo* radiocarpal joint mechanics using image-based surface contact modeling. Magnetic resonance images of ten injured and contralateral normal wrists were acquired at high resolution (hand relaxed) and during functional grasp. Three dimensional surface models of the radioscaphoid and radiolunate articulations were constructed from the relaxed images, and image registration between the relaxed and grasp images provided kinematics. The displacement driven models were implemented in a contact modeling software, Joint_Model. Contact parameters were determined from interpenetration of interacting bodies and a linear contact rule. Peak and mean contact pressures, contact forces and contact areas were compared between the normal and injured wrists. Also measured were effective (direct) contact areas and intercentroid distances from the grasp images. Means of the model contact areas were within 10 mm^2 of the direct contact areas for both articulations. With injury, all contact parameters significantly increased in the radioscaphoid articulation, while only peak contact pressure and contact force significantly increased in the radiolunate articulation. Inter-centroid distances also increased significantly with injury. This study provides novel *in vivo* contact mechanics data from scapholunate ligament injury and confirms detrimental alterations as a result of injury.

Joint mechanics, modeling, osteoarthritis, ligament injury, wrist

3.2. Introduction

Normal wrist joint function is facilitated by complex interactions between articulating geometry and ligamentous anatomy, which constrain motion and provide stability. Scapholunate interosseous ligament (SLIL) is the primary stabilizer of the scapholunate (SL) joint.[1] SLIL tears from impact loading to the base of the wrist or repetitive twisting motion (in hyperextension or intercarpal supination) can result in a common wrist injury known as SL dissociation.[2] SLIL ligament injury can cause disruption of normal SL mechanical relationship leading to loss of alignment.[3] With continued usage, there is further damage to the secondary stabilizers (such as radioscaphocapitate and dorsal intercarpal ligaments) that leads to progressive instability, thereby causing further malalignment and deformity. These changes in carpal bone orientations can lead to abnormal kinematics.[3] Loss of normal alignment (articular surface incongruity) and abnormal kinematics can alter load transfer through the joint, with subsequent degenerative changes to the articular surface.[4]

Osteoarthritis (OA) is the most common degenerative joint disease that affects not only the elderly (33.6% of Americans over 65), but also the younger population (13.9% over 25).[5-7] While attention is commonly focused on weight bearing joints (such as the hip or knee) due to functional debilitating effects, extremities such as the hand and wrist are also significantly impacted adversely. In fact, prevalence of radiographic OA is highest for the hand (7.3/100), and prevalence of symptomatic OA (8/100) is second only to the knee (12.1/100).[8,9] While age is the primary risk factor for OA, degenerative changes also occur secondary to joint injury or trauma, and this is also common in the younger population.[10] Impact joint injuries resulting in macroscopic (from fractures) and microscopic (from capsular or ligamentous injuries) damage are a frequent cause of post-traumatic OA (PTOA).[10] PTOA can be a consequence of sudden local insult to the articular surface or of progressive damage as a result of joint instability and incongruity.[10] In the lower extremity, ligamentous injuries cause a 10-fold increase in risk of developing OA and economic losses from PTOA alone amount to 3 billion dollars annually.[10]

Without treatment, SL dissociation generally leads to a progressive osteoarthritic pattern known as scapholunate advanced collapse (SLAC), which is the most common form of wrist OA.[11] Clinical manifestation of PTOA is highly variable, during which time certain biological or

mechanical factors are thought to promote repair and restoration of the joint, indicating possibility for treatment.[6] Joint contact pressures and pressure distributions are considered to be important mechanical factors.[12] However, the mechanism is unclear and its role is still under debate. Progressive instability/deformity of the SL joint as a result of SLIL injury may cause an elevation in joint contact pressures in normal contact regions or in shifted regions of contact. The ability to evaluate changes in contact pressure that occur *in vivo* may provide insight into the mechanism of PTOA.

Several cadaveric experimental studies have investigated normal wrist biomechanics and biomechanics after SLIL sectioning.[3,13-16] However, *in vivo* conditions are much more complex due to soft tissue interactions and dynamic motor stability. *In vivo* studies investigating SLIL, have mostly evaluated scaphoid and lunate kinematics after injury. Crisco et al have shown decreased lunate rotation in extension, and increased scaphoid rotation in flexion after SLIL injury.[17] While magnetic resonance imaging (MRI) is useful for early OA diagnosis[18] and is commonly used to diagnose knee injuries, such as anterior cruciate ligament tear, it is somewhat limited in its diagnostic value for wrist ligament injuries due to the small anatomy and lower spatial resolution.[2] However, MRI can be also be used to acquire *in vivo* data such as model geometry and kinematics.[19,20] Computer modeling is helpful to simulate joint abnormalities and predict joint mechanics non-invasively. Finite element (FE) modeling is the most common technique for joint contact analysis, but generating a quality FE model and solving the complex nonlinear contact problem is difficult and time consuming.[21] To evaluate articular joint changes as a result of injury, it may be sufficient to look at articular surface parameters. This can be achieved through surface contact modeling (SCM), in a relatively simple and computationally efficient manner, without the need for complex nonlinear analyses.[22] MRI when combined with SCM can be an effective tool to determine *in vivo* joint mechanics and this technique has not been extensively used.

Compared to cadaveric studies, fewer studies have investigated normal and pathologic *in vivo* wrist joint mechanics,[23,24] and there does not appear to be any prior work on the *in vivo* effects of SLIL injury on mechanics. *In vivo* data may improve understanding of how contact mechanics are altered from normal kinematics and may also improve efficacy of surgical

interventions that are performed to minimize pain, restore joint function and prevent the onset of OA. Hence, the objective of this study was to compare radiocarpal joint mechanics from MRI-based SCM between normal wrists and wrists with SLIL injury. Our hypothesis was that peak and mean contact pressures would be higher in the injured wrists.

3.3. Methods

Ten human subjects diagnosed (clinical examination, radiographs and/or MRI) with unilateral SL dissociation by a board certified physician, were enrolled for the study. The study was approved by the Institutional Review Board. While the mechanism of injury varied, subjects fell into three general categories. The most common was fall on outstretched hand, and also from athletic injuries and vehicular accidents. The contralateral hand was used as "normal" control and hence, it was ensured that the normal hand had no prior patient history or clinical symptoms of injury. The contralateral hand was used as a control to minimize the effects of variation and performance from between subject factors. It was also ensured that there was no visual indication of articular surface degeneration or inflammatory arthritis, in both wrists. Subjects were recruited with ages upward from skeletal maturity, with a mean age of 40.4 years (22 to 67), and there were eight male and two female subjects. SL dissociation can occur in younger individuals due to congenital defects and other factors, but, it is harder to differentiate between biomechanical changes arising from injury and geometric (bone and cartilage) changes due to growth. Also, the likelihood of joint degeneration increases for individuals over 60 years old. While an equal distribution of male and female subjects was targeted, due to the nature of the injury (high-impact loading), more male than female subjects were expected. It was also ensured that subjects were able to perform the functional grasp activity for the duration of the scan.

MR images were acquired using a 3T clinical scanner using a constructive interference steady state (CISS) or a dual echo steady state (DESS) sequence. Nine subjects were scanned using CISS sequence, while one subject was scanned using DESS sequence.

Two sets of images were acquired for both normal and injured wrists. High resolution scans of the injured wrist were acquired first with the hand in relaxed (unloaded) position (Fig. 3.1A). Then, lower resolution scans were acquired during active light grasp (loaded) position (Fig. 3.1B). Loaded scans were designed to minimize subject fatigue and motion artifacts by reducing

scan time, while maintaining adequate resolution for bone segmentation. The normal hand was similarly scanned in the unloaded state, followed by the loaded configuration.

The protocols for CISS were matrix: 640×416 pixels, field of view (FOV): 95×61.8 mm, slice thickness: 0.5 mm, scan time: ~12 mins, for relaxed scans and matrix: 320×208 pixels, FOV: 95×61.8 mm, slice thickness: 1.0 mm, scan time: 196 s, for grasp scans. The protocols for DESS were matrix: 448×240 pixels, FOV: 100×48 mm, slice thickness: 0.5 mm, scan time: 4.5 mins, for relaxed scans and matrix: 320×320 pixels, FOV: 100×100 mm, slice thickness: 1.0 mm, scan time: 188 s, for grasp scans.

The grasp activity involved squeezing a pre-pressurized grip device to a specified target (3.125 psi = 21.6 KPa) and maintaining it for the duration of the scan, by means of a visual feedback system (Fig. 3.2). This target pressure was previously determined in our lab to produce minimal discomfort, while maintaining grip during the grasp activity for the duration of the scan. The grasp activity was also performed with the wrist braced to ensure consistent loaded positions between the subjects (Fig. 3.2).

SCM was the primary method used to acquire contact mechanics data, which required model geometries, kinematics and a contact rule/relationship. The radius, lunate and scaphoid bones with their articular surfaces, were segmented from the high resolution unloaded images using image processing software (ScanIP, Simpleware, Exeter, UK). To ensure accuracy of boundary selection, independent quality control was performed for each segmentation. Triangular faceted surfaces were created from the segmented volumes to obtain 3D surface models (Fig. 3.3).

Kinematics were obtained from 3D voxel-based image registration to match bone orientations in the loaded images, using Analyze 5.0 (Analyze Direct, Overland Park, KS). The 3D voxel registration technique is based on normalized mutual information, which compares relative pixel information between image volumes. Bones were assumed as rigid (undergoing negligible deformation), while cartilage deformed even under the low loading of the light grasp activity. Hence, radius and carpal (lunate and scaphoid) bones without cartilage, were segmented from the image volumes. In every image set, each bone was isolated on a black background for registration. The first step was using the radius as a fixed reference to align the loaded and the

unloaded image sets. This registration was used to transform the loaded carpal bones into the unloaded image coordinate system. Finally, the unloaded carpal bones were registered to the (transformed) loaded carpal bones. These transformations were converted to a translation and rotation vector. The rotation vector initiated at the origin of the coordinate system and prescribed a single axis of rotation, which could be decomposed along the coordinate system axis (X: ulnar-radial; Y: proximal-distal; Z: volar-dorsal, first direction being the positive direction for each). The magnitude of the rotation vector specified the angle of rotation about the axis.[25] This provided kinematics from the unloaded to loaded configuration. Thus model geometries and kinematics were acquired for the normal and injured wrists and implemented in a contact modeling software.

Displacement controlled surface contact mechanics were determined using Joint_Model software.[22] The software determined contact parameters from interpenetration of interacting rigid bodies and the algorithm defined contact force as linearly proportional to strain. The kinematics placed the unloaded model geometries in the loaded configuration, from which the location of contact, contact area and strain were directly determined. The articular surface of each body was assigned a uniform thickness of 1 mm[14] based on average measured values. The region of model surface penetration yielded the contact area for each articulation. The ratio of overlap/penetration to total thickness of the articular surfaces provided the local cartilage deformation at each node, which gave a first order estimate of strain. The total deformation was distributed to the bodies in contact based on the ratio of their cartilage thicknesses and moduli, which were the same for all bodies in contact. The loaded images were acquired over a relatively long period, which was sufficient time for the cartilage to approach equilibrium. Hence, cartilage was assigned a modulus of 4 MPa, as a reasonable assumption for an effective compressive relaxation modulus.[22] Local nodal contact pressures were determined from the strain estimate and the material property. Finally, contact pressures were numerically integrated over contact area to obtain contact force. The ratio of contact force to contact area gave the mean contact pressure.

Also, the regions of articular surface contact were reasonably visible in the loaded MR images. These regions of contact were individually segmented for each contact pair (radiolunate and radioscaphoid) from every loaded image set. Lengths of the segmented contact regions were

multiplied by slice thickness to obtain an effective area, and the areas from all images were summed to obtain the total contact area for each articulation. These "direct" contact areas were compared to the model contact areas as a form of model verification. The distances between the centroids of radiolunate and radioscaphoid contacts (inter-centroid distance) were also determined from the direct contact areas.

Contact forces, contact areas, peak and mean contact pressures, contact pressure distributions and inter-centroid distances, were compared between the normal and injured wrists for both radiolunate (RL) and radioscaphoid (RS) articulations. Paired-samples t-test, with one-tailed significance defined as $p < 0.05$, was used to identify differences in contact forces, contact areas, peak and mean contact pressures and inter-centroid distances, between the normal and injured wrists. To determine the relationship between model contact areas and direct contact areas, a linear regression analysis was performed for overall (normal and injured combined) model and direct contact areas for each articulation.

3.4. Results

Data for all parameters is represented as mean ± standard error. Since positions of relaxed wrists were not fixed during MRI scanning, kinematics were not statistically compared between subjects. For the normal wrist, mean magnitude of translation vectors trended higher for scaphoid (2.22±0.28 mm) than for lunate (1.29±0.25 mm). Also, mean magnitude of rotation vectors trended higher for scaphoid (8.72±1.35°) than for lunate (5.32±1.11°). For the injured wrists, mean magnitude of translation and rotation vectors tended to increase for both lunate (1.37±0.40 mm and 8.98±1.66° respectively) and scaphoid (2.54±0.46 mm and 10.40±2.16° respectively), compared to the normal wrists.

Contact pressure distributions on the radius articular surface were different between normal and injured wrists (Fig. 3.4). For normal wrists, lunate and scaphoid contacts were located generally in the mid to dorsal region. With injury, scaphoid contact generally separated from lunate contact towards the radial styloid region. Lunate contact generally shifted volarly or widened to cover the entire lunate fossa on the radius. Figure 3.5 shows an example of scaphoid and lunate centroids of contact from normal and injured wrists that were used to determine

centroidal distances. Inter-centroid distance increased significantly from normal (15.14±0.78 mm) to injured (16.43±0.71 mm), p=0.044.

Table 3.1 shows contact parameters compared between normal and injured wrists for both articulations. Peak contact pressures significantly increased with injury in both RL (p=0.012) and RS (p=0.038) articulations (Fig. 3.6), while mean contact pressures significantly increased with injury only in the RS (p=0.029) articulation. Contact forces also significantly increased with injury in both RL (p=0.032) and RS (p=0.005) articulations (Fig. 3.7). Model contact areas significantly increased with injury in the RS (p=0.022) articulation, but not in the RL articulation. Means of the normal and injured model contact areas were within 5 mm^2 of means of corresponding normal and injured direct contact area results for RS articulation, and similarly within 10 mm^2 for RL articulation (Table 3.1). Only differences between RS overall model contact areas and direct contact areas, were non significant (p=0.17). Regression analysis however, showed a significant relationship between model and direct contact area measurements (R^2 = 0.89 and slope = 0.82 for RL articulation; R^2 = 0.79 and slope = 0.96 for RS articulation, p<0.001).

3.5. Discussion

In summary, MRI-based SCM technique was used to evaluate radiocarpal joint contact mechanics as a result of scapholunate dissociation. Contact forces, contact areas, peak and mean contact pressures significantly increased in the RS articulation, while only peak and mean contact pressures significantly increased in the RL articulation. Results confirm that contact mechanics are altered after SL ligament injury.

There is still an ongoing debate about the impact of SLIL injury on radiocarpal kinematics, though it is generally accepted that there are associated changes in carpal alignment.[3] The scaphoid is the most mobile of the carpal bones.[26] With SLIL tears and progressive injury to its secondary ligamentous stabilizers, the scaphoid is known to collapse into flexion (rotary subluxation), further increasing its mobility.[26] While kinematics were not directly compared in this study, the magnitudes of translations and rotations trended higher for the scaphoid in the normal wrists, and also appeared to increase with injury.

With injury, progressive widening of the SL interval occurs (Fig. 3.3 right). However, the amount of widening depends on the degree of injury/instability. In the dynamic stage, SL diastasis is only visible on stress radiographs. With continued usage and further damage to the secondary stabilizers, the static stage develops, where the deformity is fixed and visible on plain radiographs.[2] SL diastasis was somewhat evident from shift in contact locations and was clear according to increase in the inter-centroid distance (Fig. 3.5). Since inter-centroid distances were calculated directly from the loaded MR images, there may have may been less variability influencing the results, such that widening of the SL interval was clearly observed.

With rotary subluxation of the scaphoid, the proximal articular surface loses it congruency with its radius facet and contact is shifted to the volar and dorsal rims of the distal radius.[11] Clinically, SLAC wrist follows a pattern where degenerative changes are first observed in the RS region, initiated at the radial styloid.[11] For over half the subjects, RS contact was observed radially at the styloid region, prior to and following injury. Also, all contact parameters significantly increased with injury in the RS articulation. This may provide an explanation for the clinically observed initiation of OA in this region. Due to its more spherical fossa, the RL articulation is less sensitive to instability,[11] which may explain why only some of the parameters significantly increase with injury in the RL articulation. While magnitude and location of contact vary with wrist position, experiments have shown radiocarpal peak contact pressures to fall within 3 MPa,[14,27,28] as observed in this study. With SLIL injury there was an increase in peak contact pressure in both articulations. However, the magnitude was higher in the RL articulation, indicating a shift in load from the scaphoid to the lunate fossa. This has also been observed previously for dynamic motion after SLIL sectioning.[16] On average, only 21% of the radius articular surface is in contact with the scaphoid and lunate under normal function, and does not exceed 40% despite the magnitude of loading.[29] As cartilage matures, it may develop a conditioning to physiological loading over a period of time.[30] As such, normal regions of contact may be able to withstand increases (sudden or gradual) in contact pressures till a threshold is exceeded (after which damage occurs), while the regions that are not normally loaded may be sensitive to even minor changes in pressure distribution. While peak (both RL and RS) and mean (only RS) contact pressure increased, a shift in the location of contact may also be an OA risk factor for both articulations. This is evident in Figure 3.4 for example, where the load

transmission through the joint clearly shifted. From the results, degenerative changes do not appear to occur as a consequence of original insult to the joint (injury event), but rather due to abnormal changes in kinematics and contact locations that progressively occur following SLIL injury. As such, restoring kinematics and normal alignment may prevent the onset of degeneration.

Of interesting note was the significant increase in contact force in both articulations, even though grasp activity was the same for both normal and injured wrists. This may be due to co-contracture, where both wrist flexors and extensors are dynamically involved to minimize instability, as subjects attempt to compensate for pain by altering their grip during grasp activity. Since there are no direct motor attachments, to provide stability during physiologic loading (axial loading for instance), scapholunate motion is constrained by the intact intrinsic ligaments.[31] The wrist motors may provide additional indirect dynamic stability. The results suggest that with injury, the wrist flexors and extensors appear to be compensating for loss of this ligamentous constraint. In a physiological attempt to minimize the existing instability, there appears to be a corresponding change in the load transmission through the joint, which may increase OA risk.

Prior experimental studies have shown the reliability of direct contact area measurements in verifying modeling accuracy.[14] With *in vivo* data, there is the added possibility of motion artifacts (particularly in injured wrists) influencing results, which might explain why RL model contact area was different from direct contact area. Regression analysis indicates that this method still provides a useful means of verifying *in vivo* model results, which is otherwise not possible.

One limitation of the study was the relatively low number of subjects analyzed. Therefore, it was not possible to evaluate contact mechanics with regard to injury/instability patterns. Variation in peak and mean contact pressure results between articulations may also be due to differences in injury patterns. The subject pool for this study included three acute (2 to 4 weeks from injury), two sub-acute (4 weeks to 6 months) and five chronic (> 6 months) cases. While differences were observed by comparison of normal and injured wrists, grouping the subjects by pattern may better indicate changes in contact mechanics from initiation and progression of instability. This is particularly useful for early diagnosis, as contact mechanics at the time of evaluation can be compared with those observed at a specific/intermediate stage of injury. Also,

it was not possible to directly validate the *in vivo* models. However, the MRI-based SCM technique has been sufficiently validated and shown to be reliable to obtain contact mechanics data.[14,28] Further, the *in vivo* data compared well to prior data, and also to the directly measured contact area data.

The ability to evaluate extent of joint injuries (soft tissue or articular surface) is still limited and research is ongoing to quantify the severity of injuries, particularly to improve therapy and treatment outcomes.[10] Recent work has demonstrated the feasibility of quantifying articular fracture severity from surface fragments.[10] Even in the wrist, extracarpal or carpal fractures (distal radius and scaphoid respectively) are frequently associated with SLIL tears.[32] However, most joint injuries are more subtle in nature (microscopic damage versus fractures), making them difficult to diagnose and treat. The earlier the diagnosis, the better the chance will be for surgical intervention to be successful. However, in most cases SLIL injury is not diagnosed until the latter stages when radiographs clearly show the presence of abnormality, which further highlights the need for a tool to evaluate injury. The ability to monitor the location of peak contact pressure and contact pressure distribution *in vivo*, may provide a means to differentiate between injury/instability patterns, and also help predict tissue wear or the onset and progression of degradation. With further work, it may be possible to construct a database of pressures and pressure distributions that correspond to clinically observed patterns of degeneration. This may prove to be a valuable tool to evaluate soft tissue injuries. Studies are also investigating the relationship between biochemical changes in cartilage at the tissue level and OA risk.[33] MRI-based SCM correlated with physiological data has the potential to be a powerful tool to evaluate joint injuries.

In conclusion, this study provides novel *in vivo* data on the effects of SLIL injury on radiocarpal mechanics and results indicate detrimental alterations subsequent to injury. This has the potential to provide insight into the progression of joint instability with altered mechanics, which may improve efficacy of treatment measures to minimize risk of OA development.

Acknowledgements

We would like to acknowledge NIH R01EB008709 grant funding, Columbia University for use of Joint_Model software, A. Schmitt for technical assistance with MR imaging and M. Humphrey, E. Tobaben and M. Mandala for assistance with image processing.

3.6. References

1. Kijima, Y, Viegas, SF. 2009. Wrist anatomy and biomechanics. J Hand Surg [Am] 34: 1555-1563.

2. Manuel, J, Moran, SL. 2010. The diagnosis and treatment of scapholunate instability. Hand Clin 26: 129-144.

3. Ruby, LK, An, KN, Linscheid, RL, et al. 1987. The effect of scapholunate ligament section on scapholunate motion. J Hand Surg [Am] 12: 767-771.

4. Sokolow, C. 2001. Anatomy and histology of the scapholunate ligament. Hand Clin 17: 77.

5. Buckwalter, JA, Martin, JA. 2006. Osteoarthritis. Advanced Drug Delivery Reviews 58: 150-167.

6. Buckwalter, JA, Saltzman, C, Brown, T. 2004. The impact of osteoarthritis: implications for research. Clin Orthop: S6-15.

7. Lawrence, RC, Felson, DT, Helmick, CG, et al. 2008. Estimates of the prevalence of arthritis and other rheumatic conditions in the United States: Part II. Arthritis Rheum 58: 26-35.

8. Dillon, CF, Hirsch, R, Rasch, EK, Gu, Q. 2007. Symptomatic Hand Osteoarthritis in the United States: Prevalence and Functional Impairment Estimates from the Third U.S. National Health and Nutrition Examination Survey, 1991-1994. Am J Phys Med Rehabil 86: 12-21.

9. Dillon, CF, Rasch, EK, Gu, Q, Hirsch, R. 2006. Prevalence of knee osteoarthritis in the United States: arthritis data from the Third National Health and Nutrition Examination Survey 1991-94. J Rheumatol 33: 2271-2279.

10. Anderson, DD, Chubinskaya, S, Guilak, F, et al. 2011. Post-traumatic osteoarthritis: Improved understanding and opportunities for early intervention. J Orthop Res 29: 802-809.

11. Watson, HK, Ryu, J. 1986. Evolution of arthritis of the wrist. Clin Orthop: 57-67.

12. Andriacchi, TP, Mündermann, A, Smith, RL, et al. 2004. A Framework for the in Vivo Pathomechanics of Osteoarthritis at the Knee. Ann Biomed Eng 32: 447-457.

13. Werner, FW, Sutton, LG, Allison, MA, et al. 2011. Scaphoid and lunate translation in the intact wrist and following ligament resection: a cadaver study. J Hand Surg Am 36: 291-298.

14. Johnson, JE, McIff, TE, Lee, P, et al. 2012. Validation of radiocarpal joint contact models based on images from a clinical MRI scanner. Comput Methods Biomech Biomed Engin: Epub ahead of print.

15. Werner, FW, Short, WH, Green, JK. 2005. Changes in Patterns of Scaphoid and Lunate Motion During Functional Arcs of Wrist Motion Induced by Ligament Division. The Journal of Hand Surgery 30: 1156-1160.

16. Short, WH, Werner, FW, Fortino, MD, et al. 1995. A dynamic biomechanical study of scapholunate ligament sectioning. J Hand Surg [Am] 20: 986-999.

17. Crisco, JJ, Wolfe, SW, Neu, CP, Pike, S. 2001. Advances in the in vivo measurement of normal and abnormal carpal kinematics. The Orthopedic clinics of North America 32: 219-231.

18. Eckstein, F, Cicuttini, F, Raynauld, JP, et al. 2006. Magnetic resonance imaging (MRI) of articular cartilage in knee osteoarthritis (OA): morphological assessment. Osteoarthritis Cartilage 14: 46-75.

19. Yao, J, Salo, AD, Lee, J, Lerner, AL. 2008. Sensitivity of tibio-menisco-femoral joint contact behavior to variations in knee kinematics. J Biomech 41: 390-398.

20. Moritomo, H, Murase, T, Goto, A, et al. 2006. In vivo three-dimensional kinematics of the midcarpal joint of the wrist. J Bone Joint Surg Am 88: 611-621.

21. Fernandez, JW, Pandy, MG. 2006. Integrating modelling and experiments to assess dynamic musculoskeletal function in humans. Exp Physiol 91: 371-382.

22. Kwak, SD, Blankevoort, L, Ateshian, GA. 2000. A Mathematical Formulation for 3D Quasi-Static Multibody Models of Diarthrodial Joints. Comput Methods Biomech Biomed Engin 3: 41-64.

23. Majima, M, Horii, E, Matsuki, H, et al. 2008. Load transmission through the wrist in the extended position. J Hand Surg Am 33: 182-188.

24. Ledoux, P, Lamblin, D, Targowski, R. 2001. Modifications to the mechanical behavior of the wrist after fracture of the scaphoid. Modeling by finite element analysis. Acta Orthop Belg 67: 236-241.

25. Woltring, HJ. 1994. 3-D attitude representation of human joints: a standardization proposal. J Biomech 27: 1399-1414.

26. Fisk, GR. 1980. An overview of injuries of the wrist. Clin Orthop: 137-144.

27. Hara, T, Horii, E, An, KN, et al. 1992. Force distribution across wrist joint: application of pressure-sensitive conductive rubber. J Hand Surg [Am] 17: 339-347.

28. Fischer, KJ, Johnson, JE, Waller, AJ, et al. 2011. MRI-Based Modeling for Radiocarpal Joint Mechanics: Validation Criteria and Results for Four Specimen-Specific Models. J Biomech Eng 133: 101004.

29. Patterson, R, Viegas, SF. 1995. Biomechanics of the wrist. J Hand Ther 8: 97-105.

30. Seedhom, BB. 2006. Conditioning of cartilage during normal activities is an important factor in the development of osteoarthritis. Rheumatology (Oxford) 45: 146-149.

31. Garcia-Elias, M. 1997. Kinetic analysis of carpal stability during grip. Hand Clin 13: 151-158.

32. Larsen, CF, Amadio, PC, Gilula, LA, Hodge, JC. 1995. Analysis of carpal instability: I. Description of the scheme. J Hand Surg [Am] 20: 757-764.

33. McAlindon, TE, Nuite, M, Krishnan, N, et al. 2011. Change in knee osteoarthritis cartilage detected by delayed gadolinium enhanced magnetic resonance imaging following treatment with collagen hydrolysate: a pilot randomized controlled trial. Osteoarthritis Cartilage 19: 399-405.

3.7. Tables

Table 3.1. Means and standard errors (±) of select contact parameters compared between normal and injured wrists for both radiolunate (RL) and radioscaphoid (RS) articulations. * indicates injured parameters significantly different from normal.

Mean (± Standard Error)		**Normal**	**Injured**
RL	*Mean Contact Pressure (MPa)*	0.37 (0.06)	0.47 (0.05)
	Model Contact Area (mm^2)	53 (9)	72 (8)
	Direct Contact Area (mm^2)	58 (10)	81 (9)
RS	*Mean Contact Pressure (MPa)*	0.38 (0.04)	0.48 (0.05)*
	Model Contact Area (mm^2)	60 (5)	86 (14)*
	Direct Contact Area (mm^2)	63 (6)	90 (12)

3.8. Figures

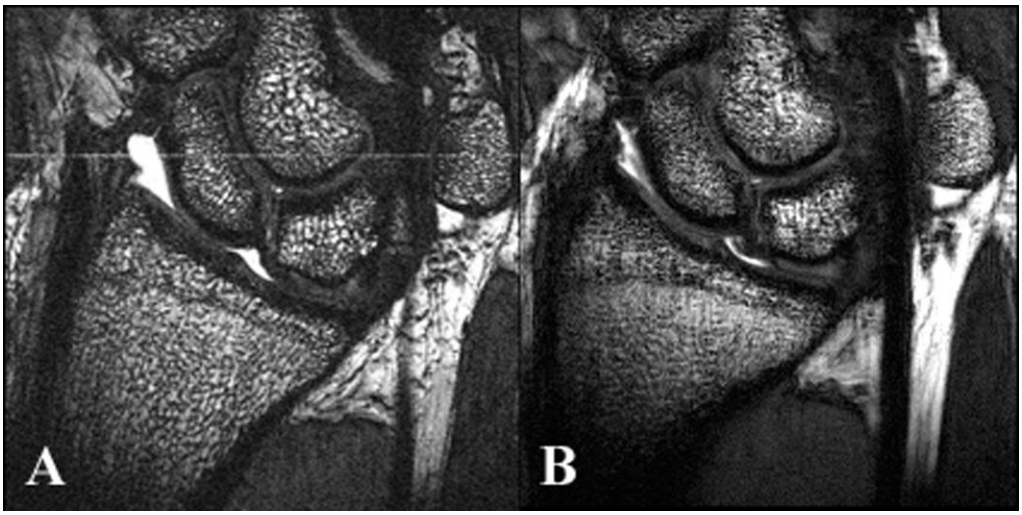

Figure 3.1. MRI of the wrist acquired using CISS sequence at (A) high resolution with the hand relaxed for model construction and at (B) low resolution during functional light grasp for image registration. Coronal views shown, which were used for image segmentation.

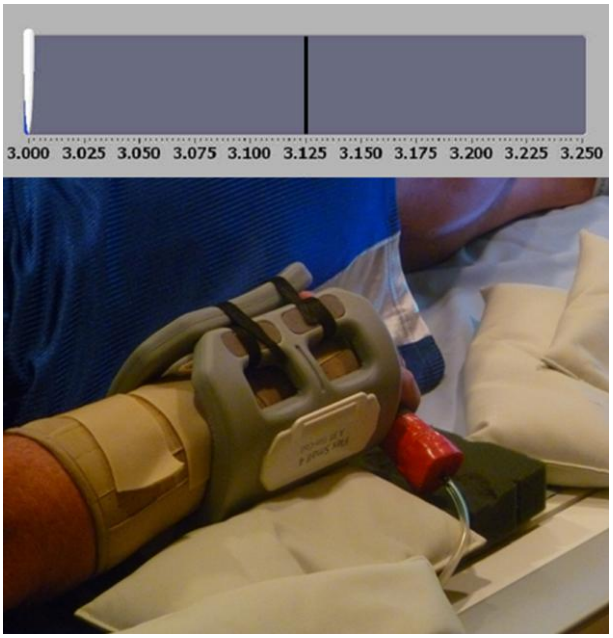

Figure 3.2. Top shows the visual feedback provided for subjects to grasp to the specified target (black line). Bottom shows the grip device for performing the grasp activity with the wrist braced for consistent loaded positions.

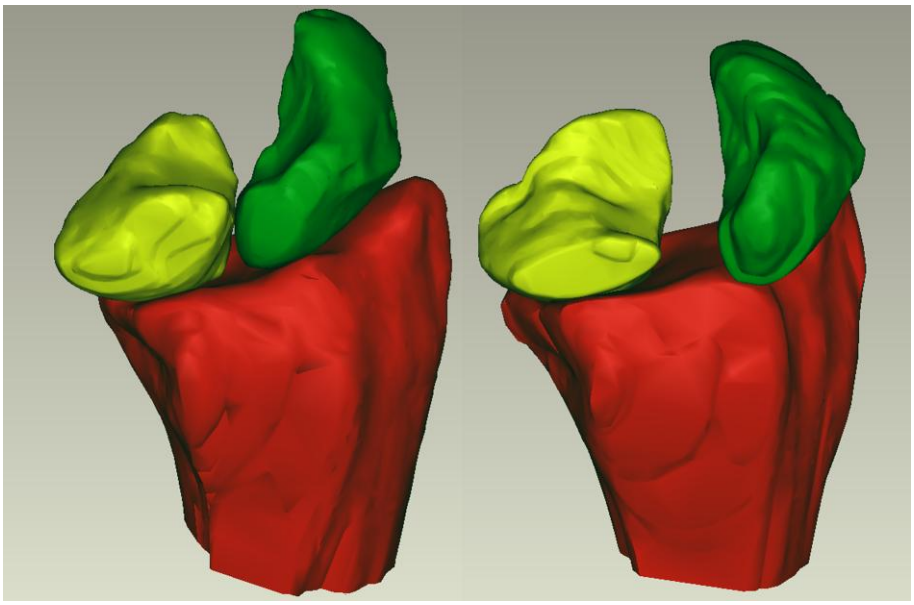

Figure 3.3. The 3D surface models of the radiocarpal joint for normal (left) and injured (right) wrists of Subject 7. Radius (red), lunate (yellow) and scaphoid (green) bones with their articulations are shown from a standard postero-anterior (dorsal) perspective.

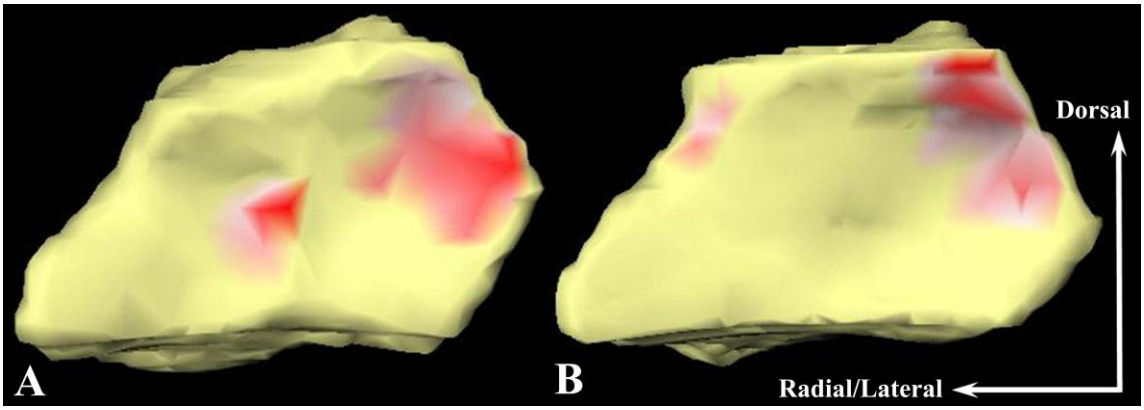

Figure 3.4. Contact patterns on the radius for normal (A) and injured (B) wrists of Subject 7. RS contact is on the left and RL contact is on the right of each radius.

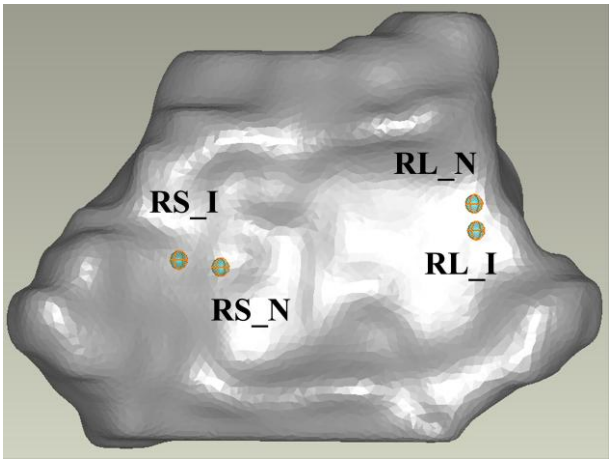

Figure 3.5. Locations of centroids of radiocarpal contact for normal (N) and injured (I) wrists of Subject 4. An increase in the intercentroid distance was observed with injury.

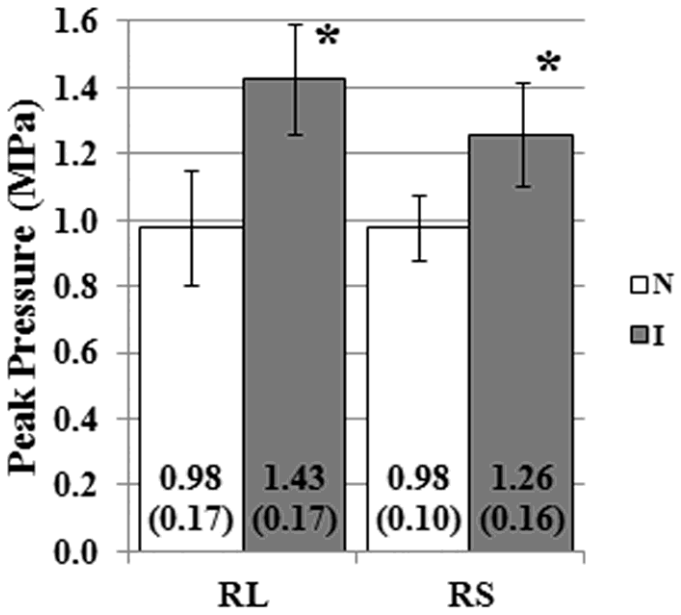

Figure 3.6. Means and standard errors of radiocarpal peak contact pressures, which were significantly higher in the injured (I) wrist compared to normal (N). * indicates $p<0.05$.

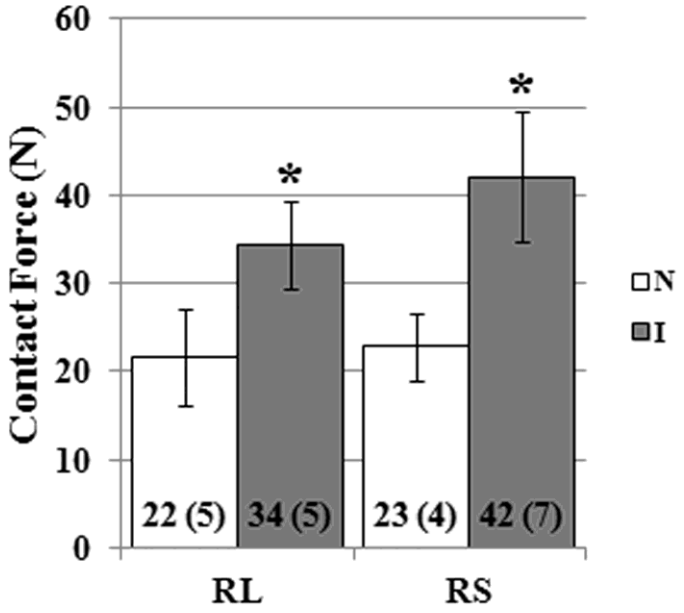

Figure 3.7. Means and standard errors of radiocarpal contact forces, which were significantly higher in the injured (I) wrist compared to normal (N). * indicates $p<0.05$.

This page left intentionally blank.

4. EFFECTIVENESS OF SURGICAL RECONSTRUCTION TO RESTORE RADIOCARPAL JOINT MECHANICS AFTER SCAPHOLUNATE LIGAMENT INJURY. AN IN VIVO MODELING STUDY

This page left intentionally blank.

Submitted to Journal of Biomechanics

Original article

EFFECTIVENESS OF SURGICAL RECONSTRUCTION TO RESTORE RADIOCARPAL JOINT MECHANICS AFTER SCAPHOLUNATE LIGAMENT INJURY. AN IN VIVO MODELING STUDY.

Joshua E. Johnson[a], Phil Lee[b], Terence E. McIff[c], E. Bruce Toby[c] and Kenneth J. Fischer[a,c,*]

[a]*Department of Mechanical Engineering, University of Kansas, 3138 Learned Hall, Lawrence, Kansas, 66045, USA*

[b]*Hoglund Brain Imaging Center, University of Kansas Medical Center, 3901 Rainbow Boulevard, Kansas City, Kansas, 66160, USA*

[c]*Department of Orthopedic Surgery, University of Kansas Medical Center, 3901 Rainbow Boulevard, Kansas City, Kansas, 66160, USA*

[*]Corresponding author

1530 W. 15th St, 3138 Learned Hall, Lawrence, Kansas, 66045, USA

Phone: +1 785 864 2994

Fax: +1 785 864 5254

E-mail address: fischer@ku.edu

Keywords: Scapholunate Dissociation, Modeling, Contact Pressure, Magnetic Resonance Imaging, Posttraumatic Osteoarthritis

Word count: 3442

4.1. Abstract

Disruption of the scapholunate ligament can cause a loss of normal scapholunate mechanics and eventually lead to osteoarthritis. Surgical reconstruction attempts to restore scapholunate relationship and shows improvement in functional outcomes, but postoperative effectiveness in restoring normal radiocarpal mechanics still remains a question. The objective of this study was to investigate the benefits of surgical repair by observing changes in contact mechanics on the cartilage surface before and after surgical treatment. Six patients with unilateral scapholunate dissociation were enrolled in the study, and displacement driven magnetic resonance image based-surface contact modeling was used to investigate normal, injured and postoperative radiocarpal mechanics. Model geometry was acquired from images of wrists taken in a relaxed position. Kinematics were acquired from image registration between the relaxed images, and images taken during functional loading. Results showed a trend for increase in radiocarpal contact parameters with injury. Peak and mean contact pressures significantly decreased after surgery in the radiolunate articulation and there were no significant differences between normal and postoperative wrists. Results indicated surgical repair improves contact mechanics after injury and that contact mechanics can be surgically restored to be similar to normal. This study provides novel contact mechanics data on the effects of surgical repair after scapholunate ligament injury. With further work, it may be possible to more effectively differentiate between treatments and degenerative changes based on in vivo contact mechanics data.

4.2. Introduction

Wrist joint motion involves a complex interplay between articulating geometries and ligamentous constraints, which play a vital role in joint stability (Berger, 1997). The scapholunate interosseous ligament (SLIL) is the primary stabilizer of the scapholunate (SL) joint (Kijima and Viegas, 2009). Disruption of the SLIL is a common injury, known as scapholunate dissociation (Kuo and Wolfe, 2008), and can lead to instability. Scapholunate instability disrupts the normal scapholunate relationship (Ruby et al., 1987). The misalignment results in abnormal radiocarpal kinematics and load transfer (Ruby et al., 1987; Sokolow, 2001). Subsequent changes in distributions of articular surface contact are associated with progressive degeneration known as scapholunate advanced collapse (SLAC), the most common cause of wrist osteoarthritis (Watson and Brenner, 1985).

Osteoarthritis (OA) is the most functionally and economically debilitating of the degenerative joint diseases (Buckwalter et al., 2004). Both age and joint injuries are known risk factors for OA (Anderson et al., 2011). Cartilage damage can occur from direct injury to the joint, or from progressive instability due to ligamentous injuries. There is a high risk of OA after ligament injuries (Anderson et al., 2011). SLIL injury, if untreated, generally leads to radiocarpal OA (Roberts et al., 2006).

Due to its subtlety, scapholunate dissociation is not often diagnosed early. Also, the rate of progression to SLAC arthropathy varies between individuals. Thus, time from SLIL injury that allows for successful repair is not established (Pomerance, 2006), and ideal treatment when the SLIL is irreparable is unknown (Pollock et al., 2010). The various treatments have inconsistent postoperative outcomes (Saffar et al., 1999), so more data on treatment methods may improve outcomes.

Contact pressure and changes in contact locations and patterns are important mechanical factors in the pathomechanics of OA (Andriacchi et al., 2004). Contact mechanics can be evaluated efficiently by surface contact modeling based on magnetic resonance image (MRI). Joint mechanics data from surface contact modeling can illustrate injury contact patterns and show effectiveness of surgical interventions.

Cadaveric studies cannot adequately assess complex in vivo conditions (active muscle forces and dynamic stability), nor the effectiveness of surgery after healing or at other future times. Cadaveric studies that have investigated treatments for scapholunate dissociation, have primarily examined limited fusions (Viegas and Patterson, 1997). Few studies have investigated in vivo wrist joint mechanics, though recent work in our lab has shown the effects of SLIL injury on radiocarpal mechanics. There does not appear to be any prior work on efficacy of surgical repair to restore normal radiocarpal joint mechanics after SLIL injury.

Hence, the goal of this study was to investigate immediate benefits of surgical repair by observing changes in contact mechanics on the cartilage surface before and after surgical treatment. Our hypothesis was that peak and mean contact pressures would increase with injury, and decrease postoperatively to values near normal.

4.3. Materials and methods

Six human subjects were enrolled for protocols approved by the internal review board. Subjects were males with a mean age of 31.3 years (22 to 55). Subjects were diagnosed with unilateral scapholunate dissociation, without visual indication of OA (no focal defects or bone-on-bone contact observed on MRI, and arthroscopic evaluation in some cases), by a board certified physician (injured wrists). Contralateral wrists, with no prior history of injury, were used as controls (normal wrists). Injured wrists were re-evaluated 12 to 15 weeks after surgical repair (postoperative wrists).

Functional data was collected for normal, injured and postoperative wrists. Grip strength levels were measured using a hand dynamometer (Baseline®). Pain levels were measured using a visual analogue scale (0=minimum to 10=maximum) for four conditions: during rest, during daily activities (with splint), during grip strength test and after grip strength test.

MRI was acquired using constructive interference steady state (CISS) or dual echo steady state (DESS) sequences in a 3T clinical scanner. Two image sets were acquired for each wrist. Injured wrists were first imaged at high resolution (CISS: in-plane voxel 0.15×0.15 mm, scan time ~ 12 mins; DESS: in-plane voxel 0.22×0.2 mm, scan time 4.5 mins; out-of-plane thickness 0.5 mm for both) with the hand relaxed (unloaded). Then, images were acquired during

functional grasp (loaded) at reduced resolution (CISS: in-plane voxel 0.30×0.30 mm, scan time 196 s; DESS: in-plane voxel 0.31×0.31 mm, scan time 188 s; out-of-plane thickness 1.0 mm for both) to minimize scan time (Fig. 4.1). Grasp involved constantly gripping to a specified target (3.125 psi) for the duration of the scan. This target was previously determined to create minimal discomfort while gripping for up to four minutes. Reduced scan times were to minimize subject fatigue and motion artifacts (especially with injury), while acquiring images with adequate resolution. Wrists were braced to ensure consistent loaded positions during grasp (Fig. 4.2). The normal and postoperative wrists were similarly scanned.

Surface contact modeling required model geometries, kinematics and a contact relationship (i.e. contact pressure linearly proportional to strain). Radius, lunate and scaphoid bones with their cartilage surfaces, were segmented from the high resolution images (ScanIP, Simpleware, Exeter, UK). These were wrapped with triangular surface elements to create undeformed 3D surface models of the radiolunate and radioscaphoid articulations for the normal, injured and postoperative wrists (Fig. 4.3).

Kinematics were acquired using markerless volume-based image registration between relaxed and functionally loaded image sets (Analyze 5.0, Analyze Direct, Overland Park, KS). Bone only segmentations were used for image registration based on the assumption that bones deformed negligibly under light grasp, while cartilage deformed even under the low loading conditions. First, the radius was used as a fixed reference to align the loaded and unloaded image sets. The transformation from this step was used to place the loaded images of carpal bones in the unloaded image coordinate system. Lastly, unloaded carpal bone image sets were registered to the "transformed" loaded carpal bone image sets. Thus, scaphoid and lunate kinematics were obtained for the normal, injured and postoperative wrists. The kinematics placed the unloaded carpal bone models in the functionally loaded state.

Model geometries and kinematics were implement in the Joint_Model program to obtain displacement constrained contact mechanics (Kwak et al., 2000). Contact areas and locations of contact were determined directly from overlapping surface elements of the rigid bodies in the functionally loaded state. A uniform thickness of 1 mm was assigned to each articular surface based on typical values (Johnson et al., 2012). While the cartilage thickness was uniform,

articular surfaces were the actual anatomical surfaces from the MR images. The overlap and total thickness were used to estimate deformation at each node, which gave a first order approximation of the local cartilage strain. Since the images were acquired over a relatively long period of time, it was assumed that the cartilage was substantially relaxed. Hence, an effective compressive relaxation modulus of 4 MPa was used as material property (Kwak et al., 2000). Local contact pressure was determined from the nodal strain and material property. The nodal contact pressures were integrated over the contact area associated with each node, to obtain contact force. The ratio of contact force to contact area gave the mean contact pressure.

We also determined contact areas directly from the loaded MR images. Regions of articular surface contact were visible in the images. These were segmented individually using b-splines from each image in the image set, to obtain arcs of contact. Each contact arc length was calculated from the b-splines and multiplied by the slice thickness. These were summed to obtain the effective contact area for each articulation. These "direct" contact areas were compared to the model contact areas to verify modeling accuracy. Locations of scaphoid and lunate centroids of contact were also determined from the loaded images to obtain scapholunate intercentroid distances, which were compared between the normal, injured and postoperative wrists.

Contact pressure distributions were qualitatively compared between normal, injured and postoperative wrists. Grip strength, peak and mean contact pressures, contact forces, model contact areas and intercentroid distances, were compared between the three conditions using one-way repeated measures analysis of variance (ANOVA). Two-way ANOVA was used to compare pain levels between state and condition, and also contact areas between method (model, direct) and condition. All data were tested for parametric assumption. Tukey's LSD was used for post hoc analysis with significance defined as $p < 0.05$. Linear regression analysis was performed to determine the relationship between model and direct contact areas. Power analysis was also performed to estimate number of subjects that would be required to observe significant differences.

4.4. Results

All data is presented as means (± standard error). For all subjects, locations of scaphoid and lunate contact on the radius were commonly in the mid to dorsal region and also along the entire

fossa (volar to dorsal). With injury, scaphoid contact appeared to shift dorsal and sometimes also laterally toward the styloid region, while lunate contact shifted away from dorsal towards the middle. Figure 4.4 shows the dorsal-lateral shift in radioscaphoid contact with injury (B) compared to normal (A). Surgery appeared to return the contacts somewhat towards their normal locations (Fig. 4.4C). There were no significant differences in intercentroid distances between the normal, injured and postoperative wrists (15.06 ± 0.69, 16.59 ± 0.78 and 16.76 ± 1.05 mm, respectively).

Grip strength significantly decreased in the injured wrists (66.8 ± 19.2 lbs) compared to the normal (110.2 ± 9.8 lbs). Grip strength was also significantly lower in the postoperative wrists (74.2 ± 13.1 lbs) compared to the normal but there were no significant differences between the injured and postoperative wrists. Pain levels were significantly higher when performing daily activities (2.0 ± 0.5), compared to when at rest (0.9 ± 0.5). There was a strong trend for increase in pain levels during the grip strength test (1.7 ± 0.6), compared to when at rest. There were no significant differences in pain levels between when at rest and after the grip strength test (1.3 ± 0.5). Also, pain levels were significantly higher in the injured wrists (3.6 ± 1.3) compared to normal (0). However, pain levels were similar to normal, postoperatively (0.8 ± 0.4).

In the radiolunate articulation, there was a trend for increase in peak and mean contact pressures with injury (Figs. 4.5, 4.6). There was a significant decrease in peak ($p = 0.023$) and mean ($p = 0.044$) contact pressures postoperatively, compared to the injured wrists (Figs. 4.5, 4.6). There were no significant differences between the normal and postoperative wrists. In the radioscaphoid joint, no significant differences were observed between normal, injured and postoperative wrists (Figs. 4.5, 4.6), though there was a strong trend for decrease in peak contact pressure postoperatively, compared to the injured wrists.

Contact force showed a trend for increase in the injured wrists for both the radiolunate and radioscaphoid articulations (Table 4.1). After surgery, contact force showed a strong trend for decrease but there were no significant differences in contact force (Table 4.1).

Similarly, model contact area showed a trend for increase with injury, and decrease after surgery in both the radiolunate and radioscaphoid articulations (Table 4.1). There were no significant differences between contact areas in both articulations. Also, there were no significant differences between model and direct contact areas in both articulations. Model contact areas

were within 10 mm^2 of the direct contact areas in the radiolunate articulation (Table 4.1). Aside from the postoperative wrists, model contact areas were within 2 mm^2 of the direct contact areas in the radioscaphoid articulation (Table 4.1). Regression analysis of all contact area data, showed a significant relationship between model and direct contact area measurements ($R^2 = 0.88$; slope = 0.79 and $R^2 = 0.78$; slope = 1.3 for the radiolunate and radioscaphoid articulations respectively, $p < 0.001$).

To differentiate between effects of surgical repair on contact parameters after injury, results from power analysis indicated that typically 7 to 10 subjects will be required. To observe changes in normal mechanics after injury, 10 to 15 subjects would be needed.

4.5. Discussion

We investigated the in vivo effects of SLIL injury on normal radiocarpal mechanics, and subsequent surgical repair to restore normal scapholunate relationship, using MRI-based surface contact modeling. An adverse mechanical response to the injury was observed from the tendency of contact parameters to increase post injury. The study showed a significant decrease in contact pressures in the radiolunate joint of the postoperative wrists, compared to the injured, and there were no significant differences between normal and postoperative wrists. A trend toward decrease in other contact parameters was also observed post surgery. The results supported our hypothesis that surgical intervention lowers elevated contact parameters after injury, returning them to near normal.

It is believed that SLIL disruption alone may not produce significant widening of the SL interval (Kuo and Wolfe, 2008). SL diastasis visible on plain radiographs, may also indicate progressive damage to the secondary stabilizers (Manuel and Moran, 2010). SL diastasis after injury, was generally observed by a separation in the locations of scaphoid and lunate contact on the radius articular surface qualitatively (Fig. 4.4), and also from the trend toward increase in intercentroid distance quantitatively. Normal intercentroid distances from this study (15.06 ± 0.69 mm) were similar to those observed in previous studies (14.91 mm) (Patterson and Viegas, 1995).

SL diastasis visible in the unloaded position (Fig. 4.3 center), suggests progressive instability from damage to the secondary stabilizers. The dorsal (scaphoid) and volar (lunate) shifts in

contact locations observed after injury are indicative of dorsal intercalated segment instability deformity, where the lunate extends and the scaphoid collapses into flexion.(Kuo and Wolfe, 2008) The radiocarpal articulations are considered incongruous (Patterson and Viegas, 1995), hence the non-uniform/unsymmetrical contact patterns were expected.

Functional data were consistent with physical examinations of SLIL injury. There is a loss of grip strength and increase in pain levels after injury (Manuel and Moran, 2010), as observed in this study, likely due to the shift in contact locations and abnormal load transfer through the joint. Surgical repair attempts to minimize pain and improve function. Pains levels were similar to normal postoperatively, which is a common outcome of surgery (Kuo and Wolfe, 2008; Manuel and Moran, 2010). No significant improvements in grip strength after surgery could be a result of subjects being cautious and protecting the repair. However, improvements in grip strength have also been observed over time (Chabas et al., 2008; Garcia-Elias et al., 2006).

Peak and mean contact pressures were expected to increase with injury in both radiolunate and radioscaphoid articulations. Prior work in our lab has shown peak and mean contact pressures to significantly increase in the radioscaphoid articulation, and peak pressure to significantly increase in the radiolunate articulation. An increase in contact pressure above a certain threshold, may be a risk factor for initiation of degenerative changes. However, a more critical mechanism may be a shift in contact location (particularly in the radioscaphoid articulation) to normally unloaded articular regions, even though increase in contact pressure is not significant.

While there were no significant differences, contact forces and model contact areas in particular, showed a trend for increase with injury in both articulations. Prior work in our lab has also shown all contact parameters to increase significantly with injury in the radioscaphoid articulation. This corresponds to the clinically observed SLAC pattern, where degenerative changes are initially observed at the radioscaphoid region, and then progress medially (Weiss and Rodner, 2007). The grasp activity was always the same, so the trend toward increase in contact forces with injury may be due to co-contracture, to stabilize the injured joint. This is also indicated by the fact that after surgery, contact forces showed a strong trend to decrease to near normal values postoperatively. Experiments have shown normal contact forces and contact areas

to be higher in the radioscaphoid articulation compared to the radiolunate articulation (Patterson and Viegas, 1995), which was observed in this study.

The significant relationship between model and direct contact area measurements from regression analysis (and no significant differences from two-way ANOVA), suggests reliability of the MRI-based surface contact modeling technique. The usefulness of the method of estimating contact area from grasp MR images to verify in vivo modeling accuracy, has been previously shown (Johnson et al., 2012). Due to the possibility of motion artifacts with human subjects (especially for loaded scans), the consistently higher values may indicate a tendency to overestimate direct contact area measurements.

The observed trends and variation in data could be attributed to the differences in injury/instability patterns between the subjects. SL instability can be clinically classified into predynamic, dynamic, static and SLAC stages (Manuel and Moran, 2010; Walsh, 2002). Of the six subjects, two were acute (< four weeks from injury and diagnosis), where the instability may have been minimal. One was subacute (between four weeks and six months). Three were chronic (> six months), which may have been sufficient time for progressive instability to develop.

Differences in stages of instability (Manuel and Moran, 2010; Walsh, 2002), variations in manifestation/progression of instability (Watson and Brenner, 1985; Werner et al., 2007), difficulty in treatment selection (Chabas et al., 2008; Garcia-Elias et al., 2006) and inconsistent outcomes (Chabas et al., 2008; Fortin and Louis, 1993; Pollock et al., 2010; Pomerance, 2006; Saffar et al., 1999), all highlight the importance of tools to evaluate soft tissue injuries and corrective measures, and the risk of OA development (Anderson et al., 2011). MRI-based surface contact modeling can be a useful tool to determine joint contact mechanics.

One limitation of the study was modeling a single pose to evaluate SLIL injury and surgical repair. Scapholunate motion occurs predominantly in flexion-extension (Gardner et al., 2006), and corresponding changes in kinematics after injury may be better visualized during this motion. However, there is minimal scapholunate motion during most functional activities (Gardner et al., 2006), and these positions may better indicate changes in mechanics with instability. The light grasp pose corresponded to the power grip activity, which the wrist

frequently undergoes during activities of daily living. Also, the clenched fist anteroposterior (longitudinal compressive load) view is commonly used to diagnose SL instability in its early stages (Manuel and Moran, 2010). Hence, the light grasp pose was considered appropriate to investigate the effects of injury and surgical repair, since subsequent mechanics have functional implications. It was also easier to acquire MR images to obtain model geometry and boundary conditions using a quasi-static pose. In the future, investigating mechanical changes during other dynamic functional activities, such as dart thrower's motion or circumduction, may also provide additional useful data.

To simplify the analysis, uniform cartilage thickness was assumed for each surface, which may have led to variation in strain estimates. This may also explain some of the variation in contact pressure results. Assigning spatially varying cartilage thickness values may further improve accuracy of acquiring subject-specific contact data. Also, the relatively low number of subjects may have resulted in fewer significant differences in contact parameters. Power analysis indicated that observed trends may become significant by doubling the number of subjects.

The surgeries performed were four direct ligament repairs, one three-ligament tenodesis (a modified Brunelli procedure according to Garcia-Elias et al. (2006)), and one scaphocapitate arthrodesis. Significant decreases in radiolunate peak and mean contact pressure postoperatively, indicated the benefits of having surgery. Surgical outcomes appeared positive from similarities in these radiolunate parameters between normal and postoperative wrists. However, the benefits may be limited by the severity of instability at the time of diagnosis. The longer the time between injury and treatment, the greater the possibility of the instability worsening. As mentioned before, with increasing severity, instability can progress to the periscaphoid region and eventually towards the lunate side. Decrease in postoperative contact pressures in the radiolunate articulation may indicate the effectiveness of treatments to correct less severe instabilities, which may not have had sufficient time to fully develop. No significant decrease in postoperative contact pressures suggests a more severe deformity in the radioscaphoid articulation, which may not have been completely corrected after surgery, indicating that more robust reconstruction techniques may be required for effective outcomes. Surgery tended to reduce the SL diastasis (Fig. 4.3 right), however not all contact locations appeared completely restored (Fig. 4.4). Lack

of significant reduction of the scapholunate interval may also suggest that longer time may be needed to heal after repair. This may provide an explanation as to why degenerative changes are sometimes observed even after surgical intervention. Due to the relatively low number of subjects, it was not possible to address effectiveness of reconstruction by technique. The mechanical outcomes of surgeries are expected to be different for ligament repairs, tendon weaves and salvage procedures, and an overall comparison of repair to injured and normal, though appearing positive, may not accurately present the complete picture. Further work is warranted to categorize reconstructive surgeries according to their biomechanical outcomes.

In conclusion, this study provides novel radiocarpal contact mechanics data on the efficacy of surgical repair after SLIL injury that further strengthens the importance of surgery to manage/halt the progression of instability and minimize/eliminate the risk of developing OA. Future work would include pooling subjects according to type of surgery and also investigating subsequent benefits at 1-2 years post surgery. The potential is to provide insight into the effectiveness of surgery from a contact mechanics perspective and better establish the extent to which each surgical repair/reconstruction restores normal joint mechanics.

Conflict of interest statement

The authors do not have any conflicts of interest to disclose.

Acknowledgements

We would like to acknowledge NIH R01EB008709 grant funding, Columbia University for Joint_Model software, A. Schmitt and F. Hunsinger for technical assistance with MR imaging and M. Humphrey, E.Tobaben, M. Mandala, S. Modaresi and Q. Zheng for assistance with image processing.

4.6. References

Anderson, D.D. Chubinskaya, S. Guilak, F. Martin, J.A. Oegema, T.R. Olson, S.A. Buckwalter, J.A., 2011. Post-traumatic osteoarthritis: Improved understanding and opportunities for early intervention. Journal of Orthopaedic Research 29, 802-809.

Andriacchi, T.P. Mündermann, A. Smith, R.L. Alexander, E.J. Dyrby, C.O. Koo, S., 2004. A Framework for the in Vivo Pathomechanics of Osteoarthritis at the Knee. Annals of Biomedical Engineering 32, 447-457.

Berger, R.A., 1997. The ligaments of the wrist. A current overview of anatomy with considerations of their potential functions. Hand Clinics 13, 63-82.

Buckwalter, J.A. Saltzman, C. Brown, T., 2004. The impact of osteoarthritis: implications for research. Clinical Orthopaedics and Related Research S6-15.

Chabas, J.-F. Gay, A. Valenti, D. Guinard, D. Legre, R., 2008. Results of the Modified Brunelli Tenodesis for Treatment of Scapholunate Instability: A Retrospective Study of 19 Patients. Journal of Hand Surgery. American Volume 33, 1469-1477.

Fortin, P.T. Louis, D.S., 1993. Long-term follow-up of scaphoid-trapezium-trapezoid arthrodesis. Journal of Hand Surgery. American Volume 18, 675-681.

Garcia-Elias, M. Lluch, A.L. Stanley, J.K., 2006. Three-Ligament Tenodesis for the Treatment of Scapholunate Dissociation: Indications and Surgical Technique. Journal of Hand Surgery. American Volume 31, 125-134.

Gardner, M.J. Crisco, J.J. Wolfe, S.W., 2006. Carpal kinematics. Hand Clinics 22, 413-420.

Johnson, J.E. McIff, T.E. Lee, P. Toby, E.B. Fischer, K.J., 2012. Validation of radiocarpal joint contact models based on images from a clinical MRI scanner. Computer Methods in Biomechanics and Biomedical Engineering, Epub ahead of print

Kijima, Y. Viegas, S.F., 2009. Wrist anatomy and biomechanics. Journal of Hand Surgery. American Volume 34, 1555-1563.

Kuo, C.E. Wolfe, S.W., 2008. Scapholunate Instability: Current Concepts in Diagnosis and Management. Journal of Hand Surgery. American Volume 33, 998-1013.

Kwak, S.D. Blankevoort, L. Ateshian, G.A., 2000. A Mathematical Formulation for 3D Quasi-Static Multibody Models of Diarthrodial Joints. Computer Methods in Biomechanics and Biomedical Engineering 3, 41-64.

Manuel, J. Moran, S.L., 2010. The diagnosis and treatment of scapholunate instability. Hand Clinics 26, 129-144.

Patterson, R. Viegas, S.F., 1995. Biomechanics of the wrist. Journal of Hand Therapy 8, 97-105.

Pollock, P.J. Sieg, R.N. Baechler, M.F. Scher, D. Zimmerman, N.B. Dubin, N.H., 2010. Radiographic Evaluation of the Modified Brunelli Technique Versus the Blatt Capsulodesis for Scapholunate Dissociation in a Cadaver Model. Journal of Hand Surgery. American Volume 35, 1589-1598.

Pomerance, J., 2006. Outcome After Repair of the Scapholunate Interosseous Ligament and Dorsal Capsulodesis for Dynamic Scapholunate Instability Due to Trauma. Journal of Hand Surgery. American Volume 31, 1380-1386.

Roberts, C. Porter, M. Wines, A.P. Shadbolt, B., 2006. The association of scapho-trapezio-trapezoid osteoarthrosis and scapholunate dissociation. Hand Surgery 11, 135-141.

Ruby, L.K. An, K.N. Linscheid, R.L. Cooney, W.P., 3rd Chao, E.Y., 1987. The effect of scapholunate ligament section on scapholunate motion. Journal of Hand Surgery. American Volume 12, 767-771.

Saffar, P. Sokolow, C. Duclos, L., 1999. Soft tissue stabilization in the management of chronic scapholunate instability without osteoarthritis. A 15-year series. Acta Orthopaedica Belgica 65, 424-433.

Sokolow, C., 2001. Anatomy and histology of the scapholunate ligament. Hand Clinics 17, 77.

Viegas, S.F. Patterson, R.M., 1997. Load mechanics of the wrist. Hand Clinics 13, 109-128.

Walsh, J.J., 2002. Current status of scapholunate interosseous ligament injuries. Journal of the American Academy of Orthopaedic Surgeons 10, 32.

Watson, H.K. Brenner, L.H., 1985. Degenerative disorders of the wrist. Journal of Hand Surgery. American Volume 10, 1002-1006.

Weiss, K.E. Rodner, C.M., 2007. Osteoarthritis of the Wrist. Journal of Hand Surgery. American Volume 32, 725-746.

Werner, F.W. Short, W.H. Green, J.K. Evans, P.J. Walker, J.A., 2007. Severity of scapholunate instability is related to joint anatomy and congruency. Journal of Hand Surgery. American Volume 32, 55-60.

4.7. Tables

Table 4.1. Contact force, model contact area and direct contact area data for normal, injured and postoperative wrists for both radiolunate (RL) and radioscaphoid (RS) articulations.

Mean (± Standard Error)		**Normal**	**Injured**	**Postoperative**
RL	*Contact Force (N)*	23 (6)	37 (6)	14 (5)
	Model Contact Area (mm^2)	58 (14)	70 (9)	46 (6)
	Direct Contact Area (mm^2)	61 (15)	79 (13)	50 (6)
RS	*Contact Force (N)*	27 (6)	40 (12)	22 (6)
	Model Contact Area (mm^2)	65 (8)	82 (23)	59 (14)
	Direct Contact Area (mm^2)	64 (8)	81 (16)	77 (8)

4.8. Figures

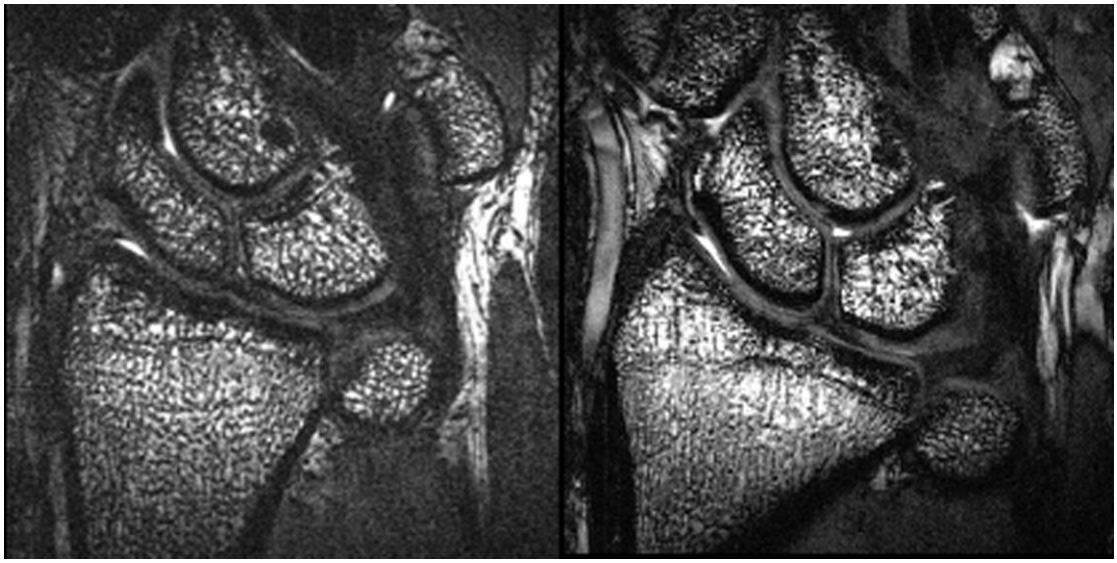

Figure 4.1. Sample MRI images of the normal wrist of Subject 1. Left shows a high resolution slice of the unloaded wrist used for model construction, while right shows a lower resolution slice acquired during functional loading for image registration.

Figure 4.2. Example wrist of a subject with the grip device in the active grasp position. The wrist was also braced for consistent loaded positions.

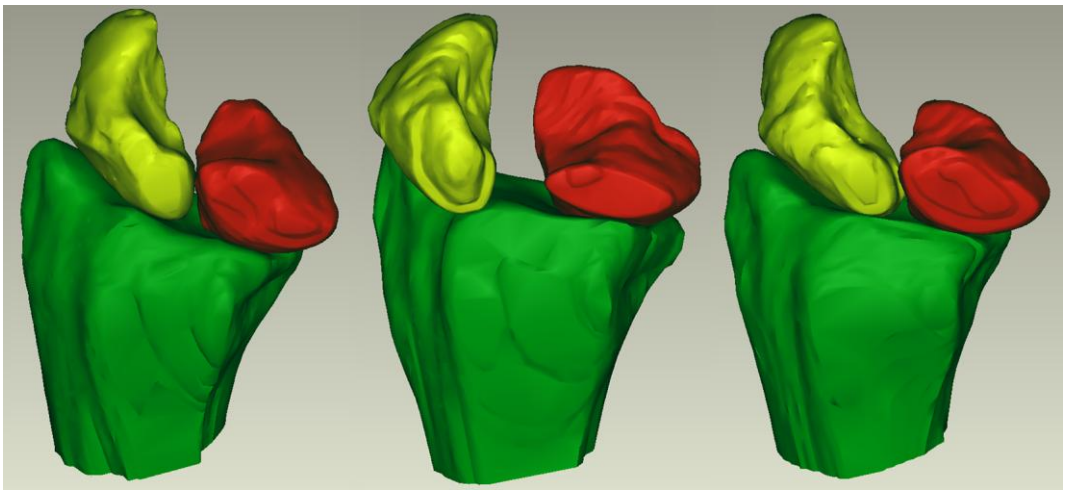

Figure 4.3. Normal (left), injured (center) and postoperative (right) surface models of the radiocarpal joint in the unloaded position, for Subject 5, from a dorsal/posterior view. Radius, lunate and scaphoid bones are colored green, red and yellow respectively.

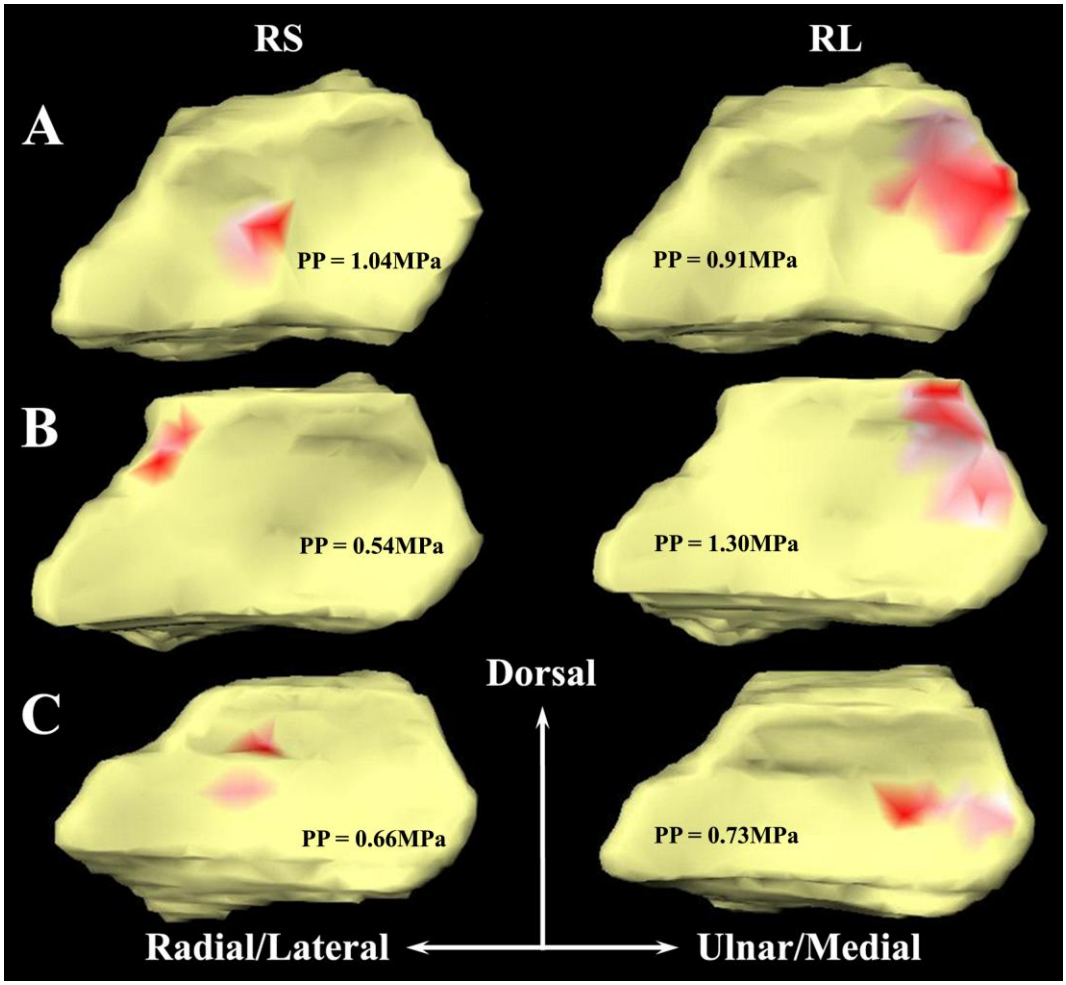

Figure 4.4. Normal (A), injured (B) and postoperative (C) contact locations of Subject 5, for radioscaphoid (RS) and radiolunate (RL) articulations, shown on the radius cartilage. Magnitude of contact pressures vary linearly from white (minimum) to dark red (maximum) for each articulation. Peak pressure (PP) values are also shown. The images for this particular subject illustrate clear separation of the scaphoid and lunate in the injured wrist, primarily due to scaphoid motion. After repair, the scaphoid moves medially to a position approaching the normal contact location. While this grossly illustrates the typical overall behavior, not all subjects exhibited these contact patterns.

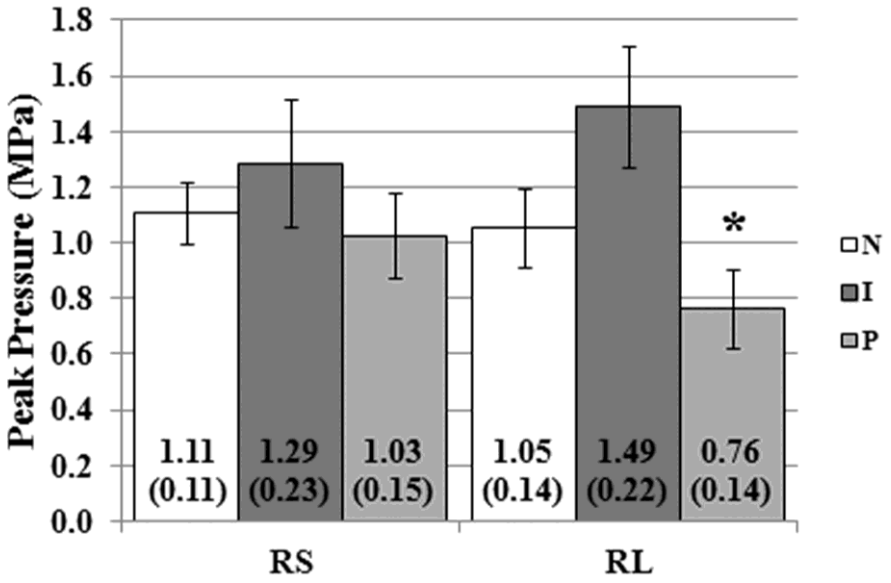

Figure 4.5. Means (± standard errors) of radioscaphoid (RS) and radiolunate (RL) peak contact pressures for normal (N), injured (I) and postoperative (P) wrists. * indicates significant difference from injured.

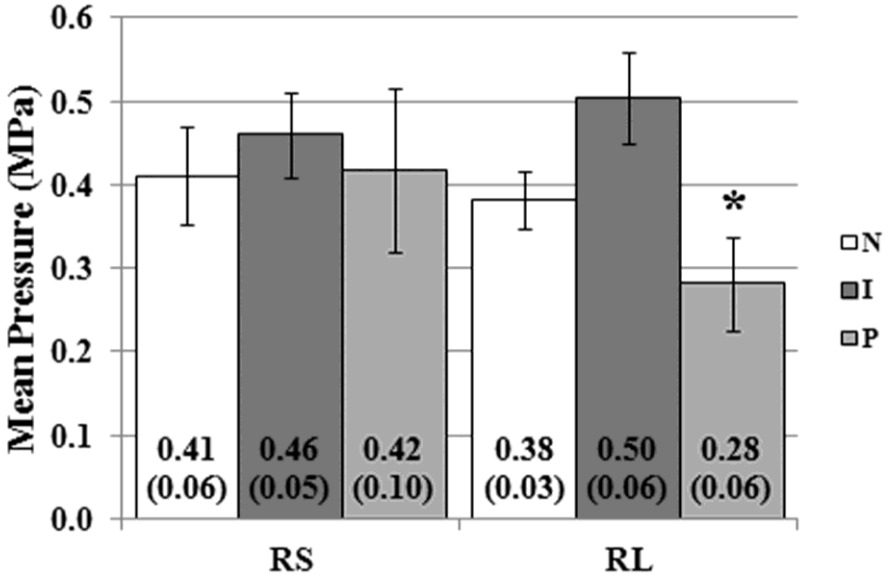

Figure 4.6. Means (± standard errors) of radioscaphoid (RS) and radiolunate (RL) mean contact pressures for normal (N), injured (I) and postoperative (P) wrists. * indicates significant difference from injured.

5. COMPUTATIONALLY EFFICIENT MRI-BASED SURFACE CONTACT MODELING AS A TOOL TO EVALUATE JOINT INJURIES AND OUTCOMES OF SURGICAL INTERVENTIONS

This page left intentionally blank.

Formatted for submission to Journal of Biomechanical Engineering

Computationally Efficient MRI-based Surface Contact Modeling as a Tool to Evaluate Joint Injuries and Outcomes of Surgical Interventions

1) Joshua E. Johnson

Department of Mechanical Engineering

University of Kansas, 3138 Learned Hall, Lawrence, KS, 66045

a2joe@ku.edu

2) Phil Lee

Hoglund Brain Imaging Center

University of Kansas Medical Center, 3901 Rainbow Boulevard, Kansas City, KS, 66160

plee2@kumc.edu

3) Terence E. McIff

Department of Orthopedic Surgery

University of Kansas Medical Center, 3901 Rainbow Boulevard, Kansas City, KS, 66160

tmciff@kumc.edu

4) E. Bruce Toby

Department of Orthopedic Surgery

University of Kansas Medical Center, 3901 Rainbow Boulevard, Kansas City, KS, 66160

btoby@kumc.edu

5) Kenneth J. Fischer[1]

Department of Mechanical Engineering, Department of Orthopedic Surgery

1530 W. 15th St, 3138 Learned Hall, Lawrence, Kansas, 66045

Phone: 785 864 2994

Fax: 785 864 5254

fischer@ku.edu

[1]Corresponding author

5.1. Abstract

Joint injuries and the resulting posttraumatic osteoarthritis (OA) are a significant problem. There is still a need for tools to evaluate joint injuries, their effect on joint mechanics, and the relationship between altered mechanics and OA. Better understanding of injuries and their relationship to OA may aid in the development or refinement of treatment methods. This may be partially achieved by monitoring changes in joint mechanics that are a direct consequence of injury. Techniques such as image-based finite element modeling can provide *in vivo* joint mechanics data, but can also be laborious and computationally expensive. Alternate modeling techniques that can provide similar results in a computationally efficient manner are an attractive prospect. It is likely possible to estimate risk of OA due to injury from surface contact mechanics data alone.

The objective of this study was to compare joint contact mechanics from image-based surface contact modeling (SCM) and finite element modeling (FEM), in normal, injured (scapholunate ligament tear) and surgically repaired radiocarpal joints. Magnetic resonance images (MRI) of the normal, injured, and postoperative wrists of three subjects were acquired when relaxed, and during functional grasp. Surface and volumetric models of the radiolunate and radioscaphoid articulations were constructed from the relaxed images for SCM and FEM analyses, respectively. Kinematic boundary conditions were acquired from image registration between the relaxed and grasp images. For the SCM technique, a linear contact relationship was used to estimate contact parameters based on interactions of the rigid articular surfaces in contact. For FEM, a pressure-overclosure relationship was used estimate parameters based on deformable body contact interactions. The SCM technique was able to evaluate variations in contact parameters arising from scapholunate ligament injury and also the effects of surgical repair, with similar accuracy to FEM. At least 80% of contact forces, peak contact pressures, mean contact pressures and contact areas from SCM were within 10 N, 0.5 MPa, 0.2 MPa and 15 mm^2 respectively, of the results from FEM, regardless of the state of the wrist. Depending on the application, the MRI-based SCM technique has the potential to provide clinically relevant subject-specific results in a computationally efficient manner compared to FEM.

5.2. Introduction

Computational modeling is very useful in biomechanics to simulate normal and pathologic joint function. It is also useful to determine the efficacies of various surgical procedures performed to treat joint pathologies and simulate their outcomes. Models can be used to estimate in situ parameters that are difficult to acquire through experiments non-invasively (such as contact pressure distributions). Currently, computational modeling is the only technique available to non-invasively evaluate *in vivo* joint contact mechanics [1]. However, most models make use of input parameters derived from various general sources such as literature, standards or experiments, and are therefore limited for patient-specific applications [2]. Joint injuries (soft tissue or articular surface) are a significant problem and there is still a need for tools to effectively evaluate joint injures and associated sequelae [3]. The ability to monitor the initiation and progression of joint instability after injury may aid in determining prognosis, leading to better treatment algorithms. In order to refine or develop treatments that are targeted towards individuals, it is important to focus on subject-specific models.

Several modeling techniques exist to evaluate *in vivo* joint mechanics. The common techniques include image-based finite element modeling (FEM) [4-13], rigid body spring modeling/discrete element analysis (RBSM) [14-16] or surface contact modeling (SCM) [17-19]. The models are either displacement driven or force driven. Generally, model geometries are acquired from modalities such as computed tomography (CT) [4-8, 14, 15, 19] or magnetic resonance imaging (MRI) [9-11, 17, 18]. Kinematics are determined through external (surface markers) or internal measures (biplanar radiography), while tendon forces are estimated from corresponding musculature (EMG and cross sectional area) and ground reaction forces are measured using force platforms [11, 20]. These loads and displacement boundary conditions are input into the model to infer joint kinetics/kinematics and resulting stresses and strains (surface and/or volumetric).

FEM is the most common and accurate method to determine stresses [20]. However, depending on the complexity of the problem, the process of developing the mesh can be laborious and obtaining a converged solution can be computationally intensive [21]. Depending on the type of problem (for instance, deformable versus rigid), more simplified analyses can be

performed based on relevant assumptions to determine appropriate solutions. This is the basis of RBSM and SCM techniques. Using these methods, joint mechanics can be evaluated in a computationally efficient manner compared to FEM [22]. The underlying question is whether these methods are competent to provide data that is sufficiently accurate for clinically relevant applications.

The ability to accurately determine joint mechanics has wide clinical implications, especially in complex joints such as the wrist. It may be possible to sufficiently evaluate changes in joint mechanics as a result of injury or surgical intervention, from surface contact mechanics data alone. This can be achieved through the SCM technique, without the need for a complex volumetric analysis [23]. However, the SCM technique has not been extensively used.

In vivo simulation studies more accurately represent physiological conditions than *ex vivo* studies (for instance, soft tissue interactions and dynamic motor stability), and can be used to assess temporal response to joint injuries and corresponding surgical treatments. Computational modeling has been extensively applied to the lower extremity to evaluate *in vivo* joint mechanics [4-11, 18]. In the wrist, studies have evaluated *in vivo* joint mechanics during functional activities [12, 14, 16, 17] and also simulated the effects of some carpal fractures and limited fusions [13, 15, 19]. In particular, scapholunate (SL) ligament injury is a commonly occurring wrist ligament injury that can lead to SL joint instability and progressive degenerative changes [24-27]. There does not appear to be any prior modeling work on the *in vivo* effects of SL ligament injury or surgical repair.

Hence, we investigated differences *in vivo* radiocarpal joint mechanics between the SCM and FEM techniques, after SL ligament injury and surgical repair. We did not intend to make comparisons between the normal, injured and postoperative states. Our goal was to show that contact parameters obtained from SCM would be comparable to those obtained from a similar FEM analysis regardless of wrist state, and to demonstrate the feasibility and applicability of the SCM technique.

5.3. Methods

Three human subjects diagnosed with unilateral SL ligament injury by a board certified physician, were enrolled for the study. Protocols were approved by the local Institutional Review Board. The subjects were all male with a mean age of 36 years. Preoperative images were first acquired of the injured and contralateral (normal) wrists. The injured wrists were imaged again 12 to 15 weeks post surgical repair (postoperative).

MR images were acquired using a constructive interference steady state (CISS) or a dual echo steady (DESS) state sequence. High resolution images were first acquired with the wrists in a relaxed position (unloaded) at 0.15 × 0.15 mm in-plane pixels for CISS sequence (field of view [FOV] = 95 × 61.8 mm^2, slice thickness = 0.5 mm, number of slices = 104, repetition time [TR] = 14.8 ms, echo time [TE] = 7.4 ms, flip angle = 60°, number of average = 1) and 0.22 × 0.2 mm in-plane pixels for DESS sequence (FOV = 100 × 48 mm^2, slice thickness = 0.5 mm, number of slices = 110, TR = 30 ms, TE = 5.7 ms, flip angle = 25°, number of average = 1). Then, images were acquired during active light grasp (loaded) at a lower resolution (CISS: voxel = 0.3×0.3 mm, slice thickness = 1.0 mm, number of slices = 52, TR = 12 ms, TE = 6 ms and DESS: voxel = 0.31×0.31 mm, FOV = 100×100 mm^2, slice thickness = 1.0 mm, number of slices = 52). The loaded scans were acquired at lower resolution to reduce scan time. This minimized subject fatigue and related motion artifacts during scanning, while maintaining adequate resolution for the modeling process. The grasp task involved gripping to a specified target with the help of a visual feedback system, and maintaining the grip for the duration of scan. The wrists were also braced in 20° extension during the scan to maintain a consistent loaded position between wrists.

Both the SCM and FEM techniques required model geometries, kinematics (displacement driven) and a contact relationship. For SCM, the radius and carpal bones (scaphoid and lunate) including their cartilage surfaces were segmented from the unloaded images using ScanIP® (Simpleware, Exeter, UK), to generate models of the radiocarpal articulations with triangular surface elements (Figure 5.1 left). The bones were assumed as rigid, that is, undergoing negligible deformation under the relatively light loading activity. Hence for FEM (Figure 5.1 right), only cartilage surfaces were segmented (same articular surfaces as SCM), which were used to generate 4-node tetrahedral meshed volumetric models using ScanFE® (Simpleware, Exeter, UK). Lunate, scaphoid and radius mesh refinement resulted in a range of 10805, 9691,

and 17740 nodes respectively, to 19301, 18286, and 28635 nodes, based on convergence analysis.

Kinematics were acquired from image registrations between the unloaded and loaded image volumes using Analyze 5.0® (Analyze Direct, Overland Park, KS). Since the bones were assumed as rigid, only the bone tissue of the radius and carpal bones was segmented from the two image sets. Briefly, the radius was used as a fixed reference to align the loaded and unloaded image sets. This reference transformation was used to reposition the loaded carpal bones into the unloaded coordinate system. Then, carpal bone transformations were determined between the unloaded carpal bones and loaded carpal bones (now in the same coordinate system as the unloaded images). This final transformation placed the unloaded carpal bone models, in the functionally loaded position.

Surface models of the radiocarpal articulations with the final kinematics, were implemented in the SCM software, Joint_Model [23]. A uniform thickness of 1 mm was assigned to each articular surface based on typical measured values. Though the thickness was uniform for analyses, the model articular surface was the actual anatomical surface from the images. Since the loaded images were acquired over a relatively long period of time, the cartilage was assumed to have had sufficient time to relax (approach equilibrium). Hence, an effective compressive relaxation modulus of 4 MPa was assigned to the articular surfaces [23]. Contact measures were determined from interactions of the rigid surfaces in contact, based on a linear contact rule. Contact area was calculated from overlapping nodes of the surface elements in contact. The depth of interpenetration/overlap was used to determine a first order estimate of normal compressive strain at each node in contact, based on the thicknesses of the cartilage surfaces at that location. These “deformations” were distributed to the nodes on each surface, based on the ratios of their thickness and modulus values. In the case of uniform thickness assumption, the thicknesses and modulii were the same for each surface in contact. Nodal contact pressures were determined from the local strains and material properties. Contact pressures were numerically integrated over the entire contact region to obtain the total compressive contact force on the articulation.

Volumetric models of the radiocarpal articulations together with kinematics, were also implemented in the FEM software, Abaqus® (Simulia, Providence, RI), on a Windows® PC with 12 processors. Since the cartilage was assumed to have substantially relaxed, time- and flow-independent material characteristics were assumed. Hence, the cartilage was modeled as an elastic, homogeneous and isotropic deformable solid. Similarly, the value of effective modulus was the same as for the SCM analysis. Due to the dual phase interstitial fluid-solid matrix interaction, the instantaneous response of articular cartilage is to behave as an incompressible material, where the hydrostatic forces support the loads applied to the joint surface. With time, fluid efflux and matrix compaction result in cartilage starting to become more compressible. Hence, Poisson's ratio $\nu = 0.20$ was chosen to model the long-term response of the hydrated cartilage matrix [28-30]. The subchondral nodes of the cartilage volumes were rigidly constrained by the kinematic boundary conditions. The linear penalty constraint method was used to enforce the pressure-overclosure relationship between the surfaces in contact. Frictionless contact was assumed between the articular surfaces (neglecting tangential behavior) and a finite sliding formulation was used to model the normal interaction between the bodies. Contact areas, contact forces, peak contact pressures and pressure distributions were determined. The solutions were accepted as converged after a less than 5% variation in contact force with mesh refinement.

To verify modeling accuracy, contact area results from the simulations were compared to contact areas directly measured from the loaded MR images. The regions where articular surfaces were visibly in contact, were segmented from each image. The lengths of these contact arcs were multiplied by slice thickness and summed to determine the effective "direct" contact areas for each articulation. Contact forces, contact areas, peak and mean contact pressures and contact pressure distributions were compared between the SCM and FEM techniques for the radiolunate (RL) and radioscaphoid (RS) articulations, from normal, injured and postoperative wrists.

5.4. Results

Qualitatively, the location of contact pressure distribution matched well between SCM and FEM for the normal, injured and postoperative wrists of all subjects (Figures 5.2 to 5.4). This was expected, since the same kinematics were implemented in both modeling approaches.

Due to the low number of subjects, no tests for statistical significance were performed. Absolute differences between SCM and FEM contact parameters for RL and RS articulations of each subject, were compared for all three conditions (18 total comparisons for each measure). Absolute differences between SCM and FEM contact parameters for both articulations averaged across subjects for each condition, were also compared (6 total comparisons for each measure).

Table 5.1 shows comparison of contact forces between SCM and FEM and also the absolute value of the difference for the normal, injured and postoperative wrists of all subjects. For all subjects, absolute differences were within 10 N for 15 out of the 18 results. Taking the average across the three subjects, absolute differences of RL and RS contact force in all wrist states were all within 6 N (Figure 5.5). The overall average (wrist states and articulations) signed difference between SCM and FEM was 1 N. Contact force signed differences for normal, injured and postoperative wrists were similar between SCM and FEM for the radiolunate articulation (Figure 5.5).

Table 5.2 shows comparison of peak contact pressures between SCM and FEM for the normal, injured and postoperative wrists of all subjects. The absolute differences were within 0.5 MPa for 13 out of the 18 results. The differences of the average of peak contact pressures across the subjects between SCM and FEM were under 0.5 MPa, except for radioscaphoid postoperative wrists (Figure 5.6). The overall average signed difference between SCM and FEM showed SCM peak pressure to be 0.34 MPa lower than FEM. For the radiolunate articulation, signed differences were similar between SCM and FEM for normal, injured and postoperative wrists (Figure 5.6).

Table 5.3 shows mean contact pressures compared between the SCM and FEM techniques for the normal, injured and postoperative wrists of all subjects. The absolute differences were within 0.2 MPa for 15 out of the 18 results, and under 0.5 MPa for all results. Except for radioscaphoid postoperative wrists, the differences of the average of mean contact pressures

across the three subjects were within 0.2 MPA (Figure 5.7). The overall average signed difference between SCM and FEM showed SCM mean pressure to be 0.14 MPa lower than FEM. Signed differences in mean contact pressures were similar between SCM and FEM for normal, injured and postoperative wrists in both articulations (Figure 5.7).

Table 5.4 shows comparison of normal, injured and postoperative contact areas between SCM and FEM, and also direct contact areas for all subjects. For 15 out of the 18 results, absolute differences between SCM and FEM were within 15 mm^2. Taking the average of contact areas across the three subjects, the difference between SCM and FEM was over 15 mm^2 only for radioscaphoid normal and injured wrists (Figure 5.8). The overall average signed difference between SCM and FEM showed FEM contact area to be 12 mm^2 lower than SCM. Signed differences for normal, injured and postoperative wrists observed between SCM and FEM were of similar magnitude, only in the radiolunate articulation (Figure 5.8). Except for radioscaphoid postoperative wrists, average contact areas from SCM were within 15 mm^2 of the average direct contact area results (Figure 5.8). Model (SCM and FEM) contact areas tended to match direct contact areas more closely for the radiolunate articulation (Figure 5.8).

5.5. Discussion

We compared radiocarpal contact mechanics as a result of scapholunate dissociation and subsequent surgical intervention determined using the SCM technique, to results of a parallel analysis using FEM. At least 80% of contact forces, peak contact pressures, mean contact pressures and contact areas from SCM were within reasonable limits (10 N, 0.5 MPa, 0.2 MPa and 15 mm^2, respectively) of the results from FEM, suggesting viability of the SCM approach. Change in wrist status did not appear to affect SCM accuracy compared to FEM, further affirming the SCM technique.

Mechanical factors are considered important in the etiology of initiation and progression of osteoarthritis (OA), and peak contact pressures and pressure distributions are considered to be key mechanical factors [31]. Increase in peak contact pressures above a physiological threshold may cause cellular damage leading to the inability of cartilage to repair and maintain a healthy extracellular matrix. Peak contact pressures tended to increase with injury, particularly in the radiolunate articulation. Peak contact pressure results from SCM and FEM were in the range

reported by prior in vitro studies [22, 32, 33]. Also, the non-uniform/asymmetrical contact distributions observed from both techniques are typical of the incongruent radiocarpal articulations [32]. While radioscaphoid peak contact pressure appeared to decrease after injury in some instances, it was observed that location of peak contact pressure and distribution had shifted more compared to radiolunate contact (Figure 5.3). Scapholunate diastasis is clinically observed after ligament disruption with increasing severity of instability [34], and a subsequent shift in contact may also be a potential OA risk factor.

Higher differences in contact parameters between SCM and FEM observed in the radioscaphoid articulation may be due to geometry and kinematics specific to this location. Scaphoid contact was mainly observed at the dorsal ridge, particularly in the injured and postoperative wrists (Figures 5.2 to 5.4). There are rapid changes in geometry associated with this region, where the radius contact surface transitions from relatively flat to areas of high curvature. As such, deformable interaction of the FEM technique may more accurately model the contact in this region compared to rigid surface interaction of SCM. Also, the lower mesh resolution of the SCM models (Figure 5.1 left) may have caused an averaging effect especially in the regions of high curvature. This may have caused an underestimation of SCM nodal strains (less overlap) resulting in lower estimates of peak contact pressures and subsequently contact forces and mean contact pressures.

FEM contact areas corresponded more closely to direct contact area measurements, than those from SCM (Figure 5.8). This was expected as the volumetric models were deformable, which would represent the apparent deformations of the articular surfaces on the loaded MR images from which the direct contact areas were calculated. While contact areas from SCM were determined from overlapping nodes of the interacting rigid bodies. Direct contact area measurements were generally higher than the model measurements. For both articulations, SCM and FEM contact areas for the normal wrists most closely matched the direct contact area measurements. With injury, the effects of motion artifacts on the loaded images may be more significant, thereby influencing segmentation and registration (kinematics) accuracy, and potentially affecting direct contact area measurements. Larger differences observed in the radioscaphoid articulation between model and direct contact area results (Figure 5.8), could be a

result of the scaphoid being more mobile than the lunate [35]. Currently, direct contact area is the only measurement available to verify our *in vivo* modeling accuracy.

Since its introduction, the application of finite element modeling has progressed rapidly in the biomechanics field. The applications are no longer just limited to basic tissue stress analysis. They now include complex multi-phasic interactions, biomechanical models that simulate physiologic/pathologic conditions, tissue response at implant interfaces, osteoporotic fracture predictions, etc. [36]. The extent of model complexity is dictated by the level of detail required of the output variables. However, as models get more complicated (non-linear contact problem for instance), more time and resources are required to prepare the models and complete the analysis [21], which questions their feasibility for clinical applications. Alternate modeling techniques that can produce similar results to the FEM "gold standard" could potentially provide clinically relevant results in an efficient manner.

MRI-based surface contact modeling has significant potential as a research and clinical tool. While CT is a common imaging modality, MRI is believed to be the best method to obtain subject-specific geometry [20]. Osseous and soft tissue geometries can be acquired from the same set of images without the need for coordinate system registration (when using multiple imaging modalities) or the use of contrast agents. With MRI-based SCM, the actual cartilage surface can be segmented, thereby eliminating the need to replace articular surfaces with a mechanical equivalent such as discrete springs [14-16]. It also eliminates the need for approximating the cartilage surfaces using half the distance between bone geometry (assuming articular contact which may not be the case during imaging). Studies have shown these methods to have lower accuracy in predicting contact mechanics [21, 37]. Inclusion of joint space with cartilage thickness and additional assumptions at joint edges (extra thickness), are thus avoided. Using fat suppressed T2-weighted sequences (DESS for example) minimizes chemical shift artifacts, providing better delineation between tissue interfaces and allowing for semi-automatic segmentation of the bone, which improves model generation efficiency [38]. Also, with quality control, boundary segmentation errors can be reduced to less than 8% [39]. There is a risk of radiation exposure in using radiographic methods to acquire kinematics [40], such as multi-planar X-ray fluoroscopy techniques. Though this technique provides accurate real-time 3D

motion, it is difficult to apply effectively to complex joints with multiple small articulating bones such as the wrist, and accuracy in such applications is not yet verified. Kinematic boundary conditions can be determined from image registration of static/quasi-static images (kinematic MRI) or from dynamic images (cine-PC MRI) acquired during functional loading [2, 17], which do not require a priori force assumptions. Intensity based volume registration is less sensitive to segmentation errors [41]. Loading conditions estimated from muscle geometry determined using diffusion tensor MRI [2] and muscle activity from EMG, can be applied to SCM for force driven models.

One limitation was that FEM contact results were not directly validated with experiments. The MRI-based SCM technique has been sufficiently validated to provide reliable joint contact mechanics data [22, 42]. Since FEM is accepted as the gold standard, it was used as the standard for comparison. As mentioned earlier, both SCM and FEM results were in reasonable agreement with published data and also with the direct contact area measurements. The low number of subjects was another limitation of the study. While data from three subjects provided a reasonable comparison between SCM and FEM, it was not sufficient (nor intended to be so) to make conclusions on the effects of injury and surgical repair. Using the SCM technique, prior *in vivo* work in our lab has shown significant increases in all contact parameters in the radioscaphoid articulation as a result of injury [Chapter 3] and a significant decrease in contact pressures in the radiolunate articulation after surgical repair [Chapter 4]. Another limitation was the uniform thickness assumption for the articular surfaces to simplify the analysis. Total articular thickness of the contacting surfaces was used to approximate local strains. Assigning higher thickness values to the cartilage surfaces can lead to lower strain estimates, and subsequently underestimate contact pressure results. Variable thickness cartilage models can also be implemented using SCM. Also, SCM mesh resolutions were comparatively lower than FEM due to processing limitations of the current modeling software version. Lower geometric fidelity may have resulted in an averaging of the nodal contact pressures from a coarser mesh distribution. To further improve SCM accuracy, future work would include comparing results from higher resolution models and also from assigning subject-specific spatially varying cartilage thicknesses determined from the MR images.

MRI-based surface contact modeling can provide useful *in vivo* joint contact mechanics data in a computationally efficient manner compared to FEM, making the technique more clinically feasible. Some differences between SCM and FEM results could also be attributed to the specific implementation of the FEM analysis. For instance, studies have shown a rigid subchondral interface assumption, used in the FEM analysis, to predict higher contact pressures than a deformable bone-cartilage interface [37]. While more complex and time consuming, FEM can be used to perform detailed analyses such as influence of depth dependent anisotropy on stresses, effects of fluid layer between articulating surfaces on contact mechanics, etc. Thus, it is likely the tool of choice for most research studies. Results from this study indicate MRI-based SCM to be a practical tool that can efficiently obtain clinically relevant data, which can differentiate between normal and abnormal conditions, and potentially assess OA risk based on contact mechanics data.

5.6. References

[1] Anderson, A. E., Ellis, B. J., Maas, S. A., Peters, C. L., and Weiss, J. A., 2008, "Validation of Finite Element Predictions of Cartilage Contact Pressure in the Human Hip Joint," J. Biomech. Eng., 130(5), pp. 051008.

[2] Blemker, S. S., Asakawa, D. S., Gold, G. E., and Delp, S. L., 2007, "Image-Based Musculoskeletal Modeling: Applications, Advances, and Future Opportunities," J. Magn. Reson. Imaging, 25(2), pp. 441-451.

[3] Anderson, D. D., Chubinskaya, S., Guilak, F., Martin, J. A., Oegema, T. R., Olson, S. A., and Buckwalter, J. A., 2011, "Post-Traumatic Osteoarthritis: Improved Understanding and Opportunities for Early Intervention," J. Orthop. Res., 29(6), pp. 802-809.

[4] Alonso-Rasgado, T., Jimenez-Cruz, D., Bailey, C. G., Mandal, P., and Board, T., 2012, "Changes in the Stress in the Femoral Head Neck Junction after Osteochondroplasty for Hip Impingement: A Finite Element Study," J. Orthop. Res., 30(12), pp. 1999-2006.

[5] Chizari, M., Snow, M., and Wang, B., 2011, "Post-Operative Assessment of an Implant Fixation in Anterior Cruciate Ligament Reconstructive Surgery," J. Med. Syst., 35(5), pp. 941-7.

[6] Harris, M. D., Anderson, A. E., Henak, C. R., Ellis, B. J., Peters, C. L., and Weiss, J. A., 2012, "Finite Element Prediction of Cartilage Contact Stresses in Normal Human Hips," J. Orthop. Res., 30(7), pp. 1133-9.

[7] Lee, H.-Y., Kim, S.-J., Kang, K.-T., Kim, S.-H., and Park, K.-K., 2012, "The Effect of Tibial Posterior Slope on Contact Force and Ligaments Stresses in Posterior-Stabilized Total Knee Arthroplasty-Explicit Finite Element Analysis," Knee Surg Relat Res, 24(2), pp. 91-98.

[8] Zou, Z., Chavez-Arreola, A., Mandal, P., Board, T. N., and Alonso-Rasgado, T., 2012, "Optimization of the Position of the Acetabulum in a Ganz Periacetabular Osteotomy by Finite Element Analysis," J. Orthop. Res., pp.

[9] Farrokhi, S., Keyak, J. H., and Powers, C. M., 2011, "Individuals with Patellofemoral Pain Exhibit Greater Patellofemoral Joint Stress: A Finite Element Analysis Study," Osteoarthritis Cartilage, 19(3), pp. 287-94.

[10] Fitzpatrick, C. K., Baldwin, M. A., and Rullkoetter, P. J., 2010, "Computationally Efficient Finite Element Evaluation of Natural Patellofemoral Mechanics," J. Biomech. Eng., 132(12), pp. 121013.

[11] Yang, N. H., Canavan, P. K., Nayeb-Hashemi, H., Najafi, B., and Vaziri, A., 2010, "Protocol for Constructing Subject-Specific Biomechanical Models of Knee Joint," Comput. Methods Biomech. Biomed. Engin., 13(5), pp. 589-603.

[12] Carrigan, S. D., Whiteside, R. A., Pichora, D. R., and Small, C. F., 2003, "Development of a Three-Dimensional Finite Element Model for Carpal Load Transmission in a Static Neutral Posture," Ann. Biomed. Eng., 31(6), pp. 718-25.

[13] Ledoux, P., Lamblin, D., and Targowski, R., 2001, "Modifications to the Mechanical Behavior of the Wrist after Fracture of the Scaphoid. Modeling by Finite Element Analysis," Acta Orthop. Belg., 67(3), pp. 236-41.

[14] Majima, M., Horii, E., Matsuki, H., Hirata, H., and Genda, E., 2008, "Load Transmission through the Wrist in the Extended Position," J Hand Surg Am, 33(2), pp. 182-8.

[15] Matsuki, H., Horii, E., Majima, M., Genda, E., Koh, S., and Hirata, H., 2009, "Scaphoid Nonunion and Distal Fragment Resection: Analysis with Three-Dimensional Rigid Body Spring Model," J. Orthop. Sci., 14(2), pp. 144-9.

[16] Schuind, F., Cooney, W. P., Linscheid, R. L., An, K. N., and Chao, E. Y. S., 1995, "Force and Pressure Transmission through the Normal Wrist. A Theoretical Two-Dimensional Study in the Posteroanterior Plane," J. Biomech., 28(5), pp. 587-601.

[17] Pillai, R. R., Thoomukuntla, B., Ateshian, G. A., and Fischer, K. J., 2007, "Mri-Based Modeling for Evaluation of in Vivo Contact Mechanics in the Human Wrist During Active Light Grasp," J. Biomech., 40(12), pp. 2781-7.

[18] Cohen, Z. A., Henry, J. H., Mccarthy, D. M., Mow, V. C., and Ateshian, G. A., 2003, "Computer Simulations of Patellofemoral Joint Surgery," The American Journal of Sports Medicine, 31(1), pp. 87-98.

[19] Murase, T., Moritomo, H., Goto, A., Sugamoto, K., and Yoshikawa, H., 2005, "Does Three-Dimensional Computer Simulation Improve Results of Scaphoid Nonunion Surgery?," Clin. Orthop. Relat. Res., 434), pp. 143-50.

[20] Fernandez, J. W., and Pandy, M. G., 2006, "Integrating Modelling and Experiments to Assess Dynamic Musculoskeletal Function in Humans," Exp. Physiol., 91(2), pp. 371-382.

[21] Clarke, S. G., Phillips, A. T., and Bull, A. M., 2011, "Evaluating a Suitable Level of Model Complexity for Finite Element Analysis of the Intact Acetabulum," Comput. Methods Biomech. Biomed. Engin., pp.

[22] Johnson, J. E., Mciff, T. E., Lee, P., Toby, E. B., and Fischer, K. J., 2012, "Validation of Radiocarpal Joint Contact Models Based on Images from a Clinical Mri Scanner," Comput. Methods Biomech. Biomed. Engin., pp. Epub ahead of print

[23] Kwak, S. D., Blankevoort, L., and Ateshian, G. A., 2000, "A Mathematical Formulation for 3d Quasi-Static Multibody Models of Diarthrodial Joints," Comput. Methods Biomech. Biomed. Engin., 3(1), pp. 41-64.

[24] Crisco, J. J., Wolfe, S. W., Neu, C. P., and Pike, S., 2001, "Advances in the in Vivo Measurement of Normal and Abnormal Carpal Kinematics," The Orthopedic clinics of North America, 32(2), pp. 219-31.

[25] Sokolow, C., 2001, "Anatomy and Histology of the Scapholunate Ligament," Hand Clin., 17(1), pp. 77.

[26] Ruby, L. K., An, K. N., Linscheid, R. L., Cooney, W. P., 3rd, and Chao, E. Y., 1987, "The Effect of Scapholunate Ligament Section on Scapholunate Motion," J. Hand Surg. [Am.], 12(5 Pt 1), pp. 767-71.

[27] Watson, H. K., and Ryu, J., 1986, "Evolution of Arthritis of the Wrist," Clin. Orthop., 202), pp. 57-67.

[28] Boschetti, F., Pennati, G., Gervaso, F., Peretti, G. M., and Dubini, G., 2004, "Biomechanical Properties of Human Articular Cartilage under Compressive Loads," Biorheology, 41(3-4), pp. 159-66.

[29] Korhonen, R. K., Laasanen, M. S., Töyräs, J., Rieppo, J., Hirvonen, J., Helminen, H. J., and Jurvelin, J. S., 2002, "Comparison of the Equilibrium Response of Articular Cartilage in Unconfined Compression, Confined Compression and Indentation," J. Biomech., 35(7), pp. 903-909.

[30] Jurvelin, J. S., Buschmann, M. D., and Hunziker, E. B., 1997, "Optical and Mechanical Determination of Poisson's Ratio of Adult Bovine Humeral Articular Cartilage," J. Biomech., 30(3), pp. 235-241.

[31] Andriacchi, T. P., Mündermann, A., Smith, R. L., Alexander, E. J., Dyrby, C. O., and Koo, S., 2004, "A Framework for the in Vivo Pathomechanics of Osteoarthritis at the Knee," Ann. Biomed. Eng., 32(3), pp. 447-457.

[32] Patterson, R., and Viegas, S. F., 1995, "Biomechanics of the Wrist," J. Hand Ther., 8(2), pp. 97-105.

[33] Hara, T., Horii, E., An, K. N., Cooney, W. P., Linscheid, R. L., and Chao, E. Y., 1992, "Force Distribution across Wrist Joint: Application of Pressure-Sensitive Conductive Rubber," J. Hand Surg. [Am.], 17(2), pp. 339-47.

[34] Manuel, J., and Moran, S. L., 2010, "The Diagnosis and Treatment of Scapholunate Instability," Hand Clin., 26(1), pp. 129-44.

[35] Fisk, G. R., 1980, "An Overview of Injuries of the Wrist," Clin. Orthop., 149), pp. 137-44.

[36] Herrera, A., Ibarz, E., Cegonino, J., Lobo-Escolar, A., Puertolas, S., Lopez, E., Mateo, J., and Gracia, L., 2012, "Applications of Finite Element Simulation in Orthopedic and Trauma Surgery," World J Orthop, 3(4), pp. 25-41.

[37] Anderson, A. E., Ellis, B. J., Maas, S. A., and Weiss, J. A., 2010, "Effects of Idealized Joint Geometry on Finite Element Predictions of Cartilage Contact Stresses in the Hip," J. Biomech., 43(7), pp. 1351-7.

[38] Eckstein, F., Cicuttini, F., Raynauld, J. P., Waterton, J. C., and Peterfy, C., 2006, "Magnetic Resonance Imaging (Mri) of Articular Cartilage in Knee Osteoarthritis (Oa): Morphological Assessment," Osteoarthritis Cartilage, 14(Supplement 1), pp. 46-75.

[39] Li, G., Lopez, O., and Rubash, H., 2001, "Variability of a Three-Dimensional Finite Element Model Constructed Using Magnetic Resonance Images of a Knee for Joint Contact Stress Analysis," J. Biomech. Eng., 123(4), pp. 341-6.

[40] Gardner, M. J., Crisco, J. J., and Wolfe, S. W., 2006, "Carpal Kinematics," Hand Clin., 22(4), pp. 413-20.

[41] Moojen, T. M., Snel, J. G., Ritt, M. J. P. F., Venema, H. W., Kauer, J. M. G., and Bos, K. E., 2003, "In Vivo Analysis of Carpal Kinematics and Comparative Review of the Literature," The Journal of Hand Surgery, 28(1), pp. 81-87.

[42] Fischer, K. J., Johnson, J. E., Waller, A. J., Mciff, T. E., Bruce Toby, E., and Bilgen, M., 2011, "Mri-Based Modeling for Radiocarpal Joint Mechanics: Validation Criteria and Results for Four Specimen-Specific Models," J. Biomech. Eng., 133(10), pp. 101004.

5.7. Tables

Table 5.1. Comparison of radiolunate (RL) and radioscaphoid (RS) contact forces from MRI-based surface contact modeling (SCM) and finite element modeling (FEM) and absolute differences (DIFF) for normal, injured and postoperative wrists of all three subjects.

		Normal			*Injured*			*Postoperative*		
		SCM	**FEM**	**DIFF**	**SCM**	**FEM**	**DIFF**	**SCM**	**FEM**	**DIFF**
	1	13	16	3	50	27	22	7	9	2
RL	**2**	46	53	8	39	41	2	9	10	1
	3	6	5	1	9	12	4	16	19	3
	1	22	13	10	34	10	24	12	13	1
RS	**2**	15	12	3	3	5	2	5	5	0
	3	11	17	6	11	18	7	15	26	11

Table 5.2. Comparison of radiolunate (RL) and radioscaphoid (RS) peak contact pressures from MRI-based surface contact modeling (SCM) and finite element modeling (FEM) and absolute differences (DIFF) for normal, injured and postoperative wrists of all three subjects.

		Normal			*Injured*			*Postoperative*		
		SCM	**FEM**	**DIFF**	**SCM**	**FEM**	**DIFF**	**SCM**	**FEM**	**DIFF**
	1	0.88	1.17	0.29	1.39	1.12	0.28	0.42	0.77	0.35
RL	**2**	0.91	1.23	0.32	1.30	1.42	0.12	0.73	1.09	0.36
	3	0.72	0.85	0.14	0.98	1.15	0.16	0.79	1.14	0.35
	1	1.15	1.24	0.09	2.18	2.20	0.02	1.59	2.55	0.96
RS	**2**	1.04	1.27	0.23	0.54	1.09	0.54	0.66	1.17	0.52
	3	0.69	1.11	0.42	0.87	1.48	0.61	0.60	1.42	0.82

Table 5.3. Comparison of radiolunate (RL) and radioscaphoid (RS) mean contact pressures from MRI-based surface contact modeling (SCM) and finite element modeling (FEM) and absolute differences (DIFF) for normal, injured and postoperative wrists of all three subjects.

		Normal			*Injured*			*Postoperative*		
		SCM	**FEM**	**DIFF**	**SCM**	**FEM**	**DIFF**	**SCM**	**FEM**	**DIFF**
RL	**1**	0.36	0.48	0.13	0.62	0.56	0.07	0.20	0.33	0.14
	2	0.46	0.63	0.16	0.48	0.56	0.08	0.21	0.31	0.10
	3	0.34	0.44	0.09	0.35	0.45	0.10	0.35	0.50	0.15
RS	**1**	0.40	0.48	0.08	0.55	0.57	0.02	0.83	1.30	0.48
	2	0.40	0.43	0.03	0.33	0.52	0.19	0.23	0.39	0.17
	3	0.20	0.40	0.20	0.30	0.60	0.30	0.25	0.50	0.24

Table 5.4. Comparison of radiolunate (RL) and radioscaphoid (RS) contact areas from MRI-based surface contact modeling (SCM) and finite element modeling (FEM) and absolute differences (DIFF), and also direct contact area measurements (DA) for normal, injured and postoperative wrists of all three subjects.

		Normal				*Injured*				*Postoperative*			
		SCM	**FEM**	**DA**	**DIFF**	**SCM**	**FEM**	**DA**	**DIFF**	**SCM**	**FEM**	**DA**	**DIFF**
RL	**1**	37	33	40	4	79	49	87	30	34	27	31	7
	2	99	85	99	14	81	72	119	8	42	31	60	12
	3	18	11	17	7	25	28	19	3	45	38	54	7
RS	**1**	57	26	62	30	62	18	49	45	15	10	65	5
	2	38	28	25	11	10	10	35	0	22	14	50	8
	3	57	43	77	14	38	30	64	8	59	53	71	6

5.8. Figures

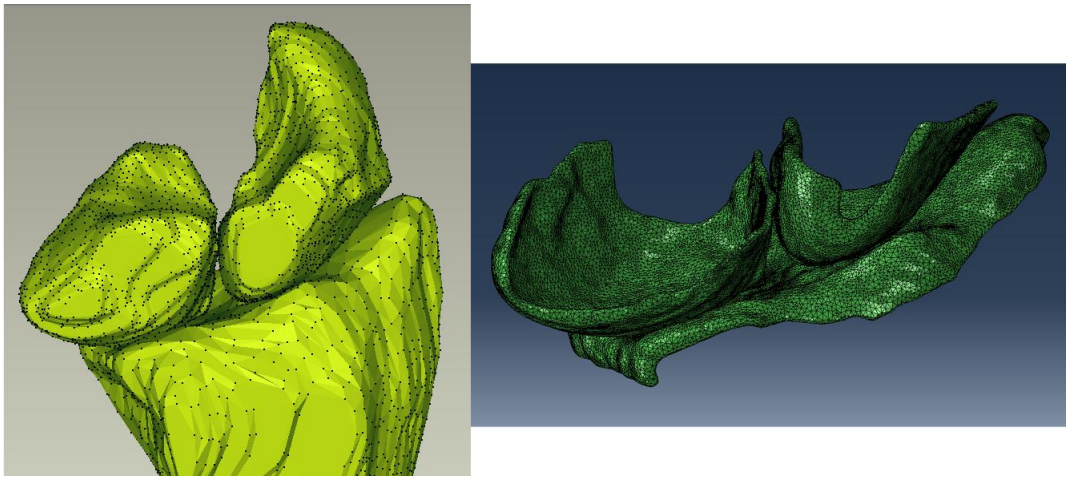

Figure 5.1. Radiocarpal surface (left) and volumetric (right) models of the normal wrist of Subject 2 used for surface contact modeling (bone and cartilage geometry) and finite element modeling (only cartilage geometry), respectively.

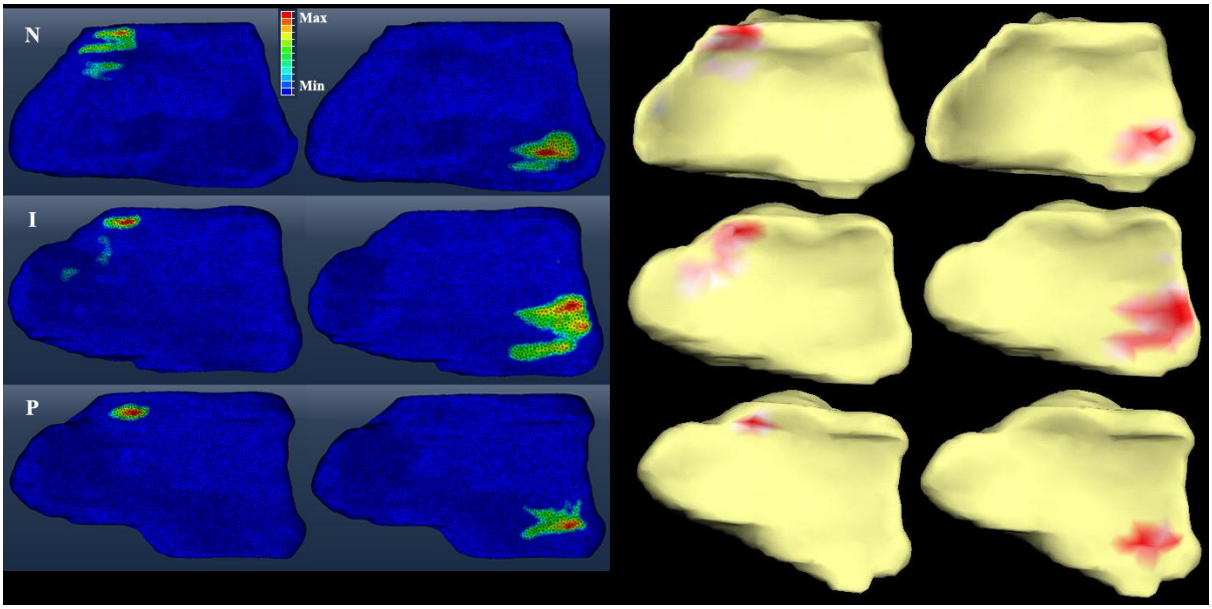

Figure 5.2. Contact pressure distributions of the normal (N), injured (I) and postoperative wrists of Subject 1 from finite element modeling (left) and surface contact modeling (right). For each technique, first column shows radioscaphoid contact and second column shows radiolunate contact. Contact varies medial/ulnar to the left and dorsal/posterior to the top.

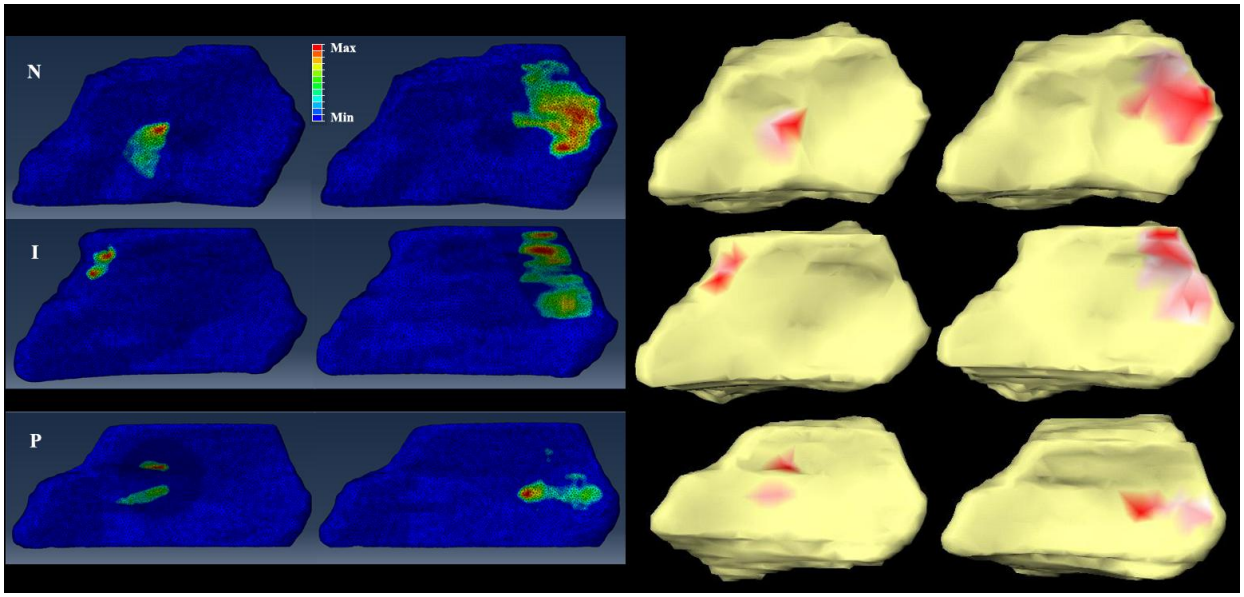

Figure 5.3. Contact pressure distributions of the normal (N), injured (I) and postoperative wrists of Subject 2 from finite element modeling (left) and surface contact modeling (right). For each technique, first column shows radioscaphoid contact and second column shows radiolunate contact. Contact varies medial/ulnar to the left and dorsal/posterior to the top.

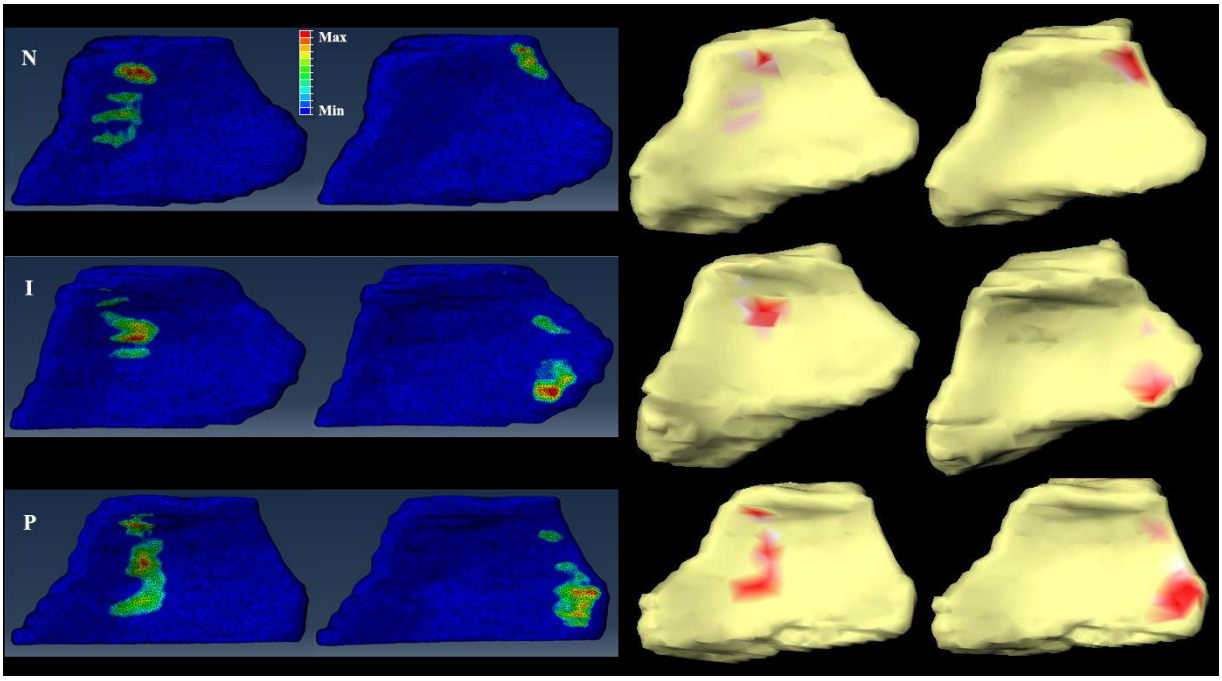

Figure 5.4. Contact pressure distributions of the normal (N), injured (I) and postoperative wrists of Subject 3 from finite element modeling (left) and surface contact modeling (right). For each technique, first column shows radioscaphoid contact and second column shows radiolunate contact. Contact varies medial/ulnar to the left and dorsal/posterior to the top.

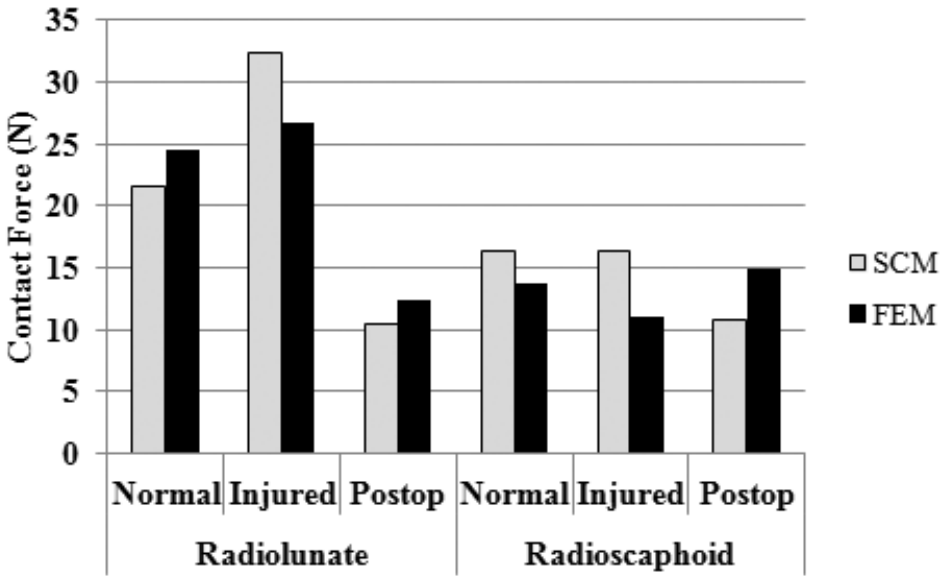

Figure 5.5. Average contact forces across the three subjects from surface contact modeling (SCM) and finite element modeling (FEM) for the three conditions.

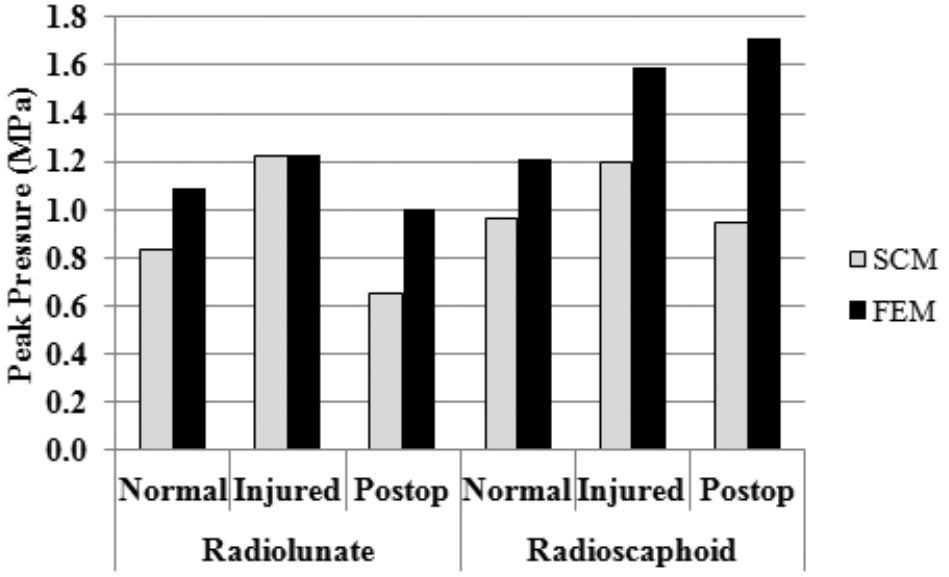

Figure 5.6. Average peak contact pressures across the three subjects from surface contact modeling (SCM) and finite element modeling (FEM) for the three conditions.

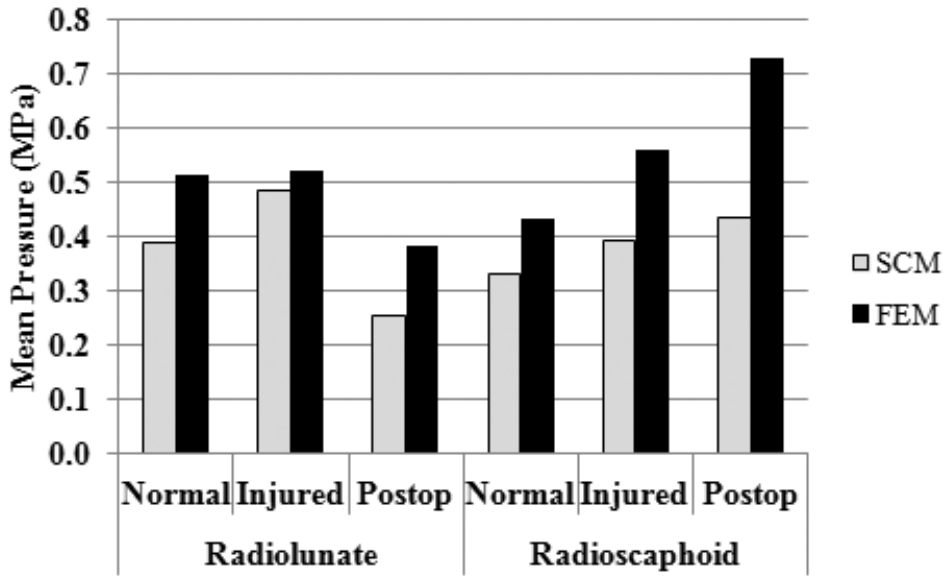

Figure 5.7. Average mean contact pressures across the three subjects from surface contact modeling (SCM) and finite element modeling (FEM) for the three conditions.

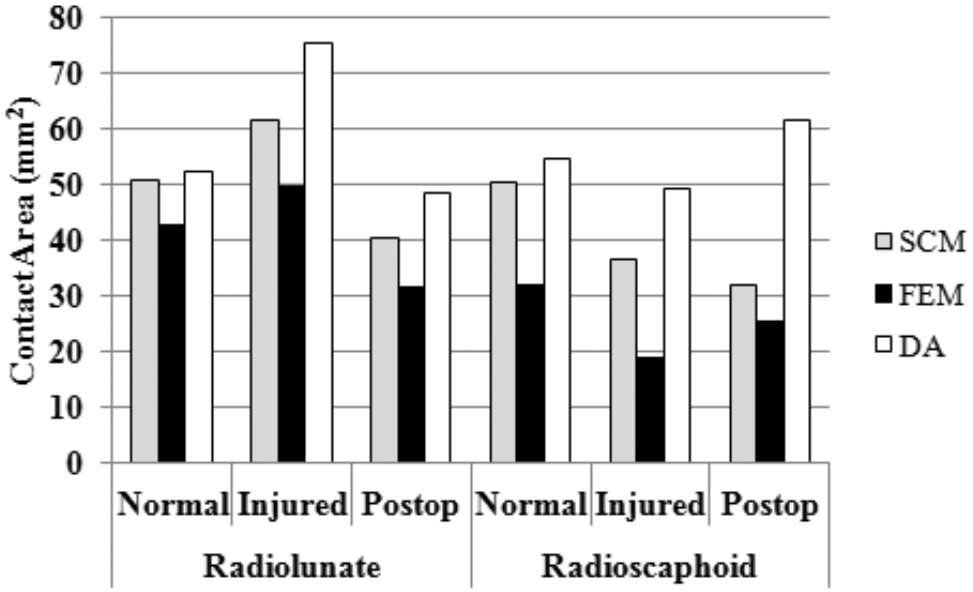

Figure 5.8. Average contact areas across the three subjects from surface contact modeling (SCM) and finite element modeling (FEM), and also from direct contact area (DA) measurements for the three conditions.

6. CONCLUSION

6.1. Summary

The study to evaluate the effects of scapholunate ligament injury and surgical repair on radiocarpal joint mechanics, has been successfully concluded. It is generally accepted that abnormal joint posture and motion are a consequence of disruption to the normal scapholunate mechanical linkage, as a result of scapholunate ligament injury. As such there is abnormal load transmission through the joint, which is manifested as altered joint mechanics. Among other factors, it is believed there is a relationship between the ensuing abnormal mechanics, particularly magnitude and distribution of contact pressures and clinically observed degenerative changes, though the mechanism is not well understood. Surgical reconstruction attempts to correct the deformity, but successful repair is commonly determined by a visual and/or functional outcome. A tool to effectively monitor in vivo joint mechanics may facilitate injury diagnosis and improve treatment efficacy.

MRI has limited diagnostic applicability for wrist ligament injuries, but is advantageous for obtaining in vivo data such as model geometry and loading or boundary conditions. MRI combined with computational modeling can be used to obtain in vivo joint mechanics. FE modeling is the most common and accurate technique for joint contact analysis. However, solving the complex non-linear contact problem is time consuming. Even performing a more computationally efficient rigid body FE analysis, requires considerable time to generate geometry with good mesh quality metrics. Surface contact mechanics may be sufficient to clinically evaluate injuries and surgical outcomes, and the MRI-based surface contact modeling technique can be used to determine joint contact mechanics in a manner that is feasible for clinical applications.

The focus of this work was to investigate the effects of scapholunate ligament injury and surgical repair through MRI-based SCM and also compare these results to a similar FE analysis. The process involved generating SCM and FE geometry (from image segmentation), acquiring boundary conditions (kinematics from image registration) and applying a contact interaction to solve for contact forces, contact areas, peak and mean contact pressures and contact pressure distributions. The following were the major findings and conclusions of the study.

6.2. Major findings and conclusions

The effect of initial manual registration on automatic registration accuracy was investigated. Results showed that manual registration to align registration volumes as close as possible prior to auto-registration, appeared to reduce errors in final kinematics and in contact mechanics. Though the results may be software specific, the study indicated that a good initial manual registration should improve kinematics results from any automated voxel registration software.

The effects of SL ligament injury on radiocarpal contact mechanics were investigated. Results showed that all contact parameters significantly increased in the radioscaphoid joint, while peak and mean contact pressures significantly increased in the radiolunate joint. There was also a significant increase in the intercentroid distances. Increase in radioscaphoid contact parameters and shift in contact locations correspond to clinically observed osteoarthritic patterns, which initiate in the lateral radioscaphoid region. While contact pressures increased, a shift in contact pressure distributions may also be a potential OA risk factor. Alterations to physiologic grasp were observed by the increases in contact forces after injury. Though the radiolunate joint is more stable, observed shift in load transfer from the scaphoid to the lunate, may explain why even the integrity of this joint is eventually compromised. Novel in vivo contact mechanics data indicated detrimental alterations to radiocarpal mechanics from SL ligament injury.

The effects of surgical repair on radiocarpal contact mechanics after SL ligament injury were investigated. Results showed significant decrease in peak and mean contact pressures after repair in the radiolunate articulation only, and no significant differences in these contact parameters between normal and postoperative wrists. There were no significant differences in intercentroid distances between the injured and postoperative wrists. Significant decrease in contact pressures indicated the benefits of having surgery. However, the benefits may be limited by the severity of instability at the time of diagnosis. The surgical technique appears to have been effective to minimize radiolunate instability, but perhaps in some cases, not the more severe radioscaphoid instability. Lack of significant reduction of the scapholunate interval also suggests that perhaps a longer time may be needed to heal after repair. In addition, contact parameters after repair suggested that perhaps more robust ligament reconstruction techniques may be required to effectively correct the deformity resulting from injury and restore normal carpal alignment. Novel radiocarpal contact mechanics data on the efficacy of surgical repair after SLIL injury,

further strengthened the importance of surgery to manage the progression of instability and minimize the risk of developing OA.

Contact mechanics results from SCM were also compared to results from a similar FE analysis. Results typically showed good agreement between SCM and FEM for contact forces, contact areas, peak and mean contact pressures. Contact pressure distributions were very similar between the two techniques. Also, model contact area results compared well to direct contact area measurements for the normal wrists, providing further verification. The study showed that based on relevant assumptions, MRI-based SCM has good potential for clinical applications to evaluate joint injuries and surgical outcomes in a computationally efficient manner, based on surface contact mechanics.

6.3. Future directions

The study on effects of injury only compared the overall effects of SL ligament injury on contact mechanics. Progression of instability varies between patients. The stages of instability (predynamic, dynamic, static and SLAC) alter carpal alignment differently, and therefore, are expected to display different mechanical behavior. Also, surgical treatments and outcomes vary with severity of instability (static versus dynamic). With more subjects, it may be possible to differentiate between the different stages of instability by investigating the variation in contact mechanics with progressive instability. Increase in peak contact pressure is expected from the least severe stage of instability (predynamic) to the most severe (SLAC stage and bone-on-bone contact).

The study on effects of surgery compared only the overall effects of surgical repair (regardless of repair type) on contact mechanics altered by injury. Degenerative changes are sometimes observed even after treatment. Surgical outcomes are expected to vary between techniques that directly repair the ligament (most mobility), reconstruct the joint with tendon weaves, or partially/totally fuse the joint (least mobility). With more subjects, it may be possible to group mechanical outcomes according to technique, to better understand how effective each technique is to restore normal joint mechanics. The potential for healing depends on the condition of the SL ligament (partial/complete tear), secondary stabilizers (intact/disrupted) and cartilage surface (healthy/degenerated). Peak contact pressures are expected to be similar to

normal for direct repairs, which have the maximum potential for healing. When the SL ligament is irreparable, peak contact pressures are expected to be close to normal for soft tissue reconstruction techniques (tenodesis) that can restore and are robust enough to maintain normal alignment. Peak contact pressures are not expected to be restored to normal for joint salvage procedures (fusions).

While the MRI-based SCM technique compared well to FE modeling, the technique can be further developed by investigating the effects of mesh resolution and spatially varying cartilage thickness on contact mechanics. Lower geometric fidelity of the current models, may have resulted in an averaging of the nodal contact pressures due to the coarser mesh distribution. The uniform cartilage thickness assumption may also have resulted in an underestimation/overestimation of contact pressures. Contact mechanics from mesh resolutions similar to FE models and also from anatomical cartilage thickness values measured from MRI, can be investigated. By increasing mesh resolution of the SCM models and also incorporating spatially varying cartilage thickness, peak contact pressures (and other contact parameters) are expected to be closer to the FEM results. Due to different methods of solving the contact problem, there will always be a difference in results between the techniques. Clearly, the deformable contact interaction using FEM is a more accurate modeling assumption than the first order estimate of strain using SCM.

With enough subjects, it may be possible to construct a database of pressures and pressure distributions that correspond to clinically observed patterns of degeneration. This may prove to be a valuable tool to evaluate soft tissue injuries. The ability to monitor the location of peak contact pressure and contact pressure distribution in vivo, may provide clinical data to aid in the selection of the most effective treatment process. Based on contact mechanics data from different instability patterns, more robust techniques can be selected that may ensure a more successful outcome.

Additionally, location of peak contact pressures and pressure distributions can potentially be correlated to physiological changes in cartilage tissue (from T2 relaxation times), to better understand the mechanism of the onset and progression of PTOA. Postoperative contact mechanics data from follow-up studies, can provide information on the short-term benefits of

surgical repair. Studies into the efficacies of immobilization devices such as braces and splints may provide useful information to facilitate the healing process. Models with ligamentous constraints can also be implemented, to investigate changes in contact mechanics from ligament laxity with progressive instability or progressive wear. Using FE modeling, it may be possible to correlate surface contact pressures with 3D internal stresses. Thus, it may also be possible to estimate internal stress parameters using SCM alone.

The subtlety of SL ligament injury, highlights the importance of early diagnosis. The computational efficiency of the MRI-based SCM method, makes it feasible for clinical applications. With advances in MR imaging techniques and automated mesh generation procedures, it is envisioned that contact mechanics data may be acquired in real-time for clinical assessment. The ability to monitor load transmission through the joint may aid in prognosis of soft tissue injuries and simulate the outcomes of surgical treatments. This method can be further applied to investigate contact mechanics in other joints.

In conclusion, the MRI-based surface contact modeling technique was used to identify clinically relevant changes in contact mechanics as a result of scapholunate ligament injury and surgical repair. The process of acquiring joint mechanics data was computationally efficient, and has good potential for clinical applications.